Fisheries and Oceans Canada | Pêches et Océans Canada
Ecosystems and Oceans Science | Sciences des écosystèmes et des océans

Canadian Science Advisory Secretariat (CSAS)

Research Document 2019/059

Québec Region

Chemical and Biological Oceanographic Conditions in the Estuary and Gulf of St. Lawrence during 2018

M. Blais, P. S. Galbraith, S. Plourde, M. Scarratt, L. Devine and C. Lehoux

Fisheries and Oceans Canada
Institut Maurice-Lamontagne
850 route de la Mer, P.O. Box 1000
Mont-Joli, QC, G5H 3Z4

September 2019

Canada

Foreword

This series documents the scientific basis for the evaluation of aquatic resources and ecosystems in Canada. As such, it addresses the issues of the day in the time frames required and the documents it contains are not intended as definitive statements on the subjects addressed but rather as progress reports on ongoing investigations.

Published by:

Fisheries and Oceans Canada
Canadian Science Advisory Secretariat
200 Kent Street
Ottawa ON K1A 0E6

http://www.dfo-mpo.gc.ca/csas-sccs/
csas-sccs@dfo-mpo.gc.ca

ISSN 1919-5044

Correct citation for this publication:

Blais, M., Galbraith, P.S., Plourde, S., Scarratt, M., Devine, L. and Lehoux, C. 2019. Chemical and Biological Oceanographic Conditions in the Estuary and Gulf of St. Lawrence during 2018. DFO Can. Sci. Advis. Sec. Res. Doc. 2019/059. iv + 64 pp.

Aussi disponible en français :

Blais, M., Galbraith, P.S., Plourde, S., Scarratt, M., Devine, L. et Lehoux, C. 2019. Les conditions océanographiques chimiques et biologiques dans l'estuaire et le golfe du Saint-Laurent en 2018. Secr. can. de consult. sci. du MPO. Doc. de rech. 2019/059. iv + 67 pp.

TABLE OF CONTENTS

ABSTRACT

An overview of chemical and biological oceanographic conditions in the Gulf of St. Lawrence (GSL) in 2018 is presented as part of the Atlantic Zone Monitoring Program (AZMP). Data from the AZMP regional monitoring program were analyzed and described in relation to long-term means in the context of a strong warming event that began in 2010. During 2018, oxygen at 300 m reached the lowest concentration observed so far in the GSL. The deep oxygen anomalies were particularly strong from Cabot Strait to the northwest GSL, while the anomaly stayed relatively stable in the Estuary compared to 2017. Nitrate inventories in the surface (0–50 m) and mid-water column (50–150 m) layers were generally below normal everywhere in the GSL during summer and fall, but were near normal in the surface layer during wintertime, suggesting that a large nitrate drawdown occurred between March and June in all regions. As well in 2018, above-normal nitrate inventories were observed in deep waters (150 m–bottom) of the eastern GSL (eGSL), a pattern associated with intrusions of warm and salty waters occurring since 2012. The annual anomalies of vertically integrated chlorophyll a (chl a; 0–100 m) were above normal in all regions mostly because of high chl a concentrations during fall. More specifically, phytoplankton biomass reached record highs during summer in the western GSL (wGSL) and during fall in eGSL. In accordance with the large spring nitrate drawdown, satellite observations show that the spring bloom started earlier, lasted longer, and showed an above-normal magnitude than normal in most regions, the main exception being the northeast GSL. Zooplankton biomass increased in 2018 compared to 2016 and 2017 but remained below normal almost everywhere in the GSL. In most regions, large calanoid abundance was also below normal in 2018, mostly related to the decline in *Calanus hyperboreus* abundance at Rimouski station and of *Calanus finmarchicus* in eGSL and southern GSL (sGSL). Small calanoid abundances were generally above normal in wGSL and sGSL and near normal in eGSL, in agreement with the trend observed since 2014. Abundances of warm-water-associated copepods were also above normal in wGSL and sGSL but near normal in eGSL. In the latter region, cold-water-associated copepod abundance was higher than the long-term mean for the fourth consecutive year. Phenology of *C. finmarchicus* at Rimouski station suggests a near-normal timing of emergence from diapause and development into the adult stage. However, the peak of the early copepodite stages (CI–CIII) was long-lasting and reached its maximum abundance only in July. The infrequent and irregular sampling at Shediac Valley limited our ability to describe seasonal patterns associated with nutrients or lower trophic levels at this station.

INTRODUCTION

The Atlantic Zone Monitoring Program (AZMP) was implemented in 1998 (Therriault et al. 1998) with the aim of (1) increasing Fisheries and Oceans Canada's (DFO) capacity to understand, describe, and forecast the state of the marine ecosystem and (2) quantifying the changes in the ocean's physical, chemical, and biological properties and the predator–prey relationships of marine resources. AZMP provides data to support the sound development of ocean activities. A critical element in the AZMP observational program is the annual assessment of the distribution and variability of nutrients and the plankton communities they support.

A description of the spatiotemporal distribution of dissolved oxygen, nutrients (nitrate, silicate and phosphate), and chlorophyll a (chl a) concentrations provides important information on water mass movements and on the location, timing, and magnitude of biological production cycles. A description of phytoplankton and zooplankton distributions provides important information on the organisms forming the base of the marine food web. Understanding plankton production cycles is essential to an ecosystem approach to fisheries management.

The AZMP derives its information on the state of the marine ecosystem from data collected at a network of sampling locations (high-frequency monitoring sites, cross-shelf sections) in each DFO region (Québec, Gulf, Maritimes, Newfoundland; see Figure 1 for Québec region locations) occupied at a frequency of weekly to once annually. The sampling design provides valuable information on the natural variability in physical, chemical, and biological properties of the Northwest Atlantic continental shelf: cross-shelf sections provide detailed geographic information but are limited in their seasonal coverage while strategically located high-frequency monitoring sites complement the sampling by providing more detailed information on seasonal-scale changes in ecosystem properties.

In this document, we review the chemical and biological oceanographic (lower trophic levels) conditions in the Gulf of St. Lawrence (GSL) in 2018. Physical oceanographic conditions that prevailed in 2018 are described in Galbraith et al. (2019). The May to November sea surface temperature average was near normal despite conditions warmer than normal during late summer. Overall, the annual average SST in 2018 was the coldest since 2002. The maximum volume of sea-ice was the ninth lowest since 1969. The annual average freshwater discharge into the Estuary was above normal. Deep-water temperatures were above normal, with inward advection from Cabot Strait: GSL annual average temperature reached record highs at 250 m and 300 m. This report describes the 2018 production cycles and community composition of phytoplankton and zooplankton in the context of these physical conditions.

METHODS

SAMPLE COLLECTION

All sample collection and processing steps meet the standards of the AZMP protocol (Mitchell et al. 2002). Field measurements included in this report were made along seven oceanographic sections during surveys carried out in winter, summer, and fall (mainly in March, June, and November) of each year and at two high-frequency monitoring sites (Fig. 1). In this document, the seven sections, as well as supplementary stations in between sections, were grouped into three subregions to better match spatial scales addressed by AZMP in other regions (Fig. 2):

(1) western GSL (wGSL): this region is generally deep (> 200 m) and cold in summer. It is strongly influenced by freshwater runoff from the St. Lawrence River and cold and dense waters from the Laurentian Channel. It includes TESL, TSI, and TASO;

(2) southern GSL (sGSL): this region is shallow (< 100 m) and warmer in summer. It is under the influence of the Gaspé Current and includes TIDM only;

(3) eastern GSL (eGSL): this region, with deep channels and a relatively wide shelf (< 100 m), is characterized by higher surface salinity and is directly influenced by the intrusion of water from the Labrador and Newfoundland shelves. It includes TCEN, TDC, and TBB.

Table 1 provides details about the 2018 sampling surveys and Figures 2 and 3 summarize the sampling effort during the seasonal AZMP surveys and at the high-frequency sampling sites, respectively. Rimouski station (depth 320 m) has been sampled since 1991 as part of a research project—about weekly throughout the summer, less frequently in early spring and late fall (once or twice a month), and rarely in winter (except during the winter survey). It has been included in AZMP's annual review of environmental conditions since 2004 to represent conditions in the St. Lawrence Estuary (SLE) and the wGSL. Since the beginning of the AZMP, Shediac Valley station (depth 84 m) has represented conditions in the sGSL and SLE outflow. The frequency of sampling at Shediac Valley station is closer to monthly and even less frequent during January–April because of its remoteness. Sampling at oceanographic sections and high-frequency monitoring sites includes a CTD profile (temperature, salinity, fluorescence, dissolved oxygen) as well as water sampling using Niskin bottles. Water from the Niskin bottles is collected for the analysis of dissolved oxygen (Winkler method), nutrients (Technicon or Alpkem AutoAnalyzer), chl a, and phytoplankton identification (inverted microscopy) (Mitchell et al. 2002). Finally, mesozooplankton (< 1 cm) is sampled with bottom-to-surface vertical ring net tows (75 cm diameter, 200 µm mesh) for identification and biomass measurements.

Since 1996, a survey of the winter surface mixed layer of the GSL has been conducted, usually in early to mid-March, using a Canadian Coast Guard (CCG) helicopter. Surface nutrients (2 m) have been sampled since 2001 (Galbraith 2006, Galbraith et al. 2006), and additional depths were sampled in March 2016 and 2017 because sampling was carried out from CCG ships rather than the helicopter during these two years. The winter survey has added a considerable amount of data to the previously sparse winter sampling in the region. Over a hundred stations were sampled by helicopter between 26 February and 13 March 2018.

OXYGEN

Oxygen concentrations at 300 m are used as a monitoring indicator of hypoxic conditions in the GSL since they are less variable over time than surface oxygen concentrations, which vary seasonally because of water column mixing and primary production. Oxygen concentration was measured using an oxygen probe (Sea-Bird SBE43) mounted on the CTD; the probe was calibrated against seawater samples collected and analyzed by Winkler titration on every cast (for the calibration procedure, see Sea-Bird application notes 61-1, -2, -3). Here, we present the mean annual distribution of deep oxygen in the GSL derived from the CTD probe along with time series of annual concentrations of deep oxygen.

NUTRIENTS AND CHLOROPHYLL A

Chl a and nutrient data collected along the AZMP sections and at the high-frequency monitoring sites were integrated over various depth intervals (i.e., 0–100 m for chl a; 0–50 m and 50–150 m for nutrients) using trapezoidal numerical integration. The concentration of the sample collected at the shallowest depth was used as the upper integration limit, and the concentration of the closest sampled depth to the lower integration limit was used as the lower limit. In 2016 and 2017, the vertical profiles of nutrients in the GSL revealed that nitrate concentrations were relatively homogeneous in the upper 50 m of the water column during winter. Thus, for years when vertical nutrient profiles were not available, including 2018, integrated nitrate values for the winter survey were calculated using surface concentrations (2 m) × 50 m, assuming homogeneity of nitrate concentrations in the winter mixed layer.

In this document, a detailed description of the seasonal patterns is provided for different nutrient and phytoplankton indices. For the high-frequency monitoring sites, we present nitrate

inventories in different water column layers, chl *a* concentration, total phytoplankton abundance, and the relative abundance of the main phytoplankton taxonomic groups. For the three GSL subregions described above, the seasonal nitrate and chl *a* concentrations integrated over different depth layers as well as the spatial distribution of nutrients (nitrate, phosphate, silicate, N:P ratio) and chl *a* are presented. Spring nutrient drawdown was estimated using the difference between March and June nitrate inventory. Anomalies were computed for these indices (see Scorecard section below) for both high-frequency monitoring sites and GSL subregions.

SATELLITE REMOTE SENSING OF OCEAN COLOUR

Satellite ocean colour data provide large-scale images of surface phytoplankton biomass (chl *a*) over the whole Northwest Atlantic. We used two-week satellite composite images of four GSL boxes (northwest and northeast GSL [NWGSL, NEGSL], Magdalen Shallows, Cabot Strait; see Fig. 4 for locations) to supplement our ship-based observations, especially regarding spring bloom phenology, and to provide seasonal coverage and a large-scale context over which to interpret our survey data. The ocean colour imagery provides information about the timing and spatial extent of the spring and fall blooms but does not provide information on the dynamics that take place below the top few meters of the water column. In addition, satellite ocean colour data for the St. Lawrence Estuary are largely biased by suspended inorganic particles and coloured dissolved organic matter. Thus, these data cannot be used in an absolute manner. While knowledge on phytoplankton dynamics at the surface of the St. Lawrence Estuary during spring is gathered using the weekly sampling at Rimouski station, the temporal resolution is not always good enough to allow the calculation of bloom metrics as discussed below. Thus, the spring bloom metrics are not presented for the Estuary, but seasonal and interannual variability of phytoplankton biomass is described. In addition, the broad-scale oceanographic surveys include a transect in the Estuary (TESL) that is used to provide an estimate of phytoplankton concentrations during summer and fall in this region.

Near-surface phytoplankton biomass has been estimated from ocean colour data collected by the Sea-viewing Wide Field-of-view Sensor (SeaWiFS) satellite launched by NASA in late summer 1997, by the Moderate Resolution Imaging Spectroradiometer (MODIS) “Aqua” sensor launched by NASA in July 2002, and most recently by the Visible Infrared Imaging Radiometer Suite (VIIRS) satellite, launched in October 2011. In this report, SeaWiFS data from 1998–2007 and MODIS data for the 2008–2011 period are combined with VIIRS data for the 2012–2018 period to construct composite time series of surface chl *a* in four GSL subregions (Fig. 4). The accuracy of the MODIS satellite in estimating chl *a* has been compared with that of SeaWiFS for some regions of the globe. Although differences in sensor design, orbit, and sampling between MODIS and SeaWiFS cause some differences in calculated chl *a* values (Gregg and Rousseaux 2014), the biases associated with these satellites are overall not significantly greater than algorithm uncertainties, especially in non-turbid waters (Zibordi et al. 2006, Arun Kumar et al. 2015). Recent studies comparing all three sensors indicate that they provide consistent global ocean colour data records, with similar patterns and magnitudes, and generally high cross-sensor fidelity (Wang et al. 2013, Barnes and Hu 2016).

All selected subregions for the imagery data are located outside of the St. Lawrence River plume because data in regions influenced by this freshwater are unreliable as a result of turbidity and riverine input of terrestrially derived coloured matter, as mentioned previously. Composite satellite images were provided by BIO’s remote sensing unit (Bedford Institute of Oceanography, DFO, Dartmouth, NS) in collaboration with NASA’s Goddard Space Flight Center. Basic statistics (mean, range, standard deviation) were extracted from two-week average composites by averaging all pixels within each box (SeaWiFS and MODIS have a 1.5 km spatial resolution while VIIRS has a 1 km spatial resolution).

A shifted Gaussian function of time model was used to describe characteristics of the spring phytoplankton bloom based on the combined satellite data (Zhai et al. 2011). Four metrics were

computed to describe the spring bloom characteristics: start date (day of year), cycle duration (days), magnitude (the integral of chl *a* concentration under the Gaussian curve), and amplitude (maximum chl *a*). In addition, seasonal mean chl *a* biomass during spring (March to May), summer (June to August), and fall (September to November) as well as its annual average (March to November) were computed. For each of these eight metrics, we computed normalized annual anomalies (see Scorecard section below) to describe temporal trends for each statistical box.

ZOOPLANKTON INDICES

We provide a detailed description of the seasonal patterns for different zooplankton indices, mostly at Rimouski and Shediac Valley stations, but also for the three GSL subregions described above. For the high-frequency monitoring sites, we present total mesozooplankton biomass (dry weight), total copepod abundance, and the relative abundance of the copepod species making up 95% of the identified taxa by abundance. In addition, we include *Pseudocalanus* spp. (Rimouski station only) and *Calanus finmarchicus* abundances and stage composition. Because of its importance to the total zooplankton biomass in the GSL, a detailed description of *Calanus hyperboreus* has been added for Rimouski and Shediac Valley stations. We also present the spring and fall total zooplankton biomass and total abundance of *C. finmarchicus*, *C. hyperboreus*, and *Pseudocalanus* spp. for the three GSL subregions since they represent distinct oceanographic regimes. Since zooplankton samples are collected over the entire water column, zooplankton indices represent depth integrated metrics.

Changes in zooplankton phenology were described using *C. finmarchicus* as an indicator. We used the time series at Rimouski station because adequate sampling and stage identification started there 25 years ago (1994). From 1994 to 2004, prior to the use of the AZMP standard 75 cm diameter, 200 µm mesh bottom-to-surface ring net tows (Mitchell et al. 2002), *C. finmarchicus* copepodite stage abundance was determined using samples collected with 333 µm (CIV–CVI) and 73 µm (CI–III) mesh nets, towed from bottom to surface and from 50 m to surface respectively, that were analyzed for seven years of the time series (see Plourde et al. 2009 for details). In other years before 2004 for which 73 µm samples were not analyzed, the abundance of CI–III in the 333 µm samples was adjusted based on a comparison done with a 158 µm mesh net (S. Plourde, DFO, Mont-Joli, QC; unpublished data). The phenology of *C. finmarchicus* was described using the following steps: (1) stage relative abundance were normalized (proportion of a copepodite stage/maximum proportion for the stage) within each year for CI–III, CIV, CV, and CVI (male and female) and (2) stage proportions were smoothed using a Loess algorithm.

Finally, we present several zooplankton indices that reflect either key copepod taxa, different functional groups, or groups of species indicative of cold- or warm-water intrusions and/or local temperature conditions specific to the GSL. These indices are for *C. finmarchicus*, *Pseudocalanus* spp., total copepods (main component of mesozooplankton in terms of biomass and abundance), non-copepods (larval stages of benthic invertebrates, many carnivores that feed on other zooplankton, and small particle-feeding taxa), large calanoids (dominated by *Calanus* spp. and *Metridia* spp.), small calanoids (depending on the region, this group can be dominated by species such as *Pseudocalanus* spp., *Acartia* spp., *Temora longicornis*, and *Microcalanus* spp.), cyclopoids (dominated by *Oithona* spp. and *Triconia* spp.; the latter is a poecilostomatoid that is included in this category because of its ecological characteristics), warm-water taxa (*Metridia lucens*, *Centropages* spp., *Paracalanus* spp., and *Clausocalanus* spp.), and cold/arctic species (*Calanus glacialis* and *Metridia longa*). A detailed list of species included in each large copepod index is presented in Appendix 1. Anomalies were computed for these groups (see Scorecard section below) for both high-frequency monitoring sites and GSL subregions. Occasionally, taxonomists cannot distinguish *C. finmarchicus* from *C. glacialis* and so record them in a common category. For this year's report, we used the results of a genetic

study based on prosome length to distinguish these species (Parent et al. 2011). This could have had a minor influence on anomaly patterns discussed in previous reports.

SCORECARDS

Standardized anomalies for the chemical and biological indices presented in scorecards were computed for the high-frequency monitoring sites and oceanographic regions. These anomalies are calculated as the difference between the variable's average for the season or for the complete year and the variable's average for the reference period (usually 1999–2015 unless otherwise noted); this number is then divided by the reference period's standard deviation to compute the normalized anomaly.

Anomalies are presented as scorecards with positive anomalies depicted as shades of red, negatives as blues, and anomalies within 0.5 SD as white (considered as normal conditions). A standard set of indices representing anomalies of nutrient concentrations, phytoplankton biomass and bloom dynamics, and the abundance of dominant mesozooplankton species and groups (*C. finmarchicus, Pseudocalanus* spp., total copepods, and total non-copepods) are produced for each AZMP region. To visualize Northwest Atlantic shelf-scale patterns of environmental variation, a zonal scorecard including observations from all AZMP regions is presented in DFO (2019).

Annual nutrient, phytoplankton, and zooplankton index anomalies are based on the mean annual concentration (mmol m^{-2} for nutrients and mg chl a m^{-2} for phytoplankton biomass) or density (cells L^{-1} for phytoplankton abundance and ind m^{-2} for zooplankton abundance) estimated at each fixed station and each GSL subregion. These annual estimates are the results of general linear models (GLM) of the form

$\text{Log}_{10}(\textit{Density}+1) = \alpha + \beta_{\textit{YEAR}} + \delta_{\textit{MONTH}} + \varepsilon$ for the high-frequency monitoring stations and
$\text{Log}_{10}(\textit{Density}+1) = \alpha + \beta_{\textit{YEAR}} + \delta_{\text{STATION}} + \gamma_{\text{SEASON}} + \varepsilon$ for the subregions,

as in Pepin et al. (2013) and Johnson et al. (2016); α is the intercept, and ε is the error. The GLM is applied to the three subregions separately. For the fixed stations, β and δ are the categorical effects for year and month, respectively. For the subregions, β, δ, *and* γ take into account the effect of year, station, and season, respectively. An estimate of the least-square mean based on type III sums of squares was used as the measure of the overall year effect. Results of the GLM analysis for high-frequency monitoring stations and GSL subregions are shown in Appendices 2–6. We log-transformed concentrations and density values before computing anomalies to compensate for the skewed distribution of the observations. One was added to the *Density* term to include observations with a value of zero. Zooplankton biomass anomalies were also computed using GLM, without log-transformation.

OBSERVATIONS

PHYSICAL ENVIRONMENT

The temperature and salinity of the 2018 water column are described in Galbraith et al. (2019) in detail. Stratification is one of the key parameters controlling primary production. For this reason, we present the upper water column stratification at the high-frequency monitoring stations (Fig. 5). Despite an annual average freshwater discharge into the Estuary that was above normal (Galbraith et al. 2019), stratification was close to normal all year round at both high-frequency monitoring stations and the seasonality of stratification followed the long-term trend.

DEEP OXYGEN

In the GSL, a dissolved oxygen value of 100 µM corresponds to approximately 30% saturation, below which the water is considered to be hypoxic and can reduce the survival of some species such as cod (Plante et al., 1998). The lowest levels of dissolved oxygen (near 15% saturation in recent years) are found in the deep waters at the head of the Laurentian Channel in the Estuary (Fig. 6). Concentrations of dissolved oxygen decreased again in the GSL in 2018 (Fig. 6), reaching time-series record lows in all regions but the Estuary, where the annual average was similar to last year (Fig. 7). The deep waters of the Estuary have consistently been hypoxic since 1984; dissolved oxygen concentration was 54 µM in 2018, corresponding to ca. 18% saturation (Fig. 7). In 2018, the strongest negative anomalies were recorded in central GSL and in the Cabot Strait region (Figs. 6, 7).

NUTRIENTS AND PHYTOPLANKTON

Distributions of the primary dissolved inorganic nutrients (nitrate, silicate, phosphate) included in AZMP's observational program strongly co-vary in space and time (Brickman and Petrie 2003). For this reason and because the availability of nitrogen controls phytoplankton growth in coastal waters of the GSL, emphasis in this document is given to the variability in nitrate concentrations and inventories, even though the distributions of other nutrients are also briefly discussed. In this document, we use the terms "nitrate" or "total nitrate" to refer to nitrate+nitrite (NO_3^-+NO_2^-).

High-frequency monitoring sites

The main highlights of 2018 in terms of nitrate inventories and phytoplankton biomass are illustrated in Figure 8 for both high-frequency monitoring sites. Detailed vertical profiles of nitrate and chl *a* and vertical anomaly patterns are shown in Figures 9 and 10 for Rimouski and Shediac Valley stations, respectively. At the Rimouski station, nitrate inventories were near normal during springtime and decreased to mostly below normal afterwards (Fig. 8a) in association with a sudden and late increase of phytoplankton biomass in late May/early June. Phytoplankton biomass generally remained close to the long-term average for the remainder of the season, except for high biomass peaks in August and again in late September (Fig. 8c). From June to September, there was notable phytoplankton biomass in the upper 40 m (Fig. 9). Overall, annual nitrate averages were below normal in all depth layers while the annual phytoplankton biomass was near normal (Fig. 8e). At Shediac Valley station, sampling was sparse and limited during winter and early spring (Fig. 8b, d), making the description of seasonal patterns difficult. From June until October, the surface nitrate inventory and chl *a* concentration were mostly below normal (Fig. 8b, d).

Phytoplankton abundance at Rimouski station was below normal most of the year, except for the spring and fall blooms (Fig. 11a). The seasonal phytoplankton community composition was similar to the reference period, except for the delay in the increase of diatom abundance during spring (Fig. 11b, c). Only dinoflagellates showed an annual negative anomaly in 2018 that resulted in a positive anomaly of the diatom:dinoflagellate ratio (Fig. 12). These anomalies continued trends observed since 2014, although the positive anomalies of the diatom:dinoflagellate ratio may also be related to the high diatom abundances observed between 2014 and 2016 (Fig. 12). In contrast, the phytoplankton assemblage at Shediac Valley during summer was largely different from the long-term average community composition. The relative abundance of diatoms decreased from about 70% to 20% with a greater proportion of smaller-sized cells (Fig. 13b, c). Annual anomalies were thus negative for diatoms and positive for dinoflagellates and ciliates (Fig. 12). Since 2014, the anomaly pattern at Shediac Valley station has suggested that a change in the size structure of the phytoplankton community might be occurring. However, one must keep in mind that these anomaly patterns are the result of fewer than 10 phytoplankton samples analyzed each year in recent years. In 2018, only four

samples were collected for phytoplankton identification and there was no sampling in April, when the spring diatom bloom usually occurs (Fig. 13a).

Gulf subregions

Overviews of the seasonal distributions of nutrients inventories, phytoplankton biomass, and their anomalies in the GSL are presented in Figures 14 to 20. Time series of regional annual and seasonal anomalies for nutrients and phytoplankton biomass are presented in Figures 21 and 22. The distributions of all nutrients in the surface layer during March 2018 were similar to the reference period (Fig. 14) while their concentrations were below normal, mostly in wGSL and sGSL, in June 2018 (Fig. 15). While not dismissing possible changes in water mass composition over the course of the year, this suggests large nutrient drawdown in these two regions during spring (Fig. 19). Nutrient concentrations in the surface layer were slightly below normal during fall, especially in sGSL and eGSL (Fig. 16). Nutrients in the surface layer showed widespread and generally strong negative anomalies in 2018, a pattern also observed in 2010–2011 (Fig. 21). Interestingly, most of the GSL surface layer showed negative N:P anomalies that were among the strongest of the time series (Figs. 15, 16, 21). The mid-layer nutrient inventory also showed negative anomalies throughout the GSL during summer, except for phosphate, which was close to normal in summer and fall in most of the GSL (Figs. 17, 18). In contrast, at 300 m in recent years, including 2018, there have been strong positive anomalies for nitrate in the eGSL, and for phosphate and silicate in the eGSL and sGSL as well as negative N:P anomalies (Fig. 21). The low surface nutrient inventory during summer was accompanied by low or near-normal phytoplankton biomass, suggesting nutrient limitation, except around the Gaspé Peninsula, where high chl a concentrations were measured (Fig. 20). However, the low nutrient inventory in the surface layer of sGSL and eGSL during fall was likely the result of phytoplankton uptake, as evidenced by the positive anomalies of phytoplankton biomass in these two regions (Fig. 20). Indeed, fall phytoplankton biomass showed a record high in eGSL (Fig. 22). These large spatial patterns were mirrored by local conditions encountered at the high-frequency monitoring stations, with generally low nutrients throughout the year and low/near-normal to high phytoplankton biomass from summer to fall (Fig. 8). The record-high phytoplankton biomass in wGSL during the June sampling was likely because the spring bloom was later than normal, as observed at Rimouski station.

Remote sensing of ocean colour

Satellite imagery suggests that the spring phytoplankton bloom started first in early April in eGSL and later in the wGSL, with the latest peak observed in the Estuary in late May/early June (Figs. 23, 24), matching observations at Rimouski station (Fig. 8). Maximum chl a concentrations in the surface layer during spring averaged ca. 4 mg chl a m^{-3} over the GSL and were close to normal in most areas (Fig. 23). Chl a concentrations during fall were either below or near normal (Figs. 23, 25), contrary to the high phytoplankton biomass measured during the fall AZMP cruise, especially in eGSL. The vertical structure of phytoplankton biomass in the water column cannot explain these diverging patterns considering that most of the biomass was in the upper part of the surface layer (data not shown). However, reduced accuracy of remote sensing during fall due to higher cloud cover might account for some of the discrepancies between satellite and field data.

The start of the spring bloom was early in all statistical boxes, with longer durations in most of them (Fig. 26). This longer duration resulted in an overall high spring bloom magnitude in the NWGSL and Cabot Strait statistical boxes. However, annual anomaly patterns suggest low phytoplankton biomass in the surface layer across the GSL mostly because of strong negative anomalies during summer and fall. Phytoplankton biomass during spring was close to the long-term mean (Fig. 26), which is somewhat in agreement with the suggested large nutrient uptake during spring.

ZOOPLANKTON

High-frequency monitoring sites

In 2018, the zooplankton biomass at Rimouski station followed the long-term seasonal pattern with below-normal values for most of the year (Fig. 27a). At Shediac Valley, however, the few zooplankton biomass data collected were generally close to normal (Fig. 27b). Despite low biomass, total copepod abundance was near normal at Rimouski station during spring and early summer and then well above normal in early fall before decreasing back to near normal in late fall (Fig. 28a). The peak of abundance coincided with a large increase in the proportion of *Acartia* spp., a small calanoid copepod, that was not part of the climatology dominant taxa. The proportion of *Microcalanus* spp., another small calanoid copepod, was also markedly higher in 2018 than during the reference period while the relative abundances of large calanoids (*C. finmarchicus, C. glacialis, C. hyperboreus*) were lower (Fig. 28b, c). Similar findings can be reported for Shediac Valley station with the arrival of *Acartia* spp. among the dominant taxa in 2018 and the decreased relative abundance of large calanoids (Fig. 29b, c).

Calanus finmarchicus and C. hyperboreus abundances in 2018 at Rimouski station were below the long-term seasonal average until mid-summer and became normal thereafter (Fig. 30a, 31a). The relative abundance of each *C. finmarchicus* copepodite stage was similar to the reference period, except for the high contribution of early stages (CI–III) in June and July (Fig. 30b, c). Adult *C. hyperboreus* made up a larger portion of the population during winter and early spring 2018 than during the reference period. Moreover, the stable composition of the population from July onward indicates that most of the new generation went into diapause at stage CIV (Fig. 31b, c). The seasonal abundance and development of *Pseudocalanus* spp. reflected almost perfectly the long-term mean at Rimouski station (Fig. 32 a-c). The few zooplankton samples collected at Shediac Valley station suggest relatively near-normal abundances for these three species (Figs. 30a, 31a, 32a). The main difference with the climatology is the very low abundance of early *C. hyperboreus* copepodite stages in June that may suggest low export from wGSL (Fig. 31e, f). No stage analysis was carried out for *Pseudocalanus* spp. at Shediac Valley station.

Gulf subregions

As observed at the high-frequency sampling stations, the average total zooplankton biomasses during spring and fall 2018 were among the lowest seen over the time series in all regions, especially during fall (Fig. 33). In wGSL, *C. finmarchicus* abundance appears to be somewhat higher compared to the 2015–2017 record low period; however, its abundance was as low as or even lower than in recent years in eGSL and sGSL (Fig. 34). *Calanus hyperboreus* abundances were near the average of the time series in all regions except sGSL during spring, when it was among the lowest values of the time series (Fig. 35). The abundance of the small calanoid *Pseudocalanus* spp. was relatively high during both seasons in wGSL and sGSL; its abundance in wGSL during fall was the second highest of the time series (Fig. 36). This positive anomaly in wGSL was likely caused by a late peak in CI–III stages at the time of sampling (data not shown) that was also observed at Rimouski station in October–November (Fig. 32c). However, *Pseudocalanus* spp. abundance in eGSL was relatively low in spring and the second lowest of the time series during fall (Fig. 36).

Copepod phenology

Changes in the timing of zooplankton development were described using the detailed seasonal pattern of the relative copepodite stage abundances of *C. finmarchicus* at Rimouski station from 1994 to 2018 (Fig. 37). Overall, there is an obvious trend towards earlier population development. Developmental timing in 2018 followed this general trend, with early moulting of

the CV copepodite stage into adult (CVI) in May. However, the maximum peak of CI–III was reached in July, which is similar to observations made at the beginning of the time series (Fig. 37).

Scorecards

The time series of annual zooplankton biomass anomalies highlights recent major changes in the community, with mostly negative anomalies across the GSL since 2010 (Fig. 38). In 2018, although the negative anomalies were not as strong as the record 2017 values, zooplankton biomass was still lower than normal everywhere in the GSL except at Shediac Valley (Fig. 38) (N.B.: n = 6 in 2018 for Shediac Valley). A synthesis of standard AZMP zooplankton indices (abundance of *C. finmarchicus*, *Pseudocalanus* spp., total copepods, non-copepods) was performed using annual standardized abundance anomalies and is presented as a scorecard (Fig. 39). The near-normal to below-normal anomalies for *C. finmarchicus* in 2018 in almost all GSL subregions were a continuation of the pattern initiated in 2010. Positive *Pseudocalanus* spp. anomalies appeared approximately during the same period, and anomalies in 2018 followed the same trend in most regions. Total copepod abundances only showed positive anomalies at both high-frequency monitoring stations, with a small negative anomaly in eGSL. Non-copepod abundance has also been increasing since 2010 and this index showed small positive anomalies in most regions in 2018 (Fig. 39).

The annual standardized abundance anomalies for six additional zooplankton indices (*C. hyperboreus* and five zooplankton groups: small calanoids, large calanoids, cyclopoids, warm-water species, and cold/arctic species) are presented in Figure 40. A detailed list of species included in each of these indices is presented in Appendix 1. *Calanus hyperboreus* abundance was above normal in eGSL and at Shediac Valley station in 2018; such positive anomalies have been less frequent in these areas since 2010. Overall since 2009, there has been a decline in large calanoid abundance and an increase in small calanoid abundance (Fig. 40). Positive anomalies for small calanoids were again observed in 2018 in all regions except eGSL, probably explaining the negative anomaly of total copepods in this region, while large calanoid anomalies were negative in most regions. A positive anomaly was observed for warm-water-associated copepods, with a near-normal anomaly of this group only occurring in the eGSL. In this region, a positive anomaly of cold-water-associated copepods has also been observed in most years—including 2018—since 2007. These annual anomalies were relatively coherent among the high-frequency sampling sites (Rimouski and Shediac Valley stations) and their associated GSL subregions (Figs. 39, 40).

DISCUSSION

ENVIRONMENTAL CONDITIONS

The timing of the onset and extent of water column stratification plays a role in defining spring bloom phenology, phytoplankton production, species succession, and trophic interactions over the complete growth season (Levasseur et al. 1984). In 2018, the timing and extent of upper water column stratification were very similar to the long-term averages. In addition to the effect of water column stratification on phytoplankton dynamics, thermal properties of the surface, intermediate (Cold Intermediate Layer [CIL], 30–125 m), and deep-water masses play a role in defining zooplankton dynamics (Plourde et al. 2002). Galbraith et al. (2019) reported on the physical conditions that prevailed in the GSL during 2018, and this document reports on the chemical and biological conditions in the GSL in the context of these conditions.

Changes in dissolved oxygen of the deep waters entering the GSL at the continental shelf are related to the varying proportions of Labrador Current water (cold/fresh, high dissolved oxygen levels) and slope water (warm/salty, low dissolved oxygen levels), which together are the source

of GSL deep water (McLellan 1957, Lauzier and Trites 1958, Gilbert et al. 2005). These waters travel from the mouth of the Laurentian Channel to the Estuary in roughly three to four years (Gilbert 2004), decreasing in dissolved oxygen as a result of *in situ* respiration and oxidation of organic material as they progress to the channel heads. Based on interdecadal variability, the inflow of warmer waters to the Estuary is expected to exacerbate the hypoxic conditions since these waters are typically poorer in dissolved oxygen (McLellan 1957, Lauzier and Trites 1958, Gilbert et al. 2005). In the St. Lawrence Estuary, temperature is well correlated with oxygen concentration over the time series (R^2 = 0.86). At 300 m in the Estuary, there has been an increase of 1.37°C from the early 1970s until 2018 (Galbraith et al. 2019). Considering the relationship of oxygen solubility with temperature, this should translate into a decrease in dissolved oxygen of 10.35 µM over the same timeframe, but the decrease has exceeded 100 µM. Moreover, given the inherent properties of GSL source waters (North Atlantic Central Water vs Labrador Current Water; Gilbert et al. 2005), changes in their mixing ratio at Cabot Strait imply that a decrease of 1.46 µM might be expected for each 0.1°C temperature increase. However, dissolved oxygen at 300 m decreased by ca. 65 µM at Cabot Strait over the time series for a 1.6°C increase (Galbraith et al. 2019). Thus, warming of bottom water and changes in the mixing ratio of source waters are not the only factors contributing to the decrease in oxygen concentrations in the GSL. Other factors that can cause variability in oxygen concentration include interannual changes in the vertical flux of organic matter to the bottom waters of the Lower St. Lawrence Estuary.

Winter mixing is a critical process for bringing nutrient-rich deep water to the surface. In the GSL, this winter convection is partly caused by buoyancy loss attributable to cooling and reduced freshwater runoff, brine rejection associated with sea-ice formation, and wind-driven mixing prior to ice formation (Galbraith 2006). Warmer than normal surface waters throughout the winter and minimal sea-ice formation imply low winter convection and may reduce the amount of nutrients available for spring production. The CIL is the winter surface mixed layer that has been insulated from the atmosphere by near-surface stratification and whose nutrient inventory will supply primary producers during the growth season through vertical mixing. In 2018, CIL-related indices suggest that winter convection was near normal but that nutrient content of the mid-layer was relatively low. This might have limited nutrient exchange between the CIL and the surface layer even though stratification was likely not strong enough to alter the regular nutrient fluxes between these layers (Galbraith et al. 2019). Negative nitrate anomalies in the surface layer have been regularly encountered in the GSL since 2010, a period over which several temperature and ice-cover indices have shown clear warming of the GSL (Galbraith et al. 2019). The sum of regional annual anomalies suggests a significant nitrate decrease of about 3 mmol m^{-2} yr^{-1} in the surface layer over the time series. Riverine nutrient input to the GSL might be another factor to consider that could improve our understanding of nutrient dynamics and interannual variability, at least in areas of significant freshwater inputs.

Positive anomalies in deep-water (300 m) nutrients have been observed since 2012 in eGSL in association with high temperature and salinity intrusions into the GSL from Cabot Strait (Galbraith et al. 2019). These higher-than-average deep inventories may be associated with a combination of a thermocline that is shallower and reduces the exchanges between the upper and bottom layers, and a water mass composition that has a greater contribution of slope water than Labrador Shelf water (Galbraith et al. 2019 and references therein). In contrast, negative deep-water nutrient anomalies were observed at Rimouski station for a third consecutive year, and possibly elsewhere in the Estuary. These could be the result of changes in the in the nitrogen cycle microbial activity, such as decreased nitrification associated with low oxygen concentrations. Routine measurement of NH_4 concentrations has recently been added to AZMP sampling in the GSL and will eventually be helpful in verifying this latter hypothesis. Moreover, modeling of processes involved in the nitrogen cycle in the GSL is ongoing (Diane Lavoie, IML) and will allow an understanding of key processes involved in nitrate distribution.

The N:P ratio is another index that requires further attention since variability in the stoichiometry of nutrient supply is a key determinant of oceanic nutrient limitation. Thus, changes in the CIL N:P ratio over time may be a better predictor of changes in the phytoplankton community and productivity than nitrate concentrations themselves. For example, if the widespread negative anomalies in the N:P ratio in 2018 were to persist through time in the GSL, they might entail a change in the productivity of this region.

PHYTOPLANKTON

Except at Rimouski station, where sampling regularly covers the spring bloom period, phytoplankton productivity during the spring bloom must be inferred either from indirect indices, such as the difference in the nutrient inventory of the surface mixed layer between the winter and the summer cruises, or from satellite observations. Interestingly, the nutrient drawdown associated with spring productivity was above normal in 2018 in all regions. The early and long-lasting spring bloom might have entailed increased nutrient consumption in most regions. Overall, field samples suggest high annual phytoplankton biomass, mostly associated with the strongly positive fall anomalies. These annual positive chl a anomalies have been regularly observed since 2013 in sGSL and eGSL, even though this increase is not significant, it may suggest that either environmental conditions are good for the growth of phytoplankton cells, or that reduced grazing pressure favours the accumulation of phytoplankton cells. Recent observations at Shediac Valley have indicated a possible phytoplankton community shift towards smaller-sized cells, which are known to perform better in nutrient-poor and stratified waters (Levasseur et al. 1984, Li and Harrison 2008). If occurring elsewhere in the GSL, the high biomass/cell size ratio suggest that changes in both grazing pressure and grazer community composition are more likely to explain these high chl a concentrations rather than ideal growth conditions. The AZMP program has not regularly documented the taxonomic composition of the phytoplankton community elsewhere in the GSL, and we must be cautious when generalizing these results to other GSL subregions. Moreover, it must be remembered that the effect of survey timing on the annual average cannot be ignored despite the use of a GLM that reduces this bias. High annual chl a concentrations may well be explained by earlier sampling during fall in recent years.

In contrast with field data, ocean colour observations suggested low phytoplankton biomass in the surface layer, especially during summer and fall. Such negative anomalies have been encountered since the use of the VIIRS satellite in 2012 and suggest a decrease of 10 to 20% of surface chl a since 2012, depending on the subregion. It is possible that the VIIRS satellite performs better in coastal waters in terms of minimizing the overestimation of chl a concentration in turbid waters compared to previous satellites. If so, this could partly explain why most satellite-derived biomass anomalies have been negative since data from this satellite have been used. Improved algorithms for the retrieval of chl a in the Gulf of St. Lawrence from the SeaWIFS satellite have recently been published (Laliberté et al. 2018) and should eventually be applied to our statistical boxes; which could modify the time series anomaly pattern. However, as far as the spring bloom metrics are concerned, the change of satellite platforms over the time series does not seem to lead to any questionable trends over time. There are no apparent trends over the time series for any of these indices, except perhaps for the timing of the spring bloom. Indeed, it seems that the strength of these anomalies has increased since 2010, suggesting that the timing of the bloom start has become much more variable in the last decade. The years 2010 and 2016–2018 show the strongest anomalies of the times series, with early bloom timing. These changes could be associated with the combined effects of warming on the onset of stratification and the reduced densities of overwintering copepods (low annual biomass) during these years (Sommer and Lengfellner 2008).

ZOOPLANKTON

Life cycle strategies vary among large copepod species, and the timing of reproduction relative to the freshet—considering its influence on water-mass circulation and transport—could explain dissimilarities in the distribution patterns of these species (Runge et al. 1999), e.g., the negative anomaly of *C. finmarchicus* versus the positive anomaly of *C. hyperboreus* in eGSL. eGSL is less influenced by freshwater than wGSL and sGSL; environmental conditions modifying the zooplankton community there might instead include the volume and temperature of cold and saline Labrador Shelf water that flows into eGSL through the Strait of Belle Isle, which have both shown negative anomalies in recent years (Colbourne et al. 2017; Galbraith et al. 2019). The differences in these environmental drivers might explain why eGSL often shows distinct anomaly patterns for the zooplankton assemblage. In 2018, eGSL was the only region that did not show a positive anomaly for *Pseudocalanus* spp., small calanoids, non-copepods, and warm-water-associated copepods whereas all these indices have shown positive trends in all regions since about 2010.

Among the most striking features in 2018 was the very low zooplankton biomass for a fourth consecutive year throughout the GSL. Depending on the subregion, the 2018 dry weight represented a decrease of approximately 15 to 40% relative to the long-term average. Lower biomass is associated with the decrease in large-sized zooplankton species abundance. The mean weight of large-sized calanoids (e.g., *C. hyperboreus*: 4 mg per adult female) is between one and two orders of magnitude higher than that of small-sized calanoids (e.g., *Pseudocalanus* spp.: 0.02 mg per adult female) (Conover and Huntley 1991). Thus, the decrease in large calanoid abundance have a greater impact on zooplankton biomass than, for instance, the increase of *Pseudocalanus* spp. abundance that was recorded in most GSL subregions in 2018. The increase in small calanoid abundance was mostly attributable to *Pseudocalanus* spp. in all regions, but also to *Temora* spp. and *Microcalanus* spp. in sGSL and wGSL, respectively. This increase also seems to be coupled with the increase in non-copepod abundance, mostly larvae of benthic organisms. Suitability of environmental conditions, competition for food and/or differential predation pressure might favor the dominance of either one of these communities, i.e., one dominated by large calanoids versus one dominated by a combination of small calanoids and non-copepod (Hall et al. 1976, Daewel et al. 2014), with potential implications for the pelagic food web and pelago–benthic coupling.

A question that may arise from these clear changes in zooplankton community composition and size-structure concerns the underlying explanatory drivers and the predicted future trends. Whereas the role of predation and of changing predator stocks in the observed trends has yet to be determined, it is possible to get a few insights regarding the effect of environmental variables using a simple correlation matrix (Fig. 41). Some obvious linkages between the community and the environmental conditions, such as the role played by temperature on the abundance of cold or warm-water-associated copepods have not been illustrated in this figure. Even though the correlations are generally not significant, temperature seems to act as an important driver in defining the zooplankton community, with cold conditions in the mid and deep layers being ideal for large calanoids and consequently high biomass, and warm conditions favouring small calanoids and non-copepods. Moreover, the magnitude of the spring bloom, which is dependent upon spring bloom amplitude and duration, is significantly correlated with the abundance of large calanoids over the time series. These environmental factors might also trigger changes in the developmental timing of zooplankton taxa, such as the earlier development of *C. finmarchicus* at Rimouski station in recent years. A regional correlation matrix could highlight some of these linkages or reveal new ones. Overall, zooplankton communities in the GSL seem to be shaped by a combination of changing water-mass properties and of bottom-up and top-down controls, although the relative importance of these processes is not yet well understood.

SUMMARY

This document reports on the chemical and biological (plankton) conditions in the GSL in 2018 in the context of a strong warming event initiated in 2010. Data from 2018 are compared to time-series observations.

- Concentrations of dissolved oxygen at 300 m reached record lows in 2018 in almost all GSL regions.
- Surface nitrate inventories (0–50 m) were below the long-term average most of the year in all GSL subregions. Positive deep-water (300 m) nutrient anomalies have been observed since 2012 in eGSL and are associated with intrusions of high temperature/high salinity water into the GSL through Cabot Strait.
- In situ nutrients and chl *a* data suggest high phytoplankton biomass during spring and fall 2018, while ocean colour data suggest near-normal and below-normal phytoplankton biomass in the surface layer during spring and fall, respectively.
- According to satellite imagery, the start of the bloom was earlier in all regions in 2018, although field measurements at Rimouski station indicated that the spring bloom was delayed. Satellite imagery showed the that duration and magnitude of the spring bloom were generally above normal in the GSL except for NEGSL satellite subregion.
- The phytoplankton community was similar to the long-term average community at Rimouski station, except for the decline of dinoflagellate abundance since 2014. At Shediac Valley, the few samples collected suggest a decrease in the abundance of diatoms concomitant with an increase of small-sized cells, also since 2014.
- Zooplankton biomass was below normal in 2018 everywhere in the GSL, because of low *C. hyperboreus* abundance at Rimouski station and low *C. finmarchicus* abundance in eGSL and sGSL.
- The 2018 abundances of small calanoids, non-copepods, and warm-water-associated copepods were once again higher than the long-term mean in all GSL subregions except eGSL, where they were near normal. These trends have generally been observed since 2010. It is also worth noting that the abundance of cold-water-associated copepods was above normal in eGSL for the fourth consecutive year.
- Despite the on-time emergence from diapause for *C. finmarchicus* at Rimouski station, early copepodite stages (CI–III) were only observed starting in late May and their abundance peaked in July; which is late compared to observations from recent years. There was only one CI–III cohort in 2018.

ACKNOWLEDGEMENTS

We thank Jean-Yves Couture, Marie-France Beaulieu, Caroline Lebel, Isabelle St-Pierre, and Caroline Lafleur for preparation and standardization of the phytoplankton and zooplankton data. The data used in this report would not be available without the work of François Villeneuve and his AZMP team (Rémi Desmarais, Marie-Lyne Dubé, Yves Gagnon, Line McLaughlin, Roger Pigeon, Michel Rousseau, Félix St-Pierre, Liliane St-Amand, Sonia Michaud, David Leblanc, and Caroline Lafleur) in organizing and carrying out AZMP surveys and analyzing samples. We thank Jeff Spry and Kevin Pauley for providing data from the Shediac Valley station and BIO's remote sensing unit for the composite satellite images. We are grateful to Erica Head, Gary Maillet and David Bélanger for their critical reviews.

REFERENCES

Arun Kumar, S.V.V., Babu, K.N., and Shukla, A.K. 2015. Comparative analysis of chlorophyll-a distribution from SeaWiFS, MODIS-Aqua, MODIS-Terra and MERIS in the Arabian Sea. Mar. Geod. 38: 40–57.

Barnes, B., and Hu, C. 2016. Dependence of satellite ocean color data products on viewing angles: A comparison between SeaWiFS, MODIS, and VIIRS. Remote Sens. Environ. 175: 120–129.

Brickman, D., and Petrie, B. 2003. Nitrate, silicate and phosphate atlas for the Gulf of St. Lawrence. Can. Tech. Rep. Hydrogr. Ocean Sci. 231: xi + 152 pp.

Colbourne, E., Holden, J., Snook, S., Han, G., Lewis, S., Senciall, D., Bailey, W., Higdon, J., and Chen, N. 2017. Physical oceanographic conditions on the Newfoundland and Labrador Shelf during 2016 - Erratum. DFO Can. Sci. Advis. Sec. Res. Doc. 2017/079. v + 50 p.

Conover, R. J., and Huntley, M. 1991. Copepods in ice-covered seas - Distribution, adaptations to seasonally limited food, metabolism, growth patterns and life cycle strategies in polar seas. J. Mar. Syst. 2: 1–41.

Daewel, U., Hjøllo, S.S., Huret, M., Ji, R., Maar, M., Niiranen, S., Travers-Trolet, M., Peck, M.A., and van de Wolfshaar, K. E. 2014. Predation control of zooplankton dynamics: a review of observations and models. ICES J. Mar. Sci. 71(2): 254–271.

DFO. 2019. Oceanographic conditions in the Atlantic zone in 2018. DFO Can. Sci. Advis. Sec. Sci. Advis. Rep. 2019/034.

Galbraith, P. S. 2006. Winter water masses in the Gulf of St. Lawrence. J. Geophys. Res. 111, C06022, doi: 10.1029/2005JC003159.

Galbraith, P. S., Desmarais, R., Pigeon, R., and Cantin, S. 2006. Ten years of monitoring winter water masses in the Gulf of St. Lawrence by helicopter. AZMP Bulletin PMZA 5: 32–35.

Galbraith, P.S., Chassé, J., Caverhill, C., Nicot, P., Gilbert, D., Lefaivre, D. and Lafleur, C. 2019. Physical Oceanographic Conditions in the Gulf of St. Lawrence during 2018. DFO Can. Sci. Advis. Sec. Res. Doc. 2019/046. v + 79 p.

Gilbert, D. 2004. Propagation of temperature signals from the northwest Atlantic continental shelf edge into the Laurentian Channel. ICES CM, 2004/N: 7, 12 pp.

Gilbert, D., Sundby, B., Gobeil, C., Mucci, A., and Tremblay, G.-H. 2005. A seventy-two-year record of diminishing deep-water oxygen in the St. Lawrence estuary: The Northwest Atlantic connection. Limnol. Oceanogr., 50(5): 1654–1666.

Gregg, W. W., and Rousseaux, C. S. 2014. Decadal trends in global pelagic ocean chlorophyll: A new assessment integrating multiple satellites, in situ data, and models. J. Geophys. Res. Oceans, 119: 5921–5933, doi 10.1002/2014JC010158.

Hall, D.J., Threlkeld, S.T., Burns, C.W., and Crowley, P.H. 1976. The size-efficiency hypothesis and the size structure of zooplankton communities. Annu. Rev. Ecol. Evol. Syst. 7: 177–208.

Johnson, C., Casault, B., Head, E., and Spry, J. 2016. Optical, chemical, and biological oceanographic conditions on the Scotian Shelf and in the Eastern Gulf of Maine in 2014. DFO Can. Sci. Advis. Sec. Res. Doc. 2016/003. v + 51 p.

Laliberté, J., Larouche, P., Devred, E., and Craig, S. 2018. Chlorophyll-a concentration retrieval in the optically complex waters of the St. Lawrence Estuary and Gulf using principal component analysis. Remote Sens. 10, 265, doi: 10.3390/rs10020265.

Lauzier, L.M., and Trites, R.W. 1958. The deep waters of the Laurentian Channel. J. Fish. Res. Board Can. 15: 1247–1257.

Levasseur, M., Therriault, J.-C., and Legendre, L. 1984. Hierarchical control of phytoplankton succession by physical factors. Mar. Ecol. Prog. Ser. 19: 211–222.

Li, W. K. W., and Harrison, W. G. 2008. Propagation of an atmospheric climate signal to phytoplankton in a small marine basin. Limnol. Oceanogr. 53(5): 1734–1745.

McLellan, H.J. 1957. On the distinctness and origin of the slope water off the Scotian Shelf and its easterly flow south of the Grand Banks. J. Fish. Res. Board Can. 14: 213–239.

Mitchell, M. R., Harrison, G., Pauley, K., Gagné, A., Maillet, G., and Strain, P. 2002. Atlantic Zonal Monitoring Program sampling protocol. Can. Tech. Rep. Hydrogr. Ocean Sci. 223: iv + 23 pp.

Parent, G.J., Plourde, S., and Turgeon, J. 2011. Overlapping size ranges of *Calanus* spp. off the Canadian Arctic and Atlantic Coasts: impact on species' abundances. J. Plankton Res. 33: 1654–1665.

Pepin, P., Maillet, G., Fraser, S., Shears, T., and Redmond, G. 2013. Optical, chemical, and biological oceanographic conditions on the Newfoundland and Labrador Shelf during 2011-12. DFO Can. Sci. Advis. Sec. Res. Doc. 2013/051. v + 38 p.

Plante, S., Chabot, D., and Dutil, J.-D. 1998. Hypoxia tolerance in Atlantic cod. J. Fish Biol. 53: 1342–1356.

Plourde, S., Dodson, J. J., Runge, J. A., and Therriault, J.-C. 2002. Spatial and temporal variations in copepod community structure in the lower St. Lawrence Estuary, Canada. Mar. Ecol. Prog. Ser. 230: 221–224.

Plourde, S., Maps, F., and Joly, P. 2009. Mortality and survival in early stages control recruitment in *Calanus finmarchicus*. J. Plankton Res. 31(4): 371–388.

Runge, J. A., Castonguay, M., de Lafontaine, Y., Ringuette, M., and Beaulieu, J. L. 1999. Covariation of climate, zooplankton biomass and mackerel recruitment in the southern Gulf of St. Lawrence. Fish. Oceanogr. 8(2): 139–149.

Sommer, U., and Lengfellner, K. 2008. Climate change and the timing, magnitude, and composition of the phytoplankton spring bloom. Global Change Biol. 14: 1199–1208.

Therriault, J.-C., Petrie, B., Pépin, P., Gagnon, J., Gregory, D., Helbig, J., Herman, A., Lefaivre, D., Mitchell, M., Pelchat, B., Runge, J., and Sameoto, D. 1998. Proposal for a Northwest Atlantic zonal monitoring program. Can. Tech. Rep. Hydrogr. Ocean Sci. 194: vii + 57 pp.

Wang, M., Liu, X., Tan, L., Jiang, L., Son, S. H., Shi, W., Rausch, K., and Voss, K. 2013. Impacts of VIIRS SDR performance on ocean color products. J. Geophys. Res. Atmos. 118: 10,347–10,360, doi:10.1002/jgrd.50793.

Zhai, L., Platt, T., Tang, C., Sathyendranath, S., and Hernández Walls, R. 2011. Phytoplankton phenology on the Scotian Shelf. ICES J. Mar. Sci. 68: 781–791, doi:10.1093/icesjms/fsq175.

Zibordi, G., Mélin, F., and Berthon, J.-F. 2006. Comparison of SeaWiFS, MODIS and MERIS radiometric products at a coastal site. Geophys. Res. Letters 33: L06617, doi:10.1029/2006GL0257.

TABLES

Table 1. List of AZMP surveys with locations, dates, and sampling activities for 2018. wGSL, eGSL, and sGSL denote the western, eastern, and southern subregions of the Gulf of St. Lawrence. See Figure 1 for station locations.

	Name	Location	Dates (2018)	Vessel	CTD/bottle	Net
Fixed	Rimouski	48º40.0'N 068º35.0'W	26 Feb – 6 Dec	Beluga II (+ others)	34	32
	Shediac Valley	47º46.8'N 064º01.8'W	3 Mar – 23 Oct	Multiple	8	6
Winter Survey	-	Estuary and Gulf	26 Feb – 13 March	GC-945 Helicopter	104	0
Summer Survey	TESL	wGSL	3 – 27 Jun	Coriolis II	7	7
	TSI	wGSL	3 – 27 Jun	Coriolis II	6	6
	TASO	wGSL	3 – 27 Jun	Coriolis II	5	5
	TIDM	sGSL	3 – 27 Jun	Coriolis II	10	10
	TDC	eGSL	3 – 27 Jun	Coriolis II	6	6
	TCEN	eGSL	3 – 27 Jun	Coriolis II	5	5
	TBB	eGSL	3 – 27 Jun	Coriolis II	7	7
	Supplementary stations		3 – 27 Jun	Coriolis II	23	0
Total					**69**	**46**
Fall Survey	TESL	wGSL	22 Oct – 3 Nov	Hudson	7	7
	TSI	wGSL	22 Oct – 3 Nov	Hudson	6	6
	TASO	wGSL	22 Oct – 3 Nov	Hudson	5	5
	TIDM	sGSL	22 Oct – 3 Nov	Hudson	10	9
	TDC	eGSL	22 Oct – 3 Nov	Hudson	6	6
	TCEN	eGSL	22 Oct – 3 Nov	Hudson	5	3
	TBB	eGSL	22 Oct – 3 Nov	Hudson	7	5
	Supplementary stations		22 Oct – 3 Nov	Hudson	7	0
Total					**53**	**41**

FIGURES

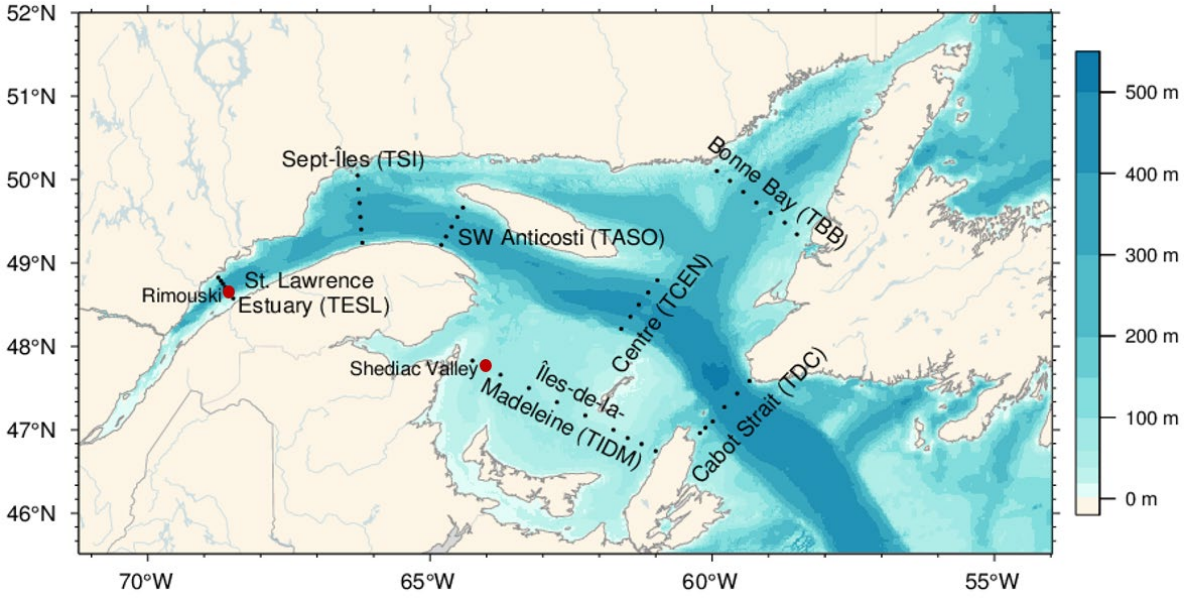

Figure 1. Bathymetric map of the Estuary and Gulf of St. Lawrence showing regular AZMP sampling stations on the different sections (dots) and at Rimouski and Shediac Valley stations (red circles).

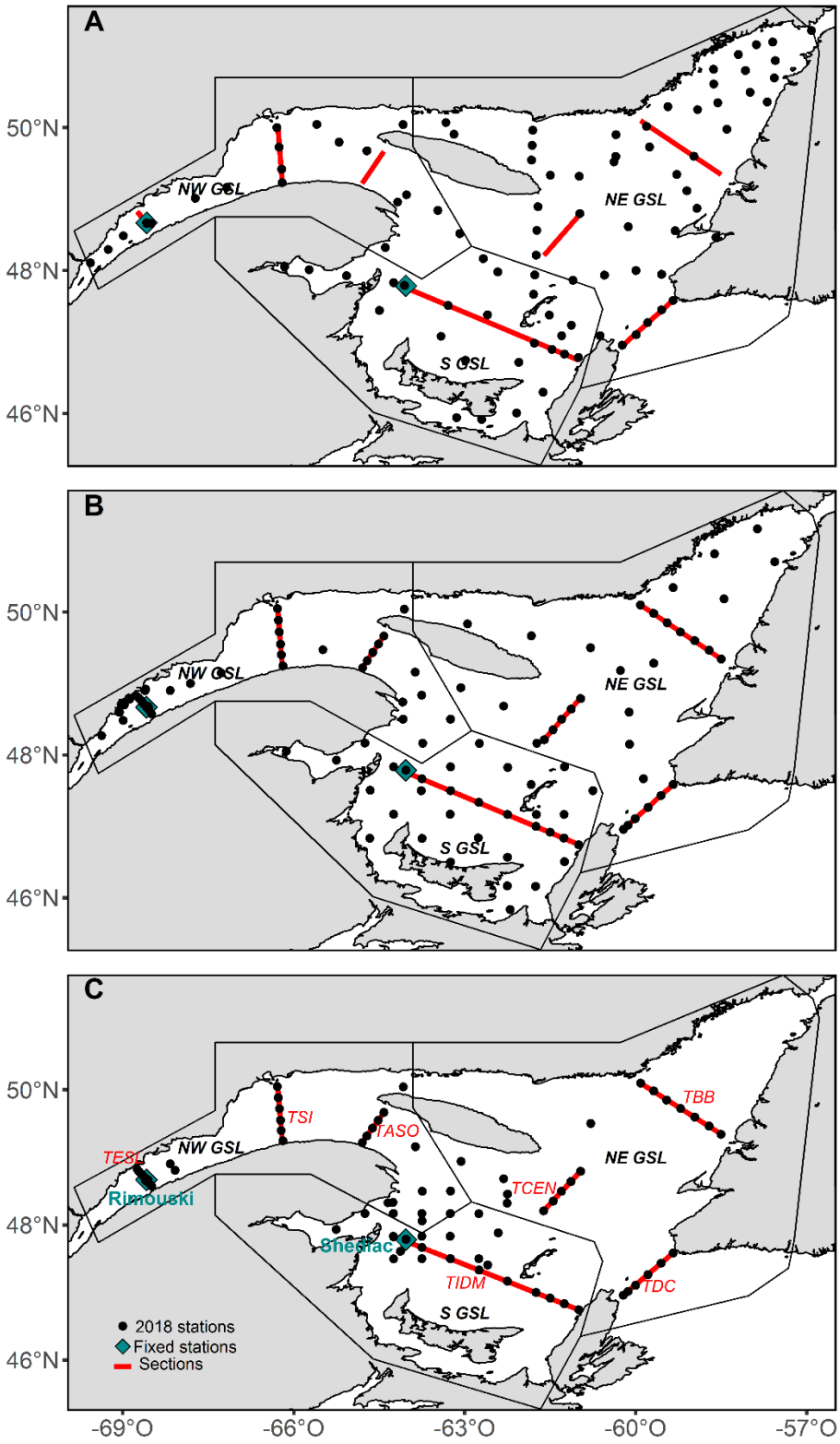

Figure 2. Locations of stations sampled during winter (A), summer (B), and fall (C) 2018. Sections are grouped to form subregions within the western GSL (TESL, TSI, TASO), southern GSL (TIDM), and eastern GSL (TBB, TCEN, TDC).

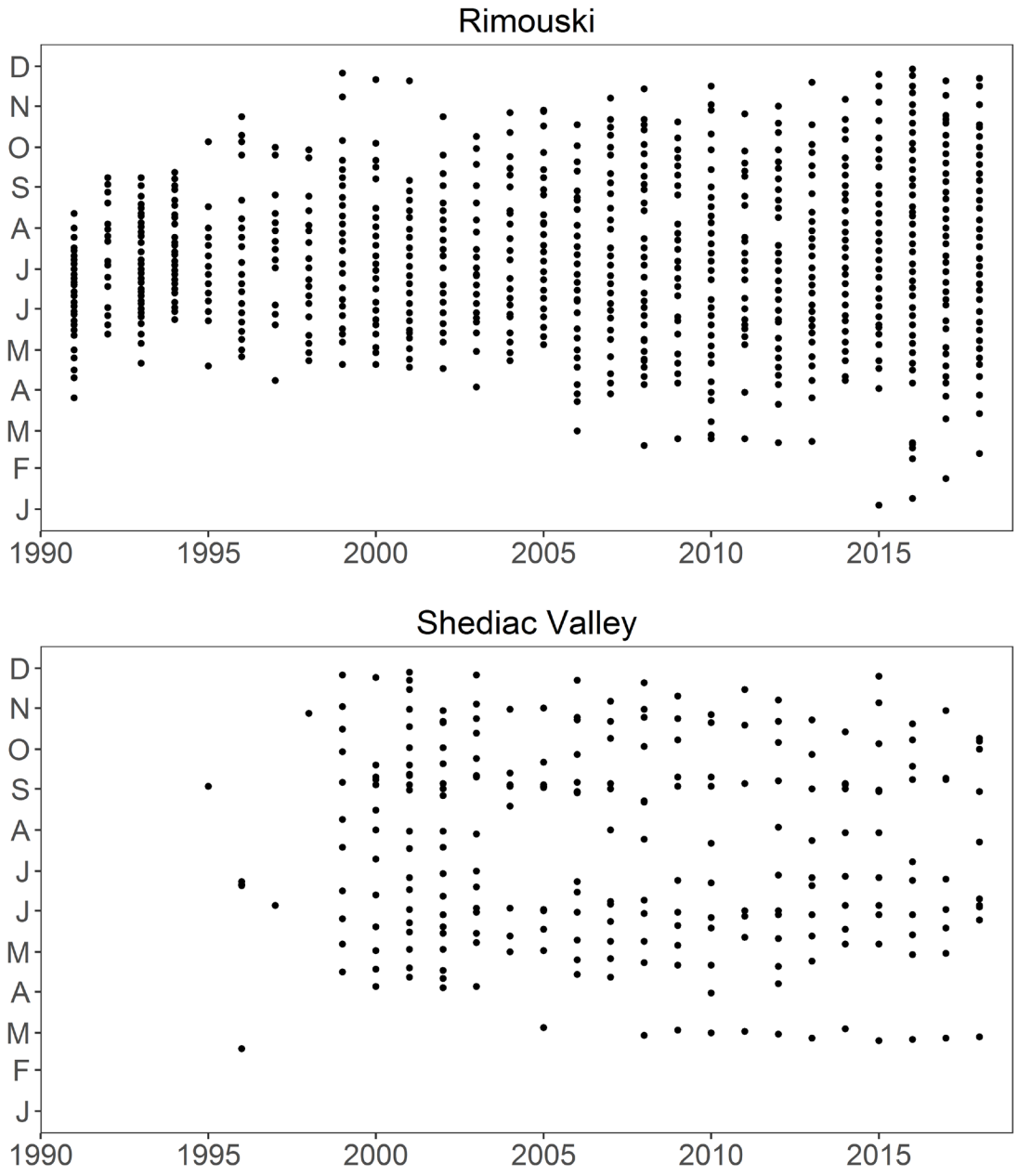

Figure 3. Sampling frequencies at Rimouski and Shediac Valley stations through 2018. Sampling included CTD/bottle as well as plankton net tows most of the time (weather permitting).

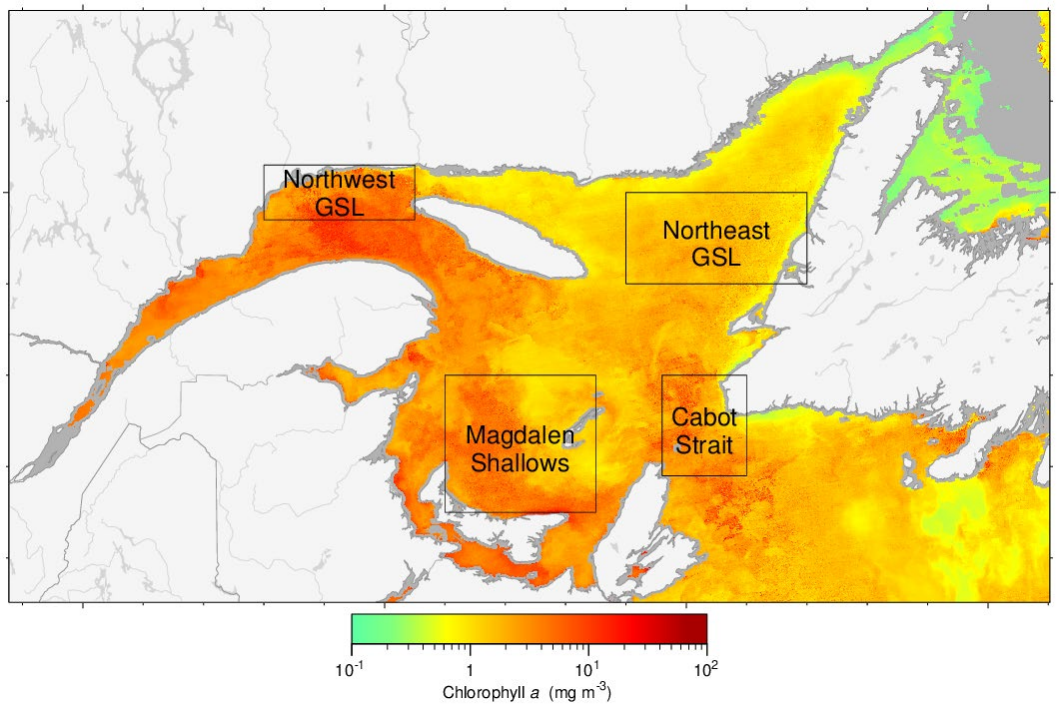

Figure 4. Statistical boxes in the GSL identified for the spatial/temporal analysis of satellite ocean colour data. The figure is a VIIRS composite image showing chlorophyll a from 16–30 April 2018. Grey areas indicate no data (in this case near-shore regions).

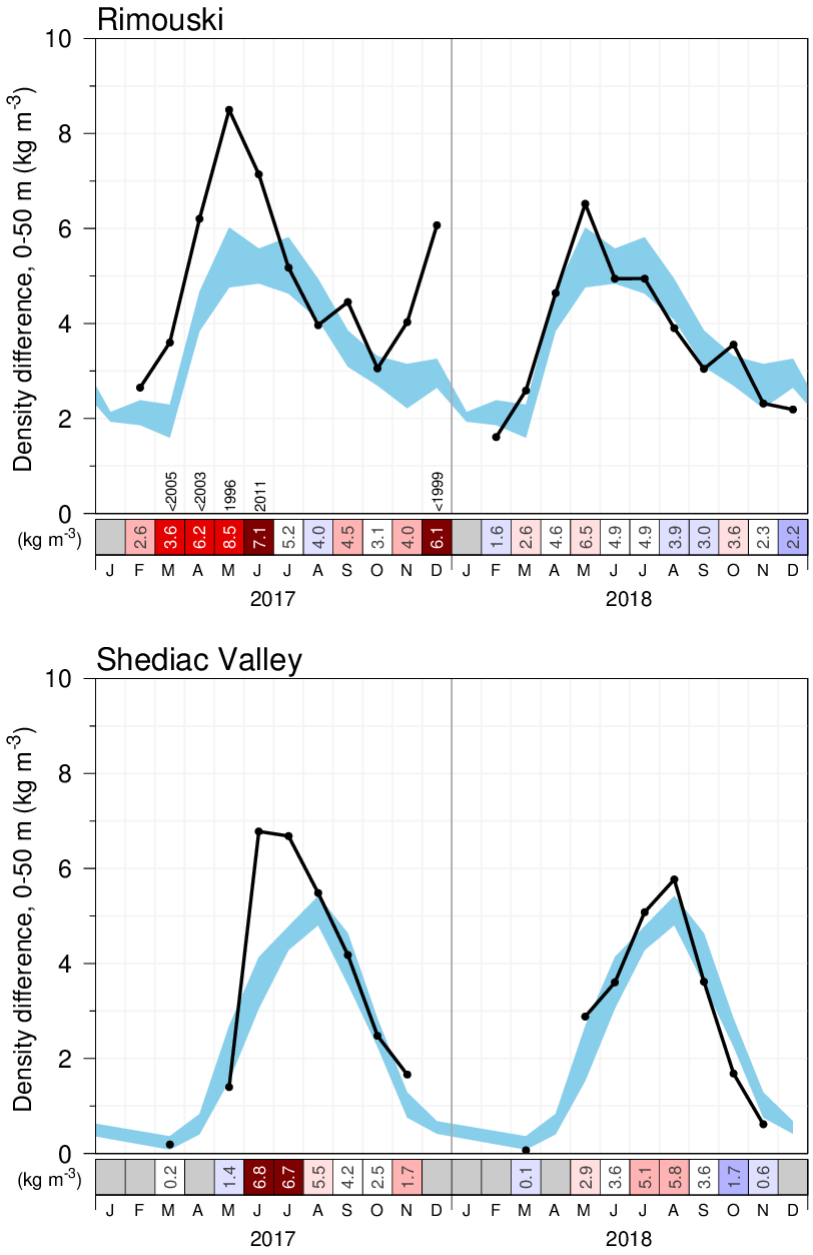

Figure 5. Seasonal stratification index (calculated as the density difference between 50 m and the surface) during 2017 and 2018 at Rimouski station (upper panel) and at Shediac Valley station (lower panel). The blue area represents the climatological monthly mean ± 0.5 SD (1991–2010 for Rimouski and 1981–2018 for Shediac Valley). The positive anomalies are shown in red and correspond to low salinity and strong stratification. Numbers in the scorecard are the monthly density differences in kg m^{-3}. For anomalies greater than 2 SD, the prior year with a greater anomaly is indicated.

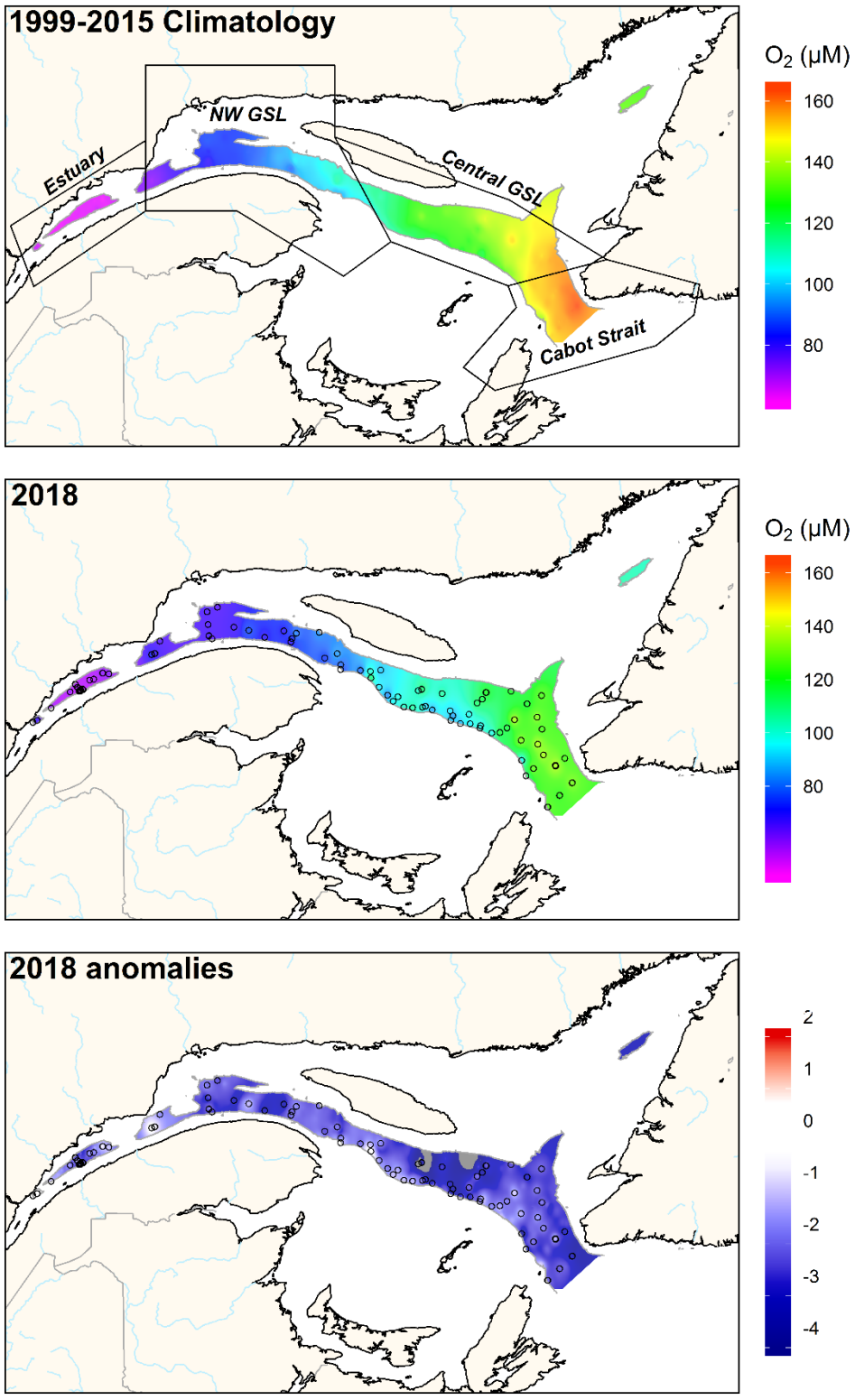

Figure 6. Annual average distribution of dissolved oxygen saturation at a depth of 300 m in the Estuary and Gulf of St. Lawrence during 2018 (upper panel). The climatology (1999–2015; middle panel) and anomalies (lower panel) are also shown. Blue colours indicate anomalies below the mean and reds are anomalies above the mean, and white represents normal conditions. Polygons in the upper panel are used to calculate regional anomalies. Open circles represent station locations in 2018.

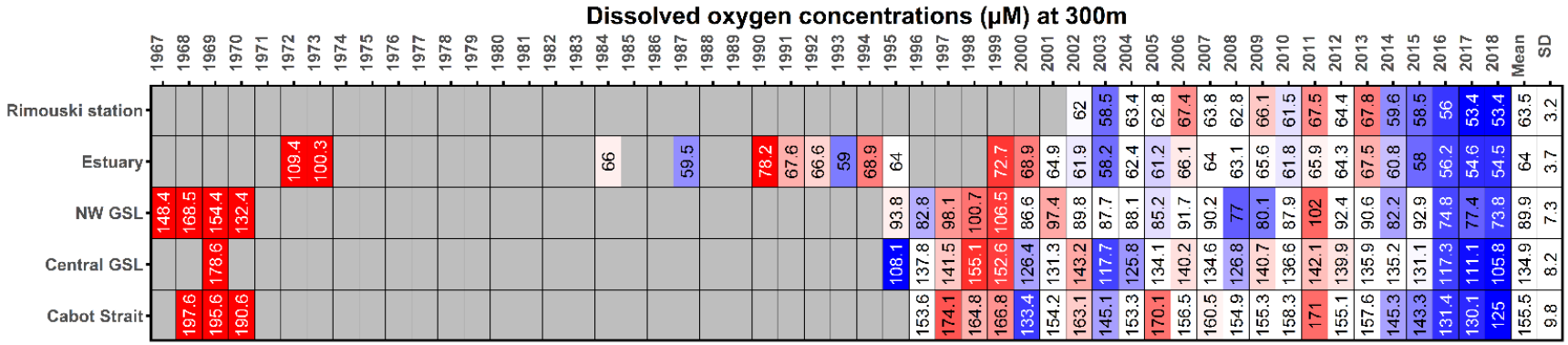

Figure 7. Time series of deep-layer dissolved oxygen concentration (µM). This figure uses the subregions presented in Figure 6. The oxygen time series presented in Gilbert et al. (2005) for the Estuary is included in our Estuary dataset. The numbers on the right are the 1999–2015 climatological means and standard deviations, and the numbers in the boxes are the oxygen concentrations. Cell colour represents the anomaly: blue colours indicate anomalies below the mean and reds are anomalies above the mean, and white represents normal conditions.

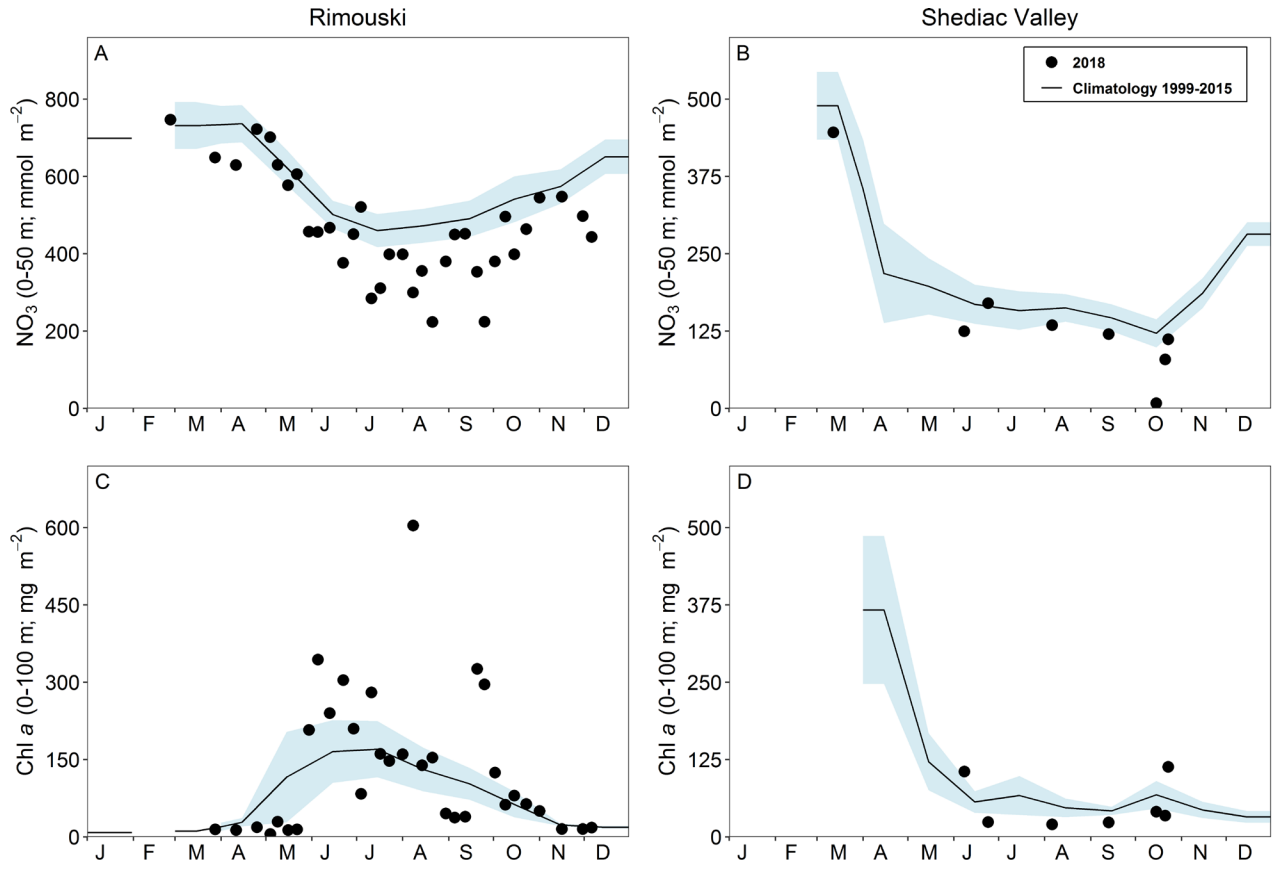

Rimouski

	1999	2000	2001	2002	2003	2004	2005	2006	2007	2008	2009	2010	2011	2012	2013	2014	2015	2016	2017	2018	Mean	SD
Chl *a* 0-100m	2.25	-0.65	0.72	-0.13	0.76	-1.37	-0.89	-0.82	0.62	-1.93	-0.17	0.01	0.02	0.47	-0.37	1.24	0.25	0.64	-0.32	0.47	35.5	19.7
NO_3 0-50m	-0.32	0.91	0.34	1.67	-0.46	1.22	-0.4	-0.03	-0.55	0.76	-1.73	-2.22	-0.65	-0.21	0.36	0.67	0.65	-1.38	0.17	-1.27	593.3	76.4
NO_3 50-150m	-1.38	-0.45	1.03	1.38	-0.67	-0.17	-0.4	1.18	1.37	-0.4	0.22	-1.73	-1.29	0.24	-0.7	1.08	0.68	0.45	-0.25	-2.16	1421.5	100.4
NO_3 150-320m	2.75	-0.91	0.27	0.18	-0.14	-0.25	0.98	1.17	0.17	-1.5	-0.15	-1.23	-0.87	-0.53	-0.35	0.31	0.11	-1.18	-1.27	-1.61	3909.7	140.3

Shediac Valley

	1999	2000	2001	2002	2003	2004	2005	2006	2007	2008	2009	2010	2011	2012	2013	2014	2015	2016	2017	2018	Mean	SD
Chl *a* 0-100m	-1.04	-1.4	-0.14	2.36	0.16	-0.38	-0.69	-0.04	1.49	1.43	-0.05	-0.69	-1.15	0.34	0.53	-0.33	-0.4	-0.92	1.22	-0.61	50.3	16.6
NO_3 0-50m	0.73	1.57	-0.11	0.53	0.59	0.75	-0.87	0.6	-2.01	-0.13	1.05	-1.98	-1.16	-0.02	0.07	0.46	-0.06	-0.25	0.8	-1.32	176.7	44
NO_3 50-84m	0.35	1.8	0.63	-0.35	0.61	-0.03	-0.7	1.49	-1.38	0.31	-0.32	-2.18	-1.19	-0.22	0.12	0.79	0.27	-0.16	0.05	-0.18	255	38.9

Figure 8. Nitrate inventories (0–50 m; top panels) and phytoplankton biomass (0–100 m Rimouski and 0–84 m Shediac Valley; bottom panels) in 2018 (black circles) with monthly mean conditions (± 0.5 SD) for the 1999–2015 reference period (black line with blue shading) at Rimouski and Shediac Valley stations. Time series of normalized annual anomalies for nitrate inventories (mmol m^{-2}) and phytoplankton biomass (mg m^{-2}) are also presented with the variable means and standard deviations for the 1999–2015 reference period to the right of the scorecard. Blue colours indicate anomalies below the mean and reds are anomalies above the mean, and white representing normal conditions.

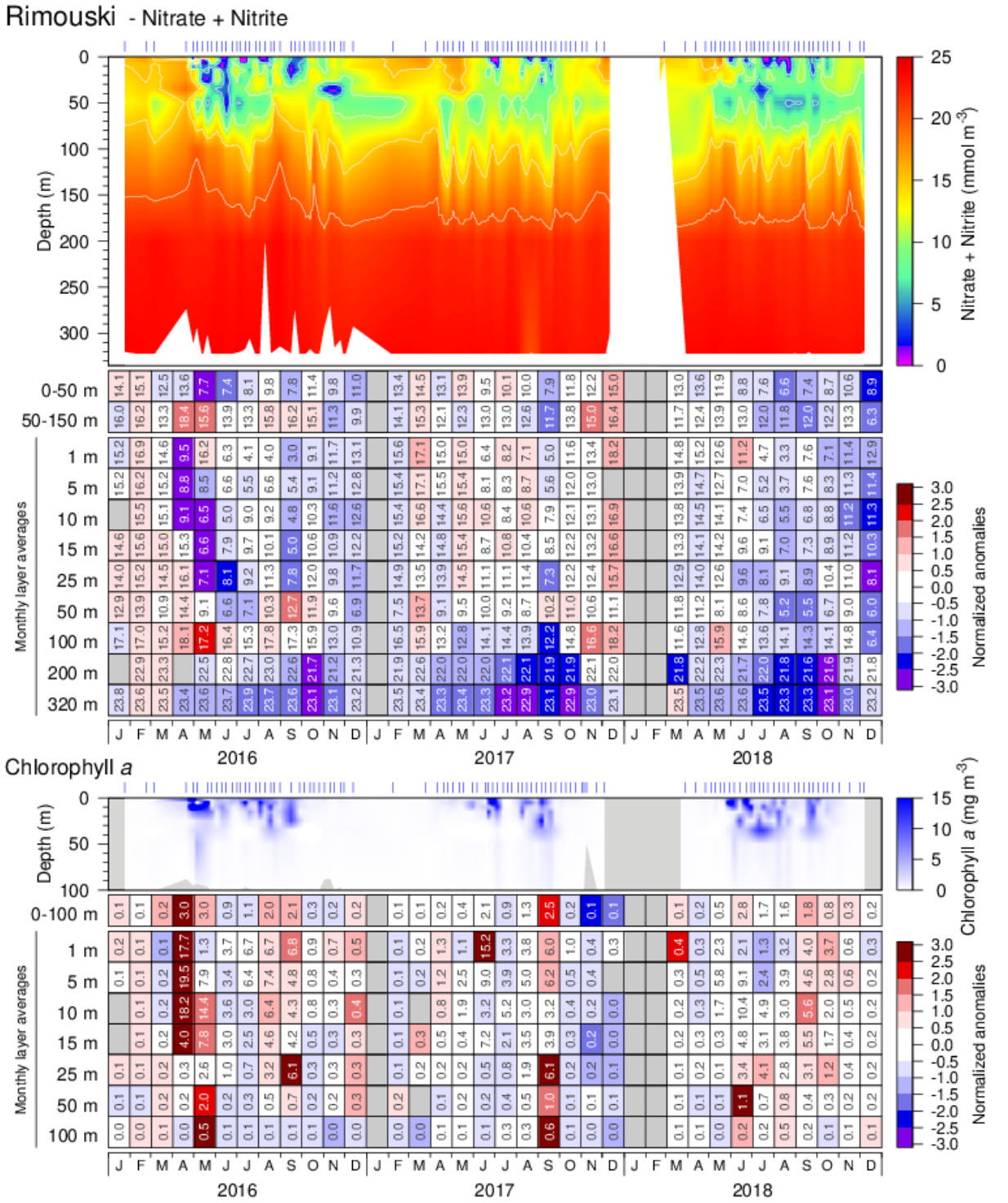

Figure 9. Nitrate (top) and chlorophyll a (bottom) concentrations at Rimouski station during the 2016 to 2018 sampling seasons. Contour plots are made with data from individual sorties while monthly means are shown in the tables below the graphics (nitrates: mmol m^{-3}; chl a: mg m^{-3}). Cell colours indicate normalized anomalies based on the 1991–2015 climatology: blue colours indicate anomalies below the mean and reds are anomalies above the mean. During March, the integrated (0–50) monthly average and the depth-specific average for nitrate for the reference period do not include the same amount of data, and this might result in inconsistent anomalies between integrated and depth-specific values.

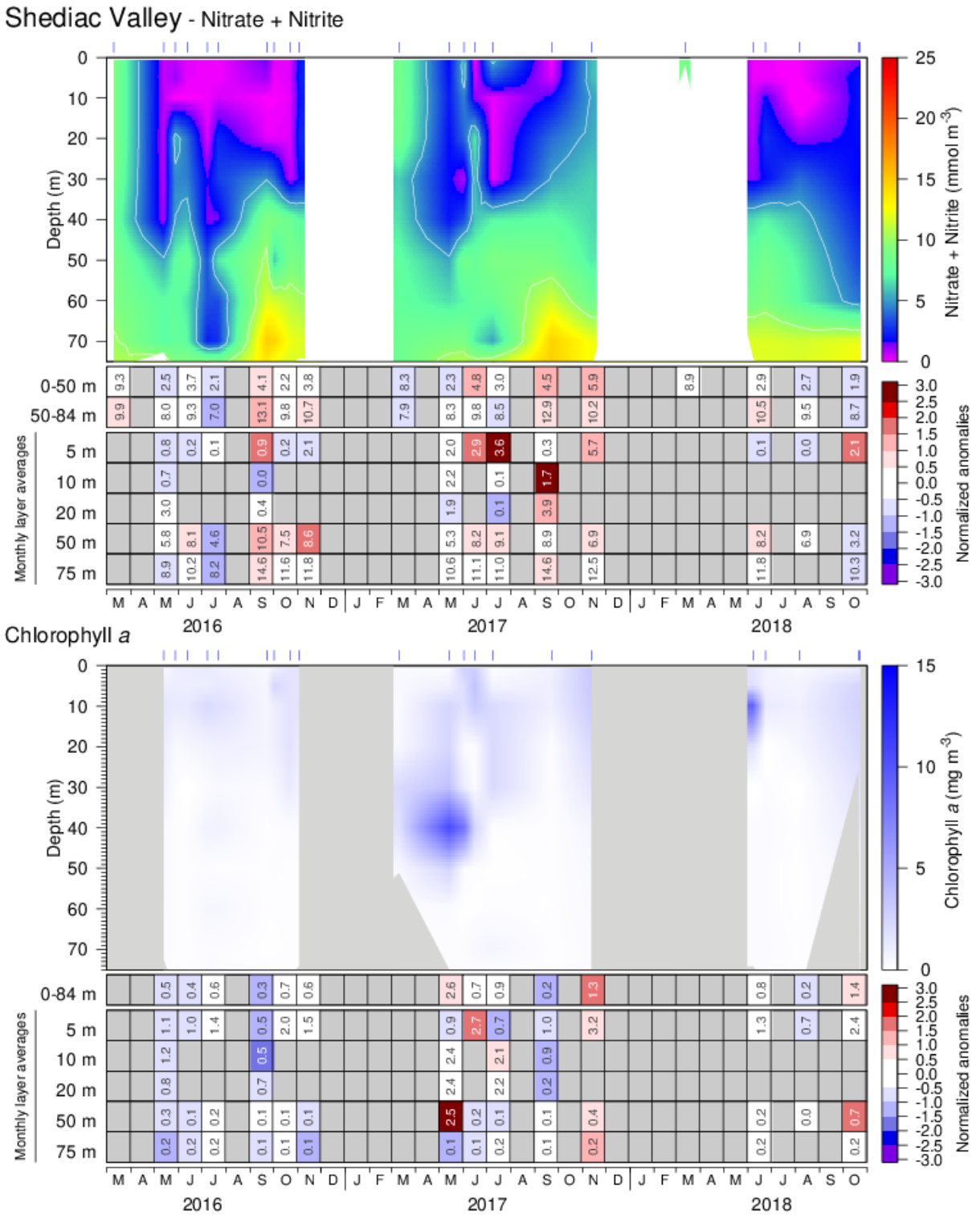

Figure 10. Nitrate (top) and chlorophyll a (bottom) concentrations at Shediac Valley station during the 2016 to 2018 sampling seasons. Contour plots are made with data from individual sorties while monthly means are shown in the tables below the graphics (nitrates: mmol m^{-3}; chl a: mg m^{-3}). Nitrate values in March are from the winter survey across the Gulf. Cell colours indicate normalized anomalies based on the 1991–2015 climatology: blue colours indicate anomalies below the mean and reds are anomalies above the mean. Only seven to ten observations per year were used to produce annual vertical profiles, so interpolation between sampling date (blue tick marks above vertical profiles) might not be accurate.

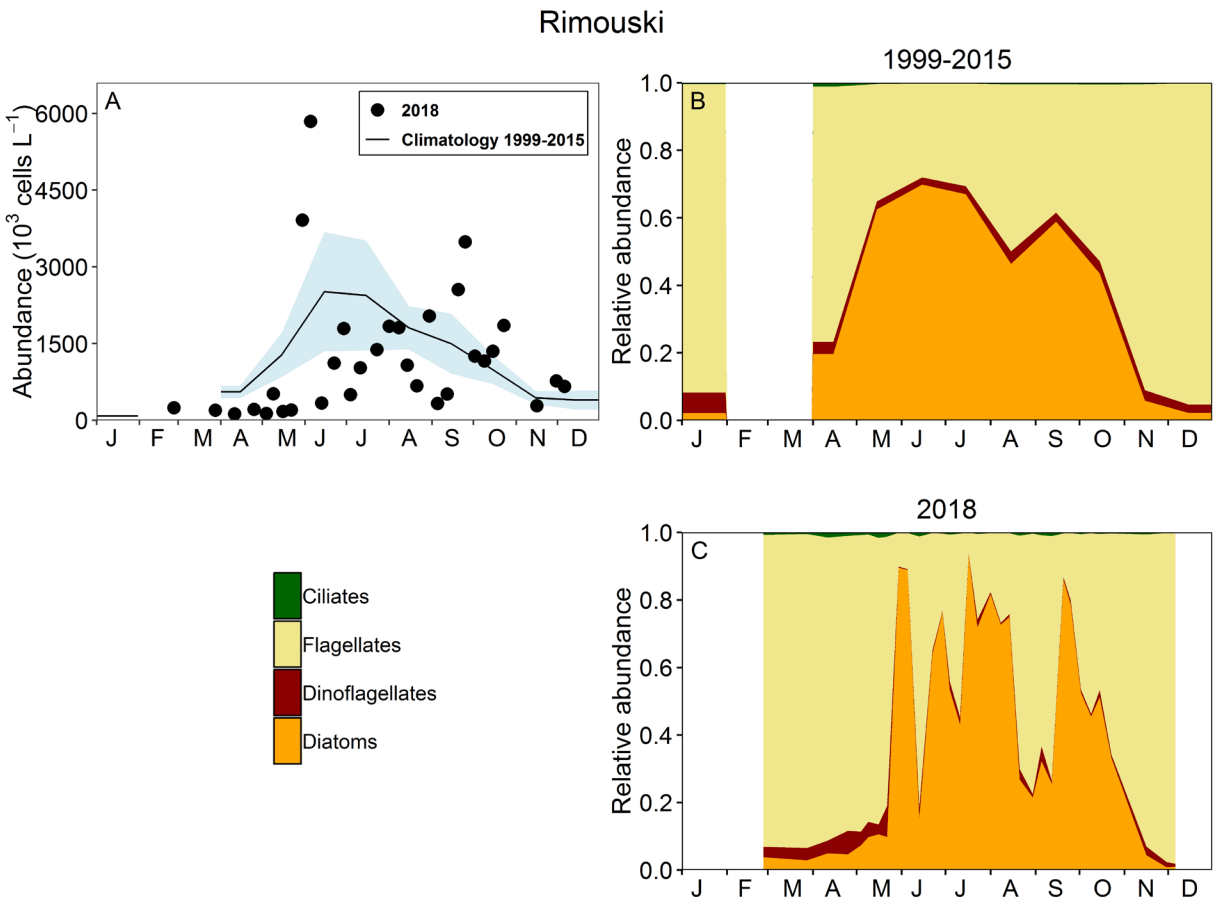

Figure 11. Phytoplankton abundance (A) and community composition at Rimouski station for the 1999–2015 reference period (B; no data in 2010) and for 2018 (C). Blue shading on panel (A) represents ± 0.5 SD of the monthly mean phytoplankton abundance for the reference period.

Rimouski

	1999	2000	2001	2002	2003	2004	2005	2006	2007	2008	2009	2010	2011	2012	2013	2014	2015	2016	2017	2018	Mean	SD
Diatom	0.56	-0.55	0.5	0.53	1.24	-1.77	-1.36	-1	0.69	-1.67	-0.62		1.07	0.65	-0.63	1.44	0.68	1.16	-1.45	0.39	49	23
Dino	-0.71	-0.39	0.46	0.45	0.74	0.23	0.75	1.44	1.85	0.62	0.88		-0.14	-0.23	-0.4	-1.22	-1.14	-1.41	-1.76	-1.53	23	12
Flag	-1.69	-1.61	-0.62	-0.95	-0.16	-0.89	1.16	1.52	1.71	0.4	0.99		-0.1	-0.77	0.36	-0.49	0.07	0.39	0.25	-0.48	396	183
Ciliate	-2.13	-1.51	0.62	0.46	0.16	-1.56	1.73	1.15	1.14	-0.07	-0.11		0.29	0.91	-0.31	-0.13	-0.31	-0.72	-1.2	-0.55	3	1
Total	0.27	-1.53	-0.08	-0.47	0.66	-2.52	0.29	0.98	1.92	-0.9	0.86		0.28	-0.51	-0.38	0.03	-0.07	1.62	-0.29	-0.3	606	171
Diat/Dino	1.21	0	0.05	-0.04	0.2	-1.35	-1.3	-1.42	-0.74	-1.44	-0.83		0.66	0.45	-0.24	1.54	0.95	1.66	0.26	1.14	4	3
Diat/Flag	2.46	0.76	0.7	0.79	0.8	-1.1	-1.3	-1.2	-0.63	-1.35	-0.58		0.4	0.59	-0.77	0.73	-0.04	0.89	-0.47	0.47	1	1

Shediac Valley

	1999	2000	2001	2002	2003	2004	2005	2006	2007	2008	2009	2010	2011	2012	2013	2014	2015	2016	2017	2018	Mean	SD
Diatom	-0.33	0.77	-0.29	1.44	0.09	0.87	-1.13	0.09	1.88	1.44	-0.22	-1.19	-0.79	-0.58	0.38	-1.19	-1.23	-1.06	0.57	-0.73	53	49
Dino	0.67	1.9	-0.19	0.36	-0.26	1.6	-0.01	-1.04	-0.49	1.24	-1.37	-1.17	-0.39	-1.05	-0.9	0.97	0.13	1.49	0.75	0.75	3	2
Flag	-1.25	0.54	0.87	0.32	0.58	1.34	-0.01	-0.79	-0.6	0.43	-0.6	-1.82	0.37	-0.8	-0.01	2.22	-0.8	2.08	1.89	0.44	12	11
Ciliate	1.29	0.51	-0.5	0.48	-0.43	2.04	-0.69	-1.29	-0.19	1.66	-1.06	-0.47	-0.05	-1.68	-0.08	0.33	0.12	1.31	0.61	3.03	1	0
Total	-0.85	0.66	-0.11	1.42	0.33	0.9	-0.45	-0.28	1.69	1.5	-0.5	-1.91	-0.76	-0.76	-0.05	0.35	-1.16	0.18	1.16	-0.51	87	56
Diat/Dino	-0.95	-0.59	-0.19	1.26	0.2	-0.32	-0.76	0.67	2.34	0.66	0.66	-0.31	-0.7	0.01	0.9	-1.52	-1.36	-2.1	-0.04	-1.3	20	18
Diat/Flag	0.54	-0.14	-1.05	1.06	-0.27	-0.57	-0.39	0.49	2.57	0.91	0.23	0.01	-1.13	0.01	0	-1.96	-0.31	-2.02	-0.87	-1	9	10

Figure 12. Time series of normalized annual (April–December) anomalies for abundance (10^3 cells L^{-1}) of the main phytoplankton taxonomic groups (diatoms, dinoflagellates, flagellates, ciliates) and total microphytoplankton, and for the diatom/dinoflagellate and diatom/flagellate ratios at Rimouski and Shediac Valley stations. Variable means and standard deviations for the1999–2015 reference period are shown to the right of the scorecard. Blue colours indicate anomalies below the mean and reds are anomalies above the mean, and white representing normal conditions. No data are available for 2010 at Rimouski station.

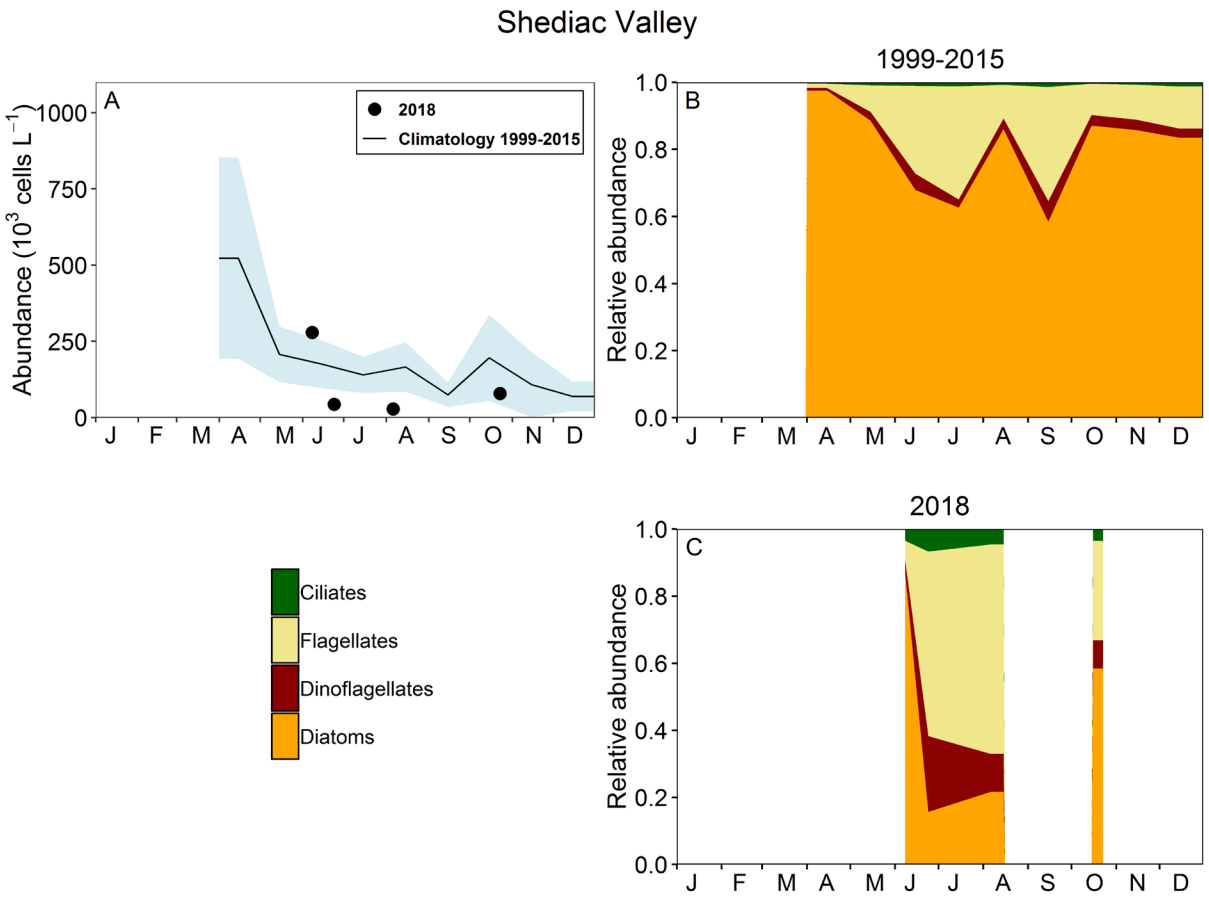

Figure 13. Phytoplankton abundance (A) and community composition at Shediac Valley station for the 1999–2015 reference period (B) and for 2018 (C). Blue shading on panel (A) represents ± 0.5 SD of the monthly mean phytoplankton abundance for the reference period.

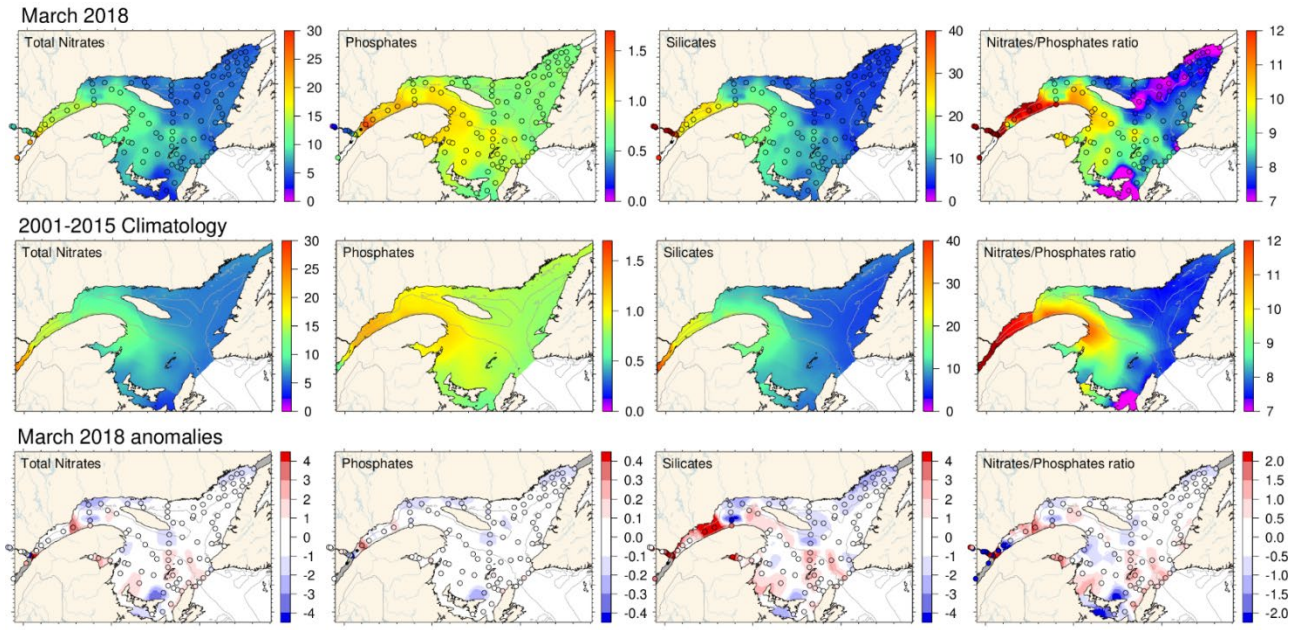

Figure 14. Total nitrate (NO_3^- + NO_2^-), phosphate, and silicate concentrations (mmol m^{-3}) and N:P ratio at 2 m in the Estuary and Gulf of St. Lawrence during early March 2018 (upper panels). The climatology (2001–2015; middle panels) and anomalies (lower panels) are shown for each nutrient. Blue colours indicate anomalies below the mean and reds are anomalies above the mean, and white representing normal conditions.

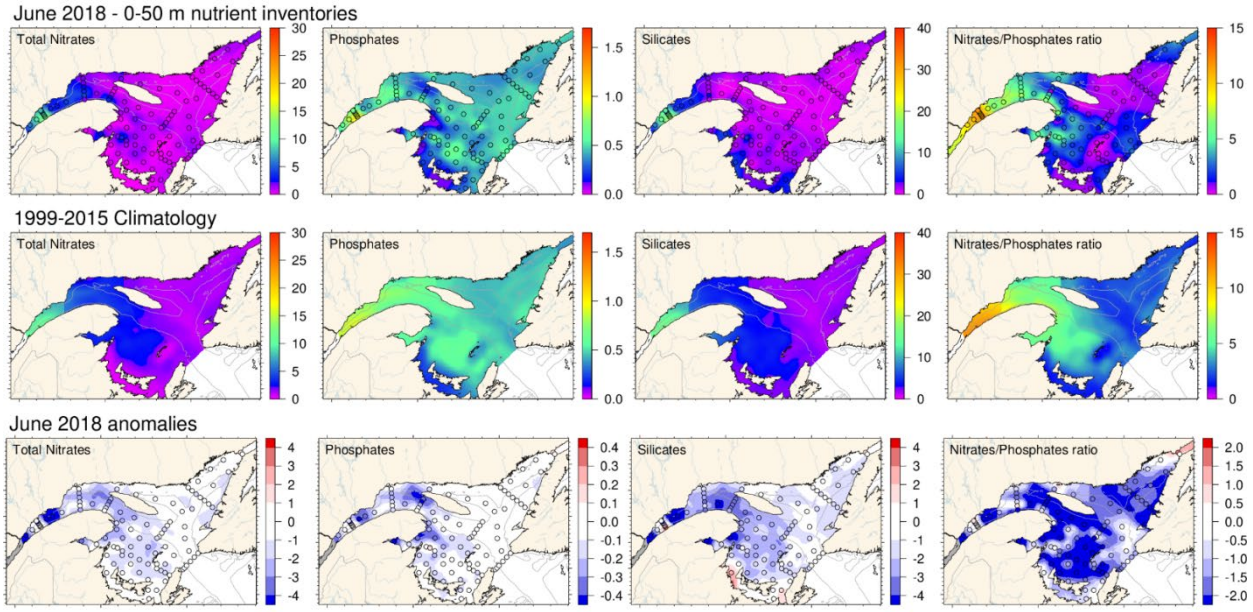

Figure 15. Total nitrate (NO_3^- + NO_2^-), phosphate, and silicate concentrations (mmol m^{-3}) and N:P ratio averaged in the surface layer (0–50 m) in the Estuary and Gulf of St. Lawrence during June 2018 (upper panels). The climatology (1999–2015; middle panels) and anomalies (lower panels) are shown for each nutrient. Blue colours indicate anomalies below the mean and reds are anomalies above the mean, and white representing normal conditions.

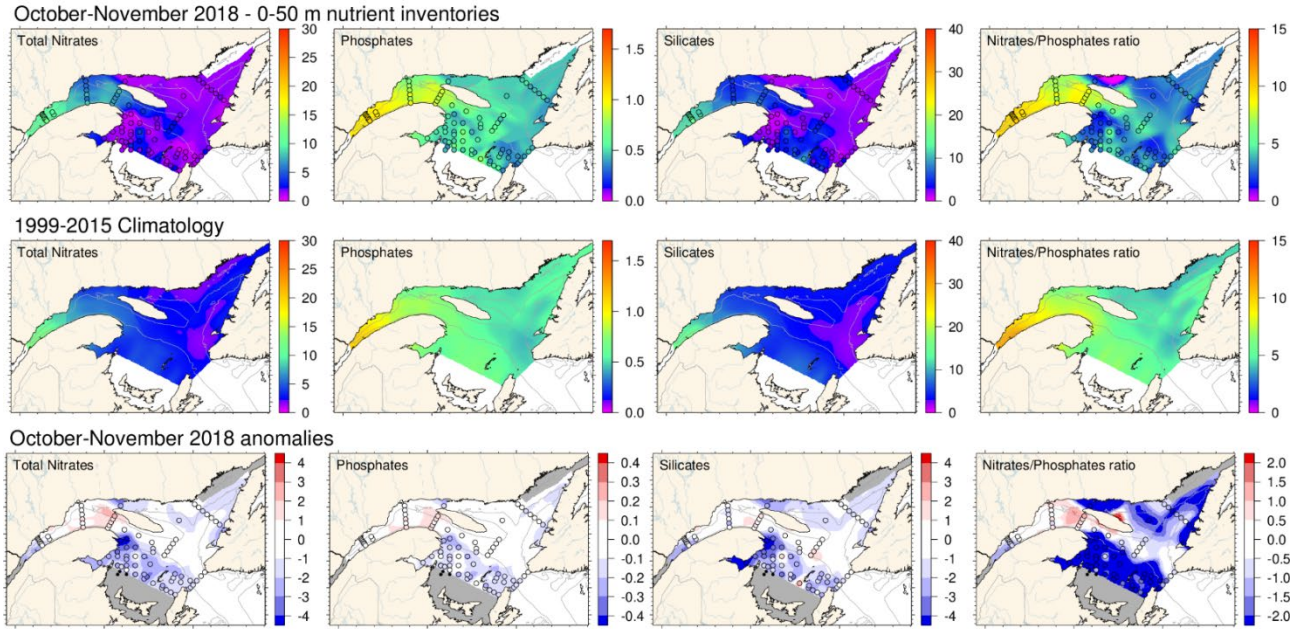

Figure 16. Total nitrate (NO3- + NO2-), phosphate, and silicate concentrations (mmol m^{-3}) and N:P ratio averaged in the surface layer (0–50 m) in the Estuary and Gulf of St. Lawrence during fall 2018 (upper panels). The climatology (1999–2015; middle panels) and anomalies (lower panels) are shown for each nutrient. Blue colours indicate anomalies below the mean and reds are anomalies above the mean, and white representing normal conditions.

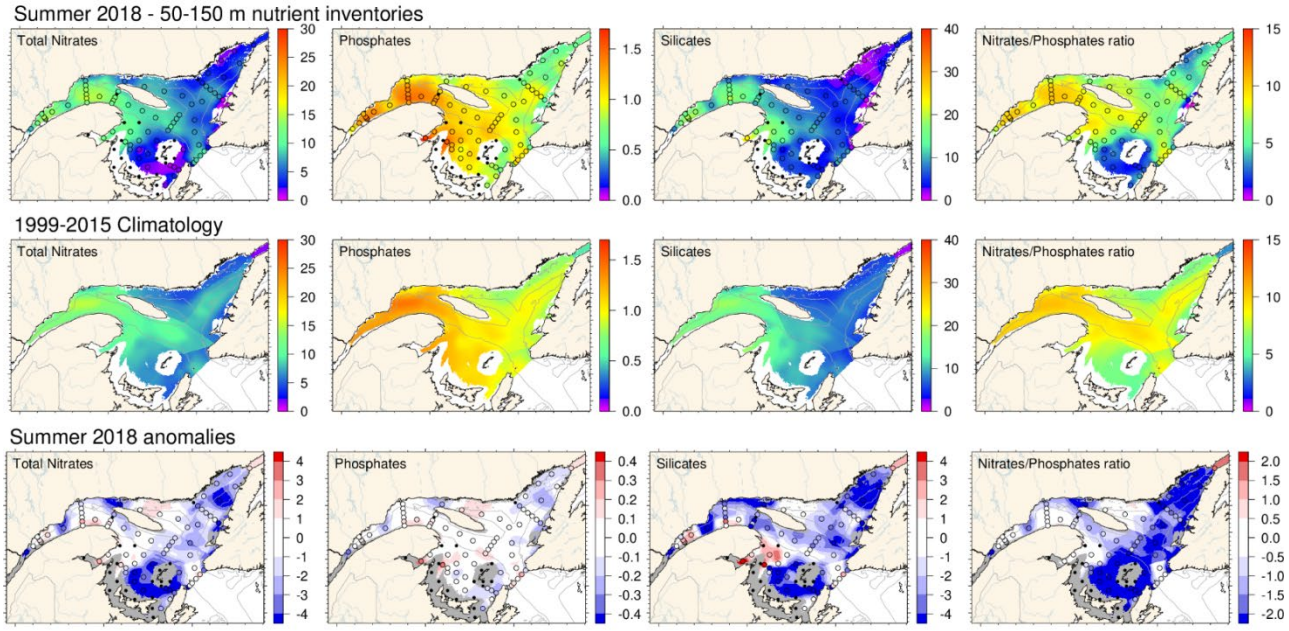

Figure 17. Total nitrate (NO_3^- + NO_2^-), phosphate, and silicate concentrations (mmol m^{-3}) and N:P ratio averaged over the mid-layer (50–150 m) in the Estuary and Gulf of St. Lawrence during June 2018 (upper panels). The climatology (1999–2015; middle panels) and anomalies (lower panels) are shown for each nutrient. Blue colours indicate anomalies below the mean and reds are anomalies above the mean, and white representing normal conditions.

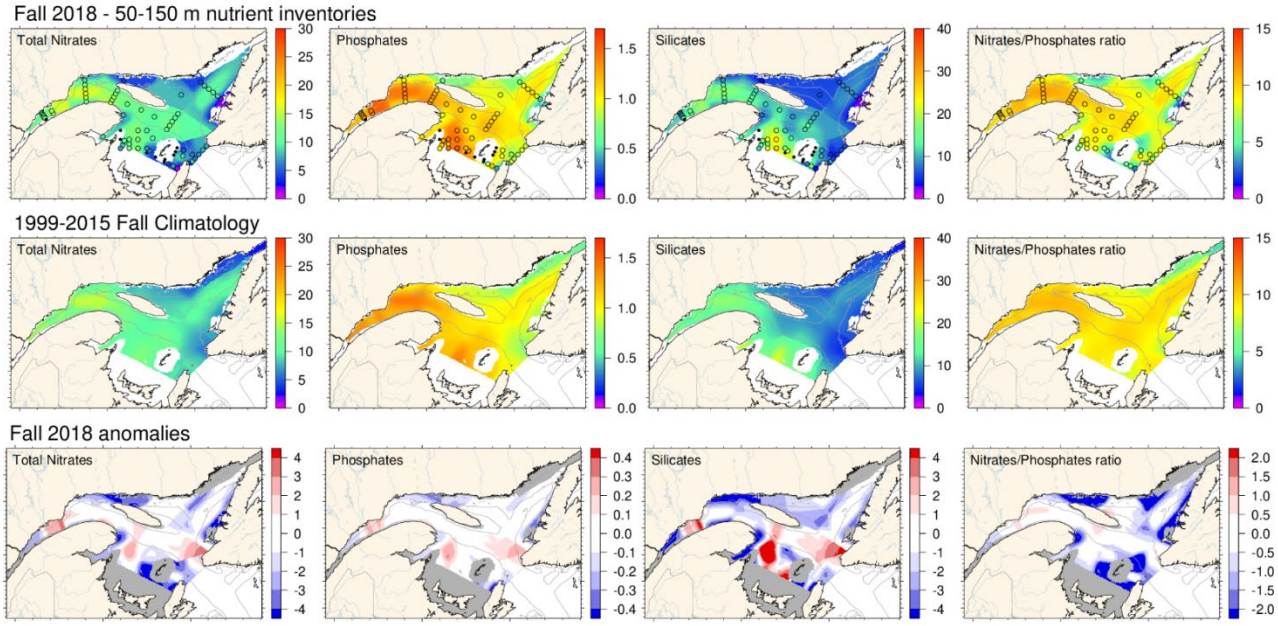

Figure 18. Total nitrate (NO_3^- + NO_2^-), phosphate, and silicate concentrations (mmol m^{-3}) and N:P ratio averaged over the mid-layer (50–150 m) in the Estuary and Gulf of St. Lawrence during fall 2018 (upper panels). The climatology (1999–2015; middle panels) and anomalies (lower panels) are shown for each nutrient. Blue colours indicate anomalies below the mean and reds are anomalies above the mean, and white representing normal conditions.

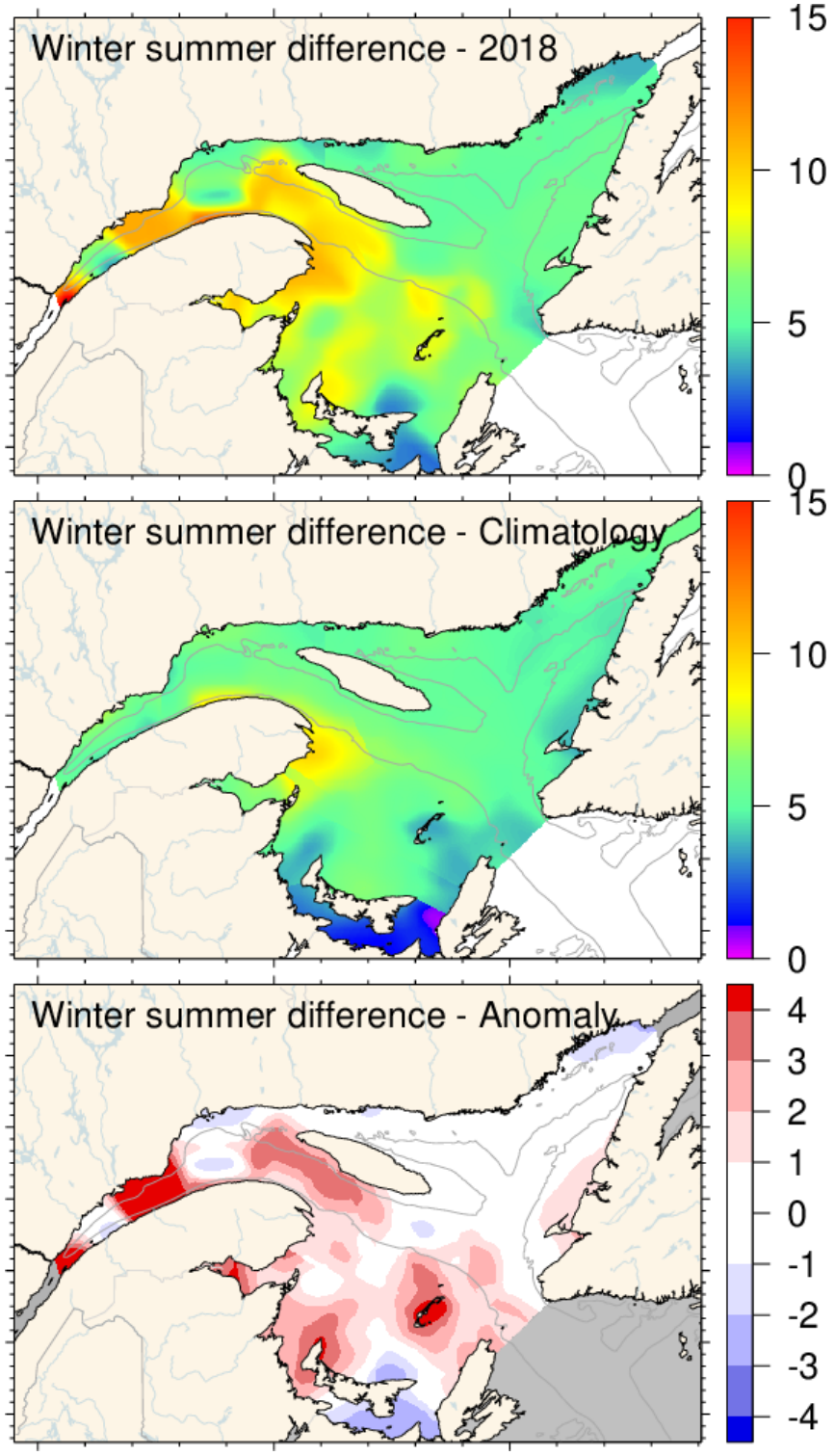

Figure 19. Difference in total nitrate (NO_3^- + NO_2^-) concentrations (mmol m^{-3}) at 2 m in the Estuary and Gulf of St. Lawrence between winter and summer. Top: winter–summer difference in 2018; middle: winter–summer climatology difference (2001–2015); bottom: winter–summer anomaly difference in 2018. Negative anomalies (blue) suggest weak nitrate drawdowns and positive anomalies (red) suggest strong nitrate drawdowns.

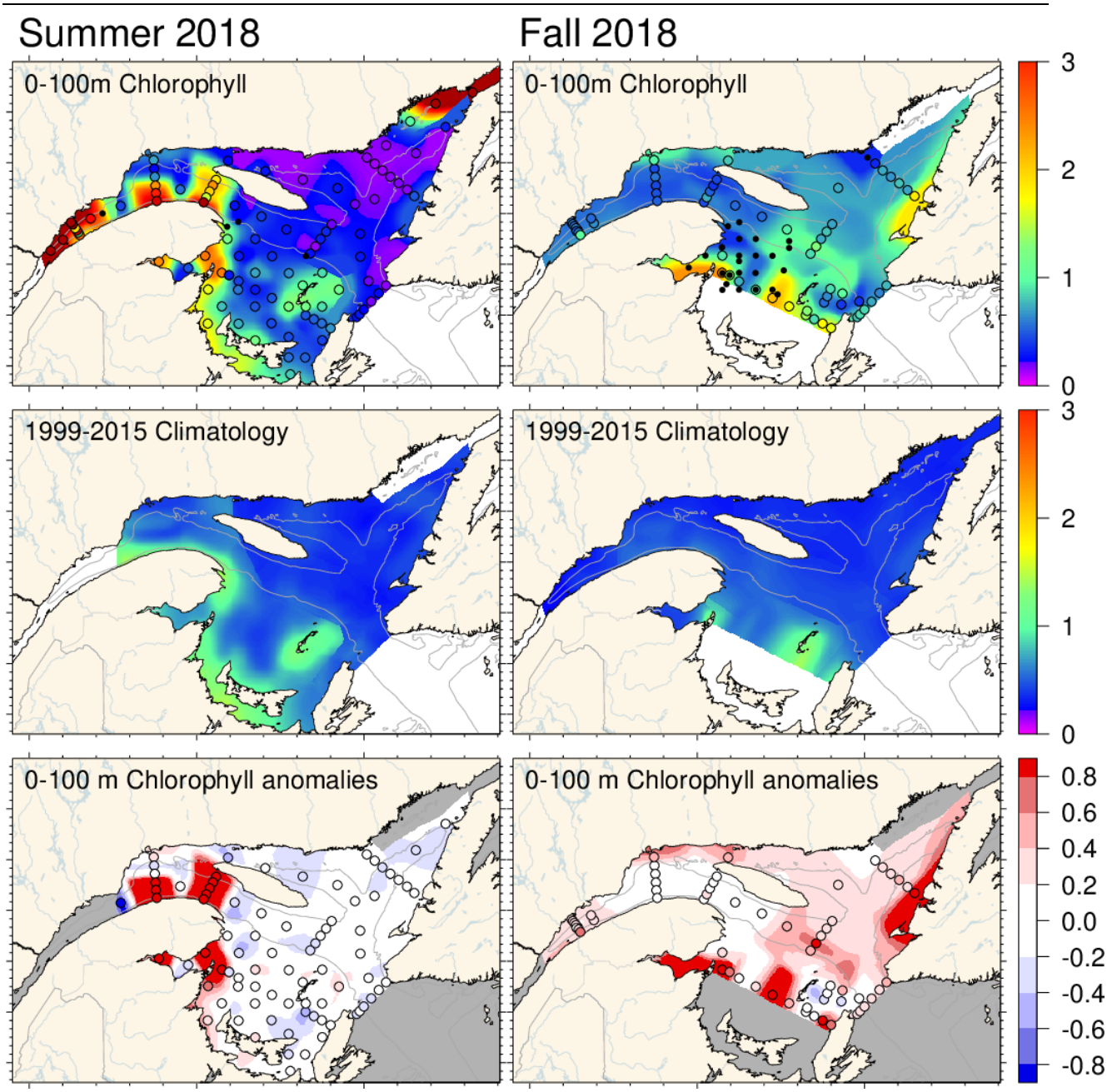

Figure 20. Vertically averaged (0–100 m) chlorophyll a concentrations (mg m^{-3}) in the Estuary and Gulf of St. Lawrence during summer (left panels) and fall (right panels) 2018. The climatology (1999–2015; middle panels) and anomalies (lower panels) are shown for both periods. Blue colours indicate anomalies below the mean and reds are anomalies above the mean, and white representing normal conditions.

Surface nutrients (0-50 m; mmol m^{-2})

		1999	2000	2001	2002	2003	2004	2005	2006	2007	2008	2009	2010	2011	2012	2013	2014	2015	2016	2017	2018	Mean	SD
N	Rimouski	-0.32	0.91	0.34	1.67	-0.46	1.22	-0.4	-0.03	-0.55	0.76	-1.73	-2.22	-0.65	-0.21	0.36	0.67	0.65	-1.38	0.17	-1.27	593.3	76.4
	wGSL	1.34	-0.46	0.77	1.49	0.32	-0.99	-0.54	-0.35	-0.41	-0.22	-0.54	-1.97	-1.4	0.05	0.87	0.5	1.53	-0.05	0.68	-1.02	347.2	56.4
	eGSL	0.9	1.46	0.56	0.4	1.13	-1.18	-0.32	-0.24	1.24	0.03	-0.04	-1.7	-1.78	-1.23	-0.19	0.16	0.77	-2	-1.19	-2.22	127.1	21.7
	S. V.	0.73	1.57	-0.11	0.53	0.59	0.75	-0.87	0.6	-2.01	-0.13	1.05	-1.98	-1.16	-0.02	0.07	0.46	-0.06	-0.25	0.8	-1.32	176.7	44
	sGSL	0.55	1.14	-0.46	0.1	0.35	0.49	0.58	1.67	0.37	0.73	0.59	-2.56	-0.74	-1.23	-0.46	-0.23	-0.89	-0.91	-0.3	-1.81	81.7	26.3
P	Rimouski	0.04	-0.04	0.83	1.71	0.1	1.21	0.12	0.74	-0.87	0.48	-1.9	-1.46	-1.62	-0.34	0.2	-0.12	0.91	-1.82	-0.36	-0.65	53.3	5.7
	wGSL	1.07	-0.18	0.85	1.45	0.84	-0.18	-0.38	-0.58	-0.18	-0.59	-1.05	-1.87	-1.68	-0.08	0.63	0.39	1.56	-0.58	0.01	-0.74	41.8	4.8
	eGSL	0.87	1.14	1.31	1.27	1.61	0.27	-0.31	-0.62	0.25	-0.55	-0.62	-1.64	-1.61	-1.18	-0.19	-0.08	0.1	-1.33	-0.72	-0.62	29.3	2.8
	S. V.	0.98	0.75	1.64	1.63	1.16	0.33	-0.86	-0.05	-1.05	-0.86	0.37	-1.42	-1.5	0.12	-0.58	-0.1	-0.57	-0.93	-0.5	-1.14	33.4	4.4
	sGSL	0.77	0.67	0.58	1.16	1.24	1.08	0	0.71	0.21	0.01	-0.02	-2.33	-1.41	-0.93	-0.25	-0.2	-1.29	-1.22	-1.74	-1.81	21.4	3
Si	Rimouski	0.18	0.7	0.11	1.23	-0.91	1.14	-0.25	0.07	-0.92	1.94	-1.76	-1.91	-0.41	0.03	0.21	0.15	0.4	-0.58	0.66	-1.69	774.5	141.8
	wGSL	1.62	-0.12	0.46	1.34	0.64	-0.25	-0.01	-0.07	-1.28	-0.26	-1.21	-1.75	-1.62	0.12	0.97	0.56	0.84	-0.43	1.49	-1.81	421.9	74.6
	eGSL	2.19	1.06	-0.25	0.05	1.29	-0.3	0.17	0.46	0.73	-0.16	-1.74	-0.62	-1.7	-0.96	0.11	0.1	-0.43	-2.09	-1.13	-1.45	166.8	38.9
	S. V.	0.62	1.28	-0.41	0.45	0.8	1.4	-0.27	0.3	-2.13	-0.12	1.31	-1.46	-0.96	-0.78	0.63	0.05	-0.73	-0.34	0.46	-1.01	248.9	63.6
	sGSL	2.3	1.3	-0.47	-0.24	0.72	0.39	-0.59	1.43	0.07	0.2	-0.24	-1.3	-0.91	-0.78	-0.23	-0.1	-1.55	-1.04	-0.66	-1.42	194.7	73.7
N:P	Rimouski	-0.67	1.77	-0.66	0.47	-1.02	0.38	-0.95	-1.23	0.31	0.67	-0.18	-1.91	1.29	0.13	0.36	1.45	-0.22	0.26	0.87	-1.38	11.1	0.8
	wGSL	1.47	-0.82	0.38	1.14	-0.74	-2.13	-0.67	0.18	-0.7	0.46	0.5	-1.53	-0.51	0.31	1.07	0.57	1.03	0.89	1.69	-1.21	8.3	0.5
	eGSL	1.15	1.22	-0.39	-0.47	0.36	-1.96	-0.32	0.07	1.79	0.43	0.4	-1.21	-1.32	-0.95	-0.09	0.28	1	-1.99	-1.19	-2.53	4.5	0.4
	S. V.	0.3	1.64	-1.24	-0.32	0	0.87	-0.55	0.82	-2.07	0.37	1.2	-1.66	-0.64	-0.17	0.52	0.67	0.26	0.25	1.46	-0.84	5.3	1
	sGSL	0.23	1.11	-1.05	-0.58	-0.32	0.08	0.79	2.03	0.34	1	0.91	-2.13	-0.23	-1.21	-0.38	-0.08	-0.5	-0.53	0.67	-1.48	4.1	0.9

Mid-layer nutrients (50-150 m; mmol m^{-2})

		1999	2000	2001	2002	2003	2004	2005	2006	2007	2008	2009	2010	2011	2012	2013	2014	2015	2016	2017	2018	Mean	SD
N	Rimouski	-1.38	-0.45	1.03	1.38	-0.67	-0.17	-0.4	1.18	1.37	-0.4	0.22	-1.73	-1.29	0.24	-0.7	1.08	0.68	0.45	-0.25	-2.16	1421.5	100.4
	wGSL	0.38	-1.6	0.66	1.11	0.47	-1.59	-0.51	0.43	-0.02	0	-0.2	-1.49	-0.83	1.04	0.14	-0.08	2.09	0.02	0.25	-0.34	1224.9	108.6
	eGSL	-1.15	-0.14	-1.37	0.03	0.27	-1.9	-0.67	0.96	0.28	-0.28	0.11	-0.72	-0.11	1.04	0.66	0.76	2.22	-0.63	-1.35	-1.52	863.3	76.5
	S. V.	0.35	1.8	0.63	-0.35	0.61	-0.03	-0.7	1.49	-1.38	0.31	-0.32	-2.18	-1.19	-0.22	0.12	0.79	0.27	-0.16	0.05	-0.18	255	38.9
	sGSL	-0.44	-0.25	-0.02	1.2	1.7	0.59	-1.99	0.77	-1.01	0.12	1.21	-0.66	0.55	0.08	-0.13	-1.79	0.09	0.36	-0.7	-0.59	34	15.2
P	Rimouski	-0.8	-1.34	1.79	1.34	-0.11	0.07	0.42	1.91	0.06	-0.03	-0.42	-1.01	-1.71	0.02	-0.52	-0.19	0.51	-0.54	-0.41	-1.9	141.1	9.2
	wGSL	0.59	-0.99	0.95	1.59	1.04	-0.44	-0.4	-0.01	-0.03	-0.28	-1.06	-1.45	-1.07	0.51	-0.35	-0.72	2.11	-0.47	0.08	-0.02	125.2	7.8
	eGSL	-1.22	0.52	-0.44	1.29	1.17	-0.53	-0.82	0.5	0.12	-0.92	-1.13	-1.13	-0.6	0.01	0.47	0.32	2.4	-0.59	-1.02	-0.01	98	5.3
	S. V.	-0.02	0.57	1.71	1.64	0.94	-0.59	-0.54	1.1	-0.55	0.34	-1.09	-2.12	-0.66	-0.42	-0.71	0.03	0.38	-0.43	-0.41	0.73	34.2	2.6
	sGSL	-0.17	-0.57	0.28	1.31	1.76	0.57	-2	0.55	-0.83	0.06	1.09	-0.43	0.53	0.16	-0.41	-1.9	-0.02	0.23	-0.81	-0.19	7.5	2.3
Si	Rimouski	-1.57	-0.67	0.87	1.2	-0.35	-0.18	0.07	0.7	1.12	1.37	-0.9	-1.6	-1.21	0.64	-0.87	0.96	0.43	0.45	0.47	-1.26	1884.7	214.2
	wGSL	0.95	-1.51	0.82	0.89	0.94	-1.12	-0.18	0.39	0.02	0.1	-1.04	-1.66	-1.15	1.03	-0.09	-0.06	1.67	-0.4	0.66	-0.59	1524.6	186.7
	eGSL	1.26	-0.02	-1.6	-0.11	0.68	-1.45	-0.2	1.34	0.83	-0.71	-0.9	-1.19	-0.8	0.37	0.04	0.92	1.53	-0.52	-1.17	-1.16	895.1	94.5
	S. V.	-0.16	1.23	0.44	0.28	0.92	0.38	-0.64	1.91	-0.78	-0.32	0.02	-2.43	-1.14	-0.57	0.34	0.82	-0.29	-0.24	0.53	0.08	389	48.6
	sGSL	0.31	-0.4	-0.13	1.28	1.85	0.51	-1.95	0.75	-0.86	-0.09	1.18	-0.59	0.38	0.02	-0.22	-1.83	-0.2	0.35	-0.97	-0.66	46.4	22.5
N:P	Rimouski	-0.94	1.14	-0.9	0.23	-0.84	-0.35	-1.15	-0.83	1.94	-0.56	0.88	-1.19	0.39	0.33	-0.32	1.84	0.32	1.38	0.18	-0.63	10.1	0.5
	wGSL	-0.04	-1.72	0	0.01	-0.47	-2.4	-0.45	0.82	0.01	0.36	0.99	-0.91	-0.18	1.29	0.71	0.78	1.2	0.64	0.35	-0.61	9.8	0.4
	eGSL	-0.57	-0.61	-1.55	-1.04	-0.62	-2.21	-0.23	0.92	0.27	0.39	1.11	-0.02	0.35	1.44	0.53	0.77	1.06	-0.39	-1.04	-2.08	8.8	0.5
	S. V.	0.38	2.01	-0.38	-1.01	0.1	0.42	-0.58	1.21	-1.64	0.2	0.34	-1.66	-1.18	-0.11	0.67	1.11	0.12	0.1	0.37	-0.74	7.6	0.8
	sGSL	-1.59	1.47	-0.84	-0.03	-0.59	-0.35	-0.34	1.71	-0.75	0.73	0.77	-1.84	-0.31	-0.32	0.86	0.96	0.45	-0.04	0.39	-2.06	7.4	0.8

Bottom nutrients (300 m; mmol m^{-3})

		1999	2000	2001	2002	2003	2004	2005	2006	2007	2008	2009	2010	2011	2012	2013	2014	2015	2016	2017	2018	Mean	SD
N	Rimouski	-0.64	-2.21	-1.75	0.34	0.49	0.7	1.2	1.4	0.38	-1.06	0.7	-0.37	-0.29	-0.49	0.52	0.92	0.19	-1.17	-1.69	-1.39	24.4	0.7
	wGSL	-2.77	-1.86	-0.49	0.17	0.28	-0.4	0.18	1.14	0.07	0.33	0.09	0.12	-0.13	0.53	0.98	0.94	0.85	-0.08	-0.15	0.27	23.7	1
	eGSL	-2.71	-0.66	0.12	-0.3	0.88	-1.17	-0.57	0.73	-0.41	0.22	-0.35	-0.2	0.29	0.97	1.16	0.57	1.43	1.21	1.3	1.67	22.5	0.9
P	Rimouski	-1.89	-0.22	-0.61	-0.06	0.4	0.19	2.04	1.73	-0.46	0.14	-0.46	0.29	-1.46	-0.48	0.53	-0.7	1	-0.53	-0.36	-0.39	2.5	0.1
	wGSL	-2.02	-0.06	-0.05	0.53	0.56	0.89	0.14	-0.37	-1.23	0.37	-0.88	0.82	-1.39	-0.59	0.58	0.61	2.08	0.83	0.74	1.99	2.2	0.1
	eGSL	-2.31	0.9	1.04	0.99	1.3	0.05	-0.69	-0.47	-0.53	-0.33	-1.07	-0.52	-0.47	-0.45	0.45	0.43	1.67	1.24	2.31	2.54	1.7	0.1
Si	Rimouski	-2.97	-1.56	0.11	0.48	1.16	0.04	0.2	-0.32	0.14	0.98	-0.64	0.18	0.15	0.62	-0.06	0.87	0.62	1.35	1.11	0.76	56.2	4.8
	wGSL	-2.35	-1.17	-0.47	0.17	1.15	-0.53	-0.71	-0.27	-0.03	1.03	-0.78	0.37	-0.27	0.96	0.38	1.78	0.74	2.35	2.06	2.13	48.7	2.6
	eGSL	-0.73	-0.99	0.63	-0.68	2.07	-0.22	-1.73	0.54	0.85	0.64	-1.34	-0.55	-0.68	0.25	-0.14	1.26	0.81	2.53	3.48	3.44	28.7	1.3
N:P	Rimouski	1.83	-1.2	-0.41	0.31	-0.08	0.24	-1.47	-1	0.33	-0.86	1	-0.59	1.52	0.24	-0.25	1.43	-1.03	-0.15	-0.7	-0.47	9.7	0.4
	wGSL	-1.01	-2.08	-0.51	-0.28	-0.2	-1.26	0.12	1.7	0.8	0.02	0.9	-0.61	1.14	1.14	0.57	0.49	-0.91	-0.86	-0.87	-1.55	10.8	0.4
	eGSL	0.01	-1.77	-1.14	-1.52	-0.63	-1.31	0.25	1.33	0.2	0.63	0.92	0.41	0.86	1.55	0.67	0.06	-0.5	-0.22	-1.34	-1.24	13.3	0.5

Figure 21. Time series of normalized annual anomalies for nitrate, phosphate, and silicate inventories as well as N:P ratio, in the surface and mid layers and at 300 m for GSL subregions and the high frequency monitoring stations. For Shediac Valley, the mid-layer integration depth is 50–84m Variable means and standard deviations for the 1999–2015 reference period are shown to the right of the scorecard. Blue colours indicate anomalies below the mean and reds are anomalies above the mean, and white representing normal conditions.

NO_3 (0-50 m; mmol m^{-2})

		1999	2000	2001	2002	2003	2004	2005	2006	2007	2008	2009	2010	2011	2012	2013	2014	2015	2016	2017	2018	Mean	SD
Winter	wGSL	1.75	-0.58	-0.23	-0.09	0.85	0.36	0.06	0.13	1.38	-0.5	0.25	-2.09	-1.96	-0.19	0.43	0.91	-0.45	-0.09	-1.07	0.14	568	94.9
	eGSL	-0.65		0.24	0.08	1.53	1.14	-0.54	-0.11	1.02	-0.22	-0.08	-2.88	-0.45	-0.52	0.45	0.4	0.58	-0.9	-0.33	-0.19	308.5	43.4
	sGSL	0.68	0.55	0.21	0.29	-0.03	0.71	-0.08	0.69	0.39	-0.14	0.54	-2.77	-0.47	-1.66	-0.77	0.32	1.53	-0.04	-0.03	0.46	263.8	109
Summer	wGSL	-0.01	-0.09	0.65	1.09	0.29	0.07	-0.62	-0.07	-0.47	0.43	-0.49	-2.38	-1.31	-0.91	1.22	1.64	0.96	-0.43	0.75	-2.12	228.2	47.3
	eGSL	-0.55	0.38	-0.02	-0.61	1.4	-1.41	-0.34	0.43	0.78	0.91	-0.09	-0.88	-1.78	-1.09	-0.05	1.66	1.26	-1.61	-1.49	-2.53	60.7	21.2
	sGSL	0.42	0.82	-0.72	-0.02	0.51	-0.04	0.69	1.72	0.4	1.37	0.53	-2.14	-0.47	-0.47	-0.07	-0.84	-1.7	-1.01	-0.2	-2.08	39.6	16.2
W - S	wGSL	2.24	-0.59	-0.67	-0.82	0.81	0.34	0.35	0.15	1.95	-0.82	0.51	-0.95	-1.25	0.21	-0.31	-0.03	-1.11	0.09	-1.57	1.08	339.7	87
	eGSL	-0.49		0.31	0.39	1.15	2.11	-0.46	-0.38	0.87	-0.84	-0.05	-2.45	0.17	-0.13	0.59	-0.68	-0.1	-0.38	0.22	0.66	248.1	37.9
	sGSL	0.67	0.38	0.13	0.16	-0.33	0.79	-0.43	0.38	0.22	-0.65	0.42	-1.71	-0.63	-1.44	-0.95	0.3	2.7	-0.14	-0.22	0.59	224.2	107.8
Fall	wGSL	1.62	-0.43	0.73	1.51	-0.07	-1.89	-0.55	-0.65	-0.96	-0.62	-0.65	0.24	-0.41	1.24	0.21	-0.74	1.41	0.21	0.71	0.47	352.6	79.8
	eGSL	1.61	1.18	1.15	1.41	0.24	-1.58	0.06	-0.59	1.08	-0.46	0.25	-0.17	-1.26	-0.79	-0.57	-1.28	-0.28	-1.43	-0.03	-1.32	114.3	29.7
	sGSL	0.55	1.48	-0.06	-0.12	-0.15	1.49	0.69	1.53	-0.8	0.21	-0.3	-0.35	-1.99	-0.27	0.11	-0.18	-1.85	-0.53	-0.58	-3.99	157.8	44.9

Chl *a* (0-100 m; mg m^{-2})

		1999	2000	2001	2002	2003	2004	2005	2006	2007	2008	2009	2010	2011	2012	2013	2014	2015	2016	2017	2018	Mean	SD
Summer	wGSL	0.51	-1.34	0.47	1.29	1.39	-0.04	-1.06	-0.03	0.37	-1.07	0.7	0.71	-0.44	0.87	-2.35	0.36	-0.35	-0.82	0.2	1.85	69.5	26
	eGSL	0.3	0.49	0.01	2.13	-1.25	-0.51	-0.79	-0.45	-0.3	0.29	-0.19	-0.62	-1.19	-0.69	0.77	-0.31	2.3	-0.81	0.69	-0.93	35.8	12.7
	sGSL	0.63	-2.21	-0.12	2.58	-0.17	-0.18	-0.82	0.58	-0.15	-0.64	-0.41	0.86	-0.53	-0.29	0.38	-0.48	0.96	1.06	2.66	0.29	31.9	9.6
Fall	wGSL	-0.67	-1.46	-0.32	0.05	0.8	-0.35	0.35	-0.14	-0.2	2.91	-0.66	-0.63	-1	0.42	-0.68	0.51	1.08	-0.27	-1.1	1.39	33.1	16.1
	eGSL	-0.79	-1.89	-0.43	0.82	0.89	-0.5	-1.19	-0.25	0.35	-0.38	0.64	-0.38	-0.85	-0.17	0.52	1.71	1.91	1.06	0.94	4.08	37	6
	sGSL	-0.36	-2.66	0.37	1.38	0.59	-0.93	-1.1	-0.88	1	-0.18	-0.18	-0.2	0.26	0.78	1.17	0.5	0.44	0.33	0.92	1.02	38.9	14.1
Annual	wGSL	-0.19	-2.01	0.3	0.95	1.68	-0.31	-0.39	-0.1	0.33	1.01	0.05	0.13	-0.91	0.88	-2.19	0.51	0.26	-0.93	-0.83	2.15	46.8	12.2
	eGSL	-0.3	-0.69	-0.16	1.67	-0.22	-0.61	-1.18	-0.45	-0.02	-0.06	0.21	-0.56	-1.2	-0.57	0.81	0.59	2.74	0.01	1.16	0.63	35.1	7.5
	sGSL	0.38	-2.48	0.16	2.3	0.31	-0.63	-1.11	-0.08	0.28	-0.6	-0.42	0.51	-0.35	0.07	1.01	-0.13	0.78	0.67	2.22	0.66	34.9	9.6

Figure 22. Time series of normalized seasonal anomalies for nitrate and chlorophyll a inventories as well as normalized annual anomalies for chlorophyll a in the 0–50 m (nitrates) and 0–100 m (chl a) layers for GSL subregions. Variable means and standard deviations for the 1999–2015 reference period are shown to the right of the scorecard. Blue colours indicate anomalies below the mean and reds are anomalies above the mean, and white representing normal conditions. *W–S is the difference in the nitrate inventory between winter and summer.*

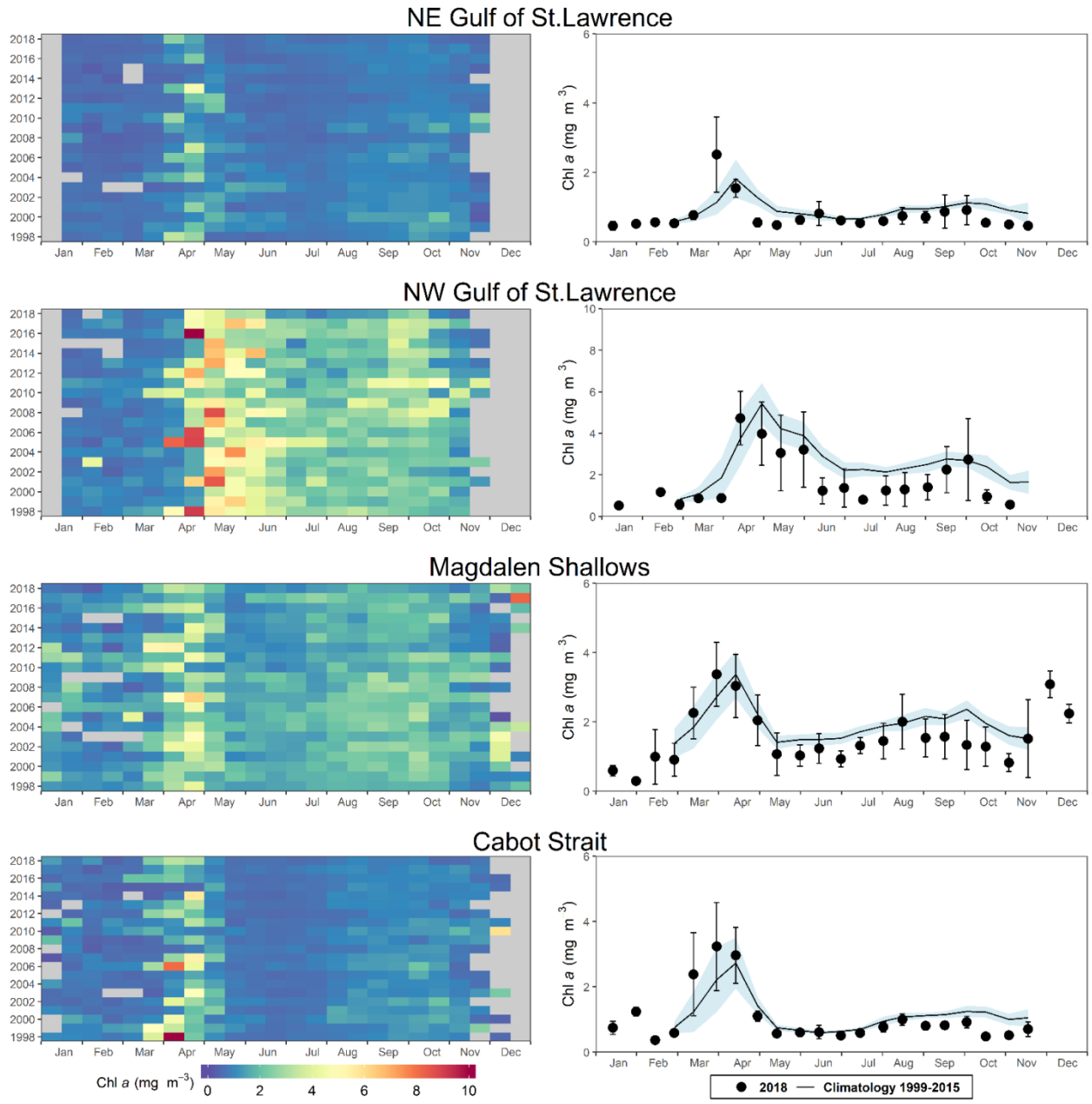

Figure 23. Left panels: Time series of surface chlorophyll a concentrations from twice-monthly SeaWiFS (1998–2007), MODIS (2008–2011), and VIIRS (since 2012) ocean colour data in the northeast Gulf of St. Lawrence, northwest Gulf of St. Lawrence, Magdalen Shallows, and Cabot Strait statistical boxes (see Fig. 4). Right panels: comparison of mean 2018 (black circles) surface chlorophyll a estimates using satellite ocean colour data with mean (± 0.5 SD) conditions from 1999–2015 (solid line with blue shading) for the same statistical boxes.

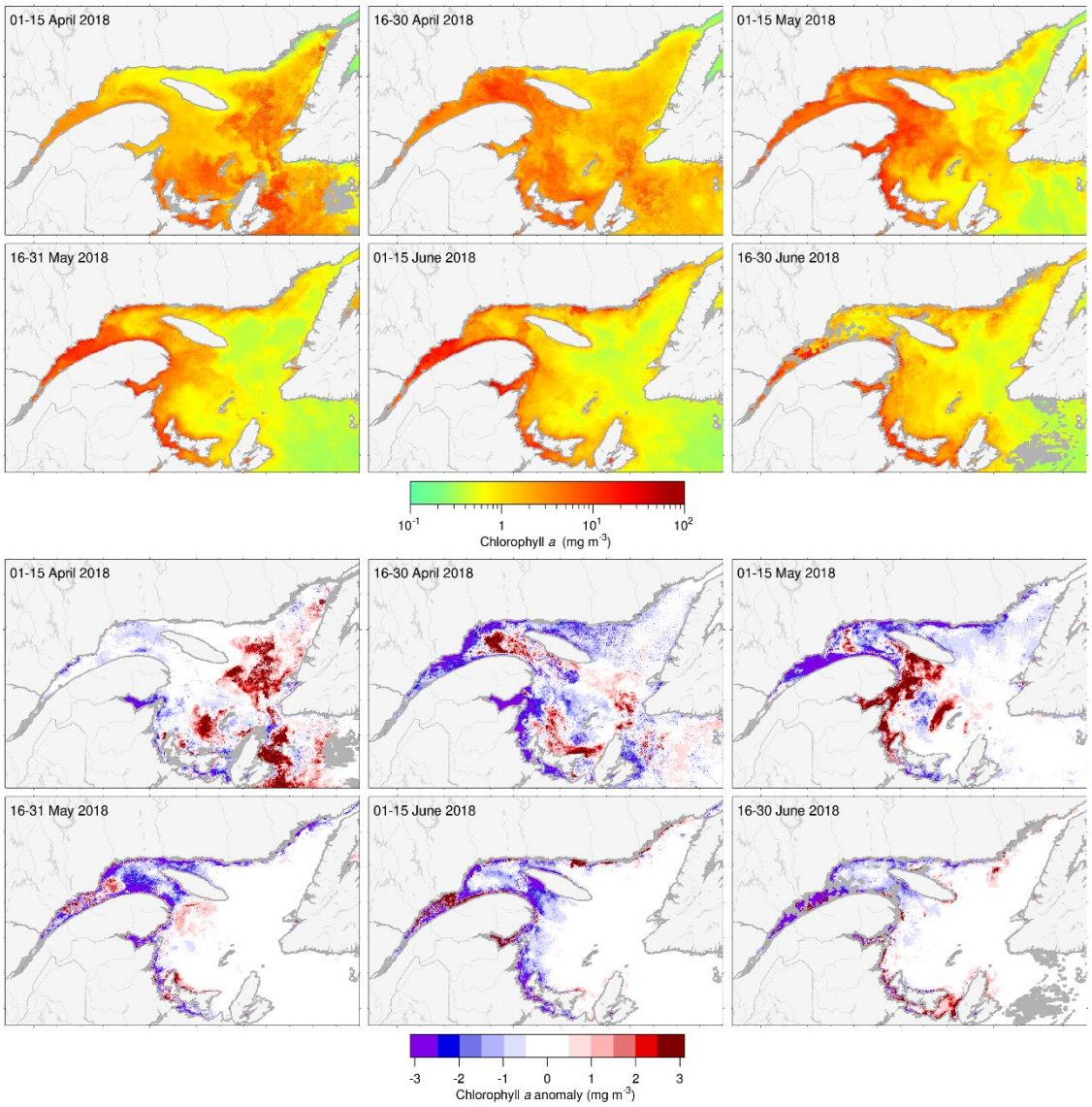

Figure 24. VIIRS twice-monthly composite images of surface chlorophyll a *(upper panels) and chlorophyll* a *anomaly based on the 1999–2015 climatology (lower panels) in the Gulf of St. Lawrence during spring/summer 2018.*

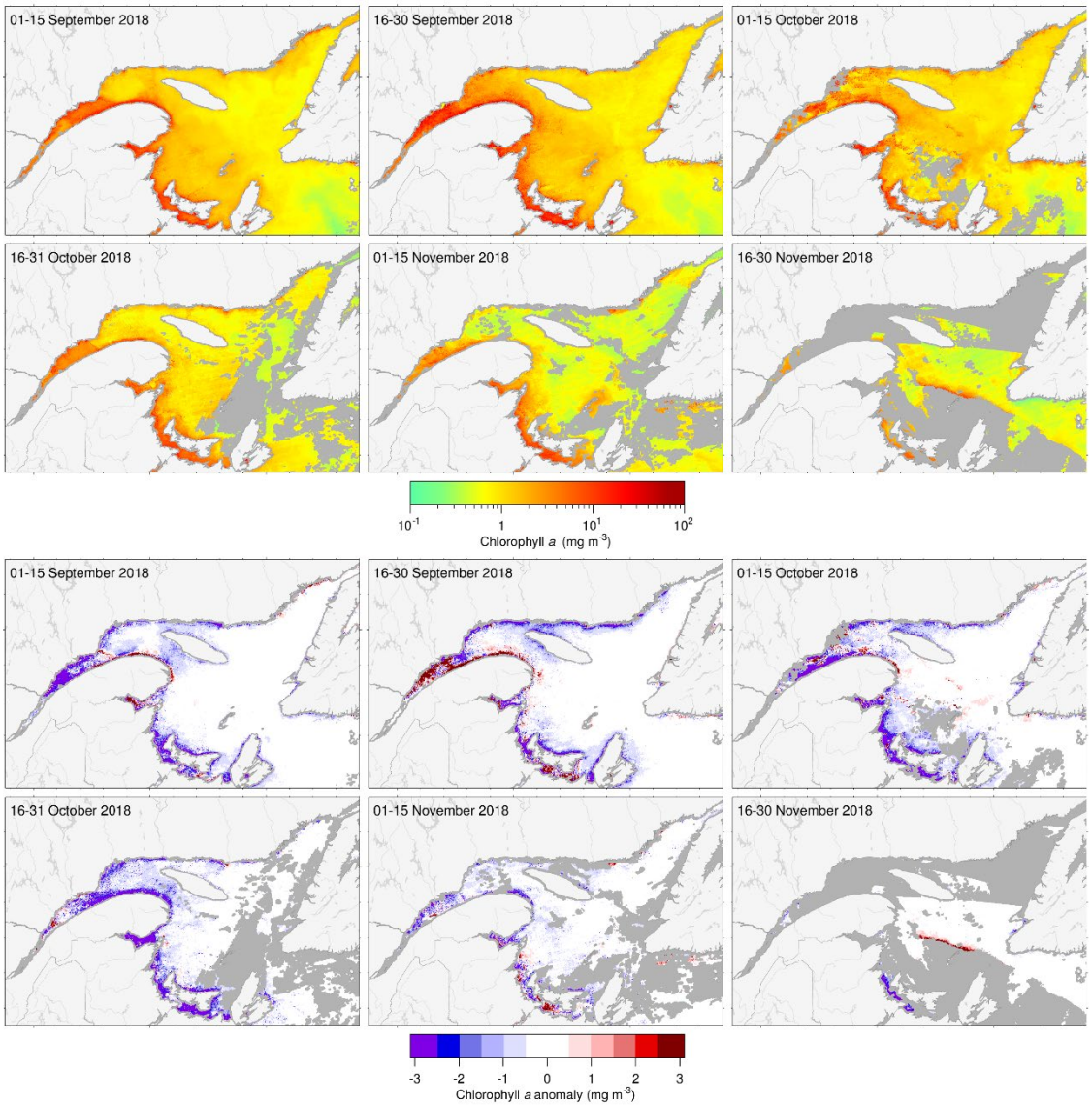

Figure 25. VIIRS twice-monthly composite images of surface chlorophyll a *(upper panels) and chlorophyll* a *anomaly based on the 1999–2015 climatology (lower panels) in the Gulf of St. Lawrence during fall 2018.*

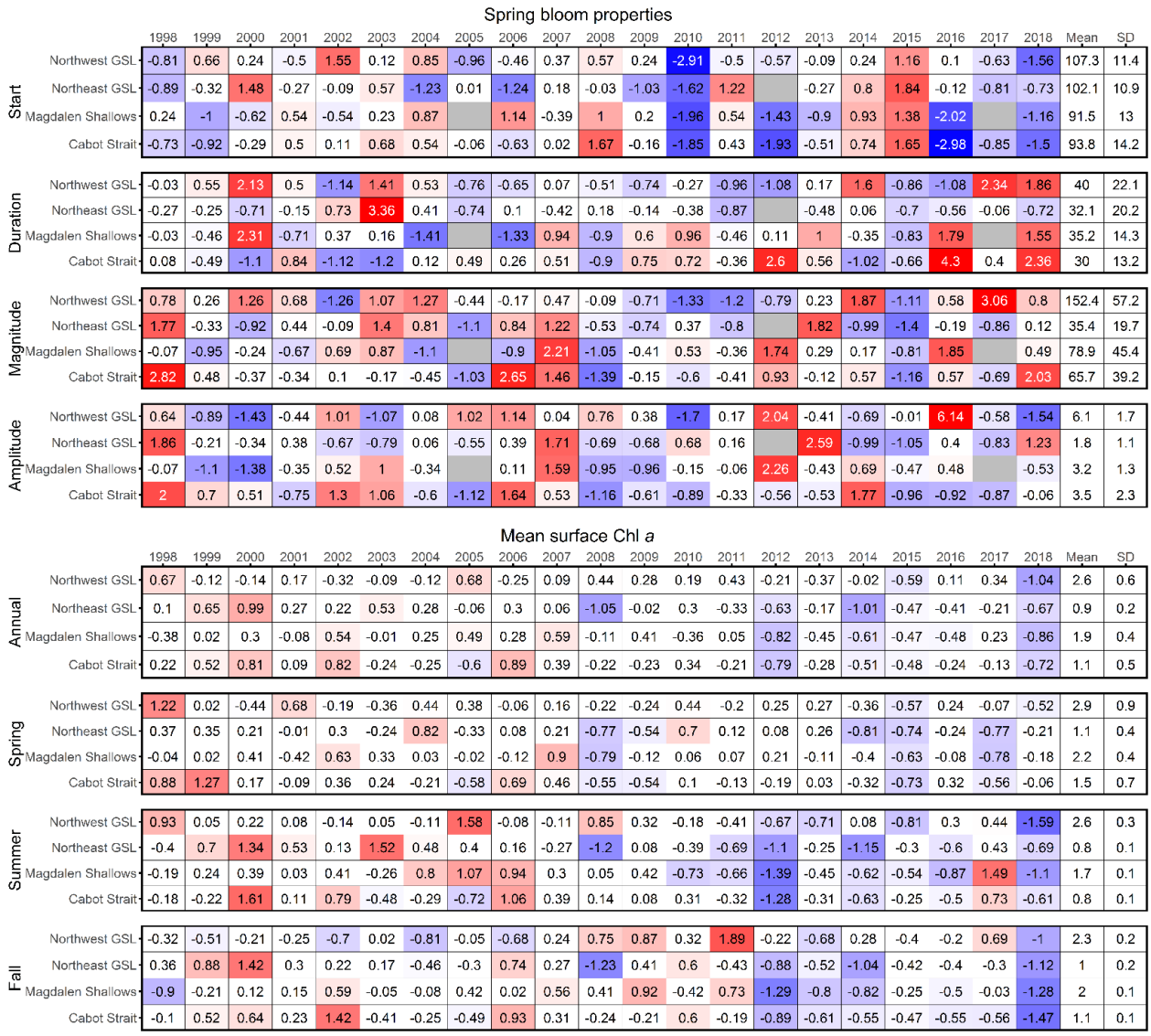

Figure 26. Time series of normalized anomalies for indices of change in spring bloom properties (upper section) and annual/seasonal mean surface chlorophyll a (lower section; mg m^{-3}) estimated from satellite ocean colour data (SeaWiFS: 1998–2007; MODIS: 2008–2011; and VIIRS since 2012) across the Gulf of St. Lawrence statistical boxes (see Fig. 4). The spring bloom indices are start (day of the year), duration (days), magnitude (mg chl m^{-2}), and amplitude (mg chl m^{-3}). Variable means and standard deviations for the 1999–2015 reference period are shown to the right of the scorecard. Blue colours indicate anomalies below the mean and reds are anomalies above the mean. Spring is from March to May, summer from June to August, and fall from September to November.

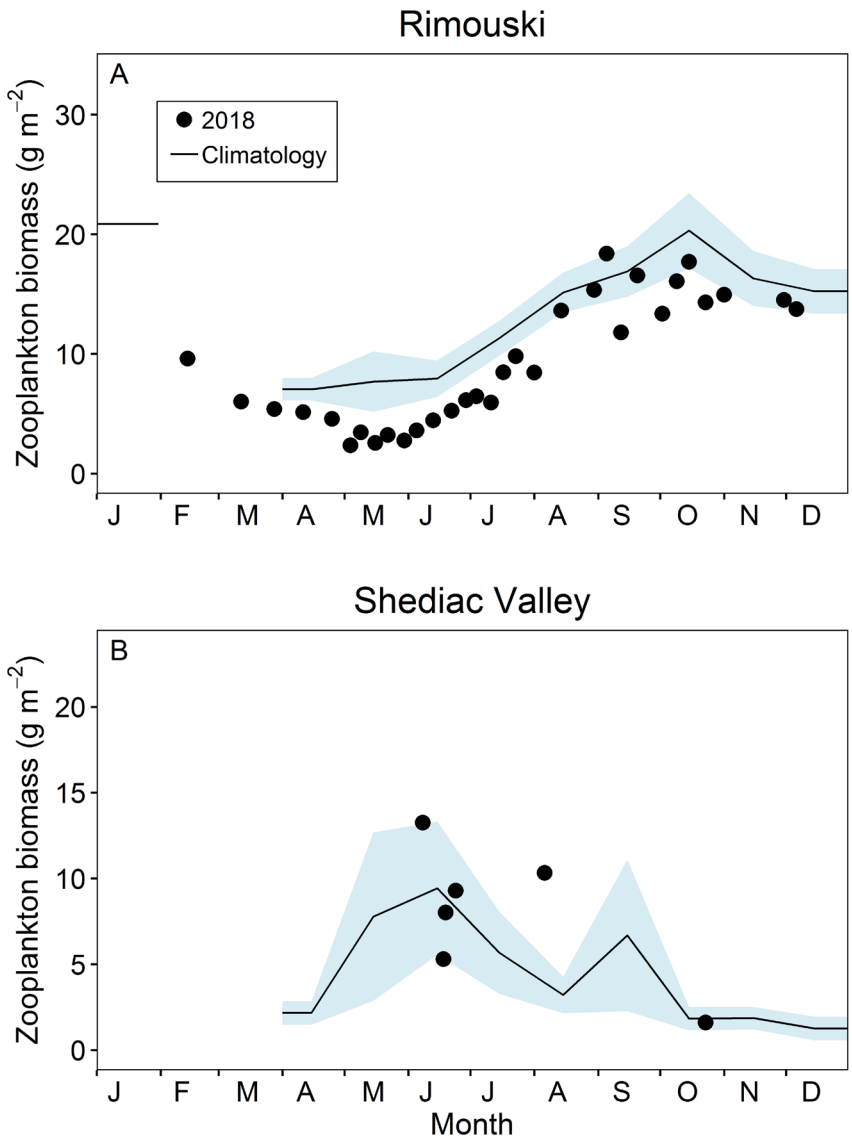

Figure 27. Comparison of total zooplankton biomass (dry weight) in 2018 (circles) with the monthly climatology from (A) Rimouski (2005–2015) and (B) Shediac Valley (1999–2015) stations (black line with blue shading). Blue shading represents 0.5 SD of the monthly means.

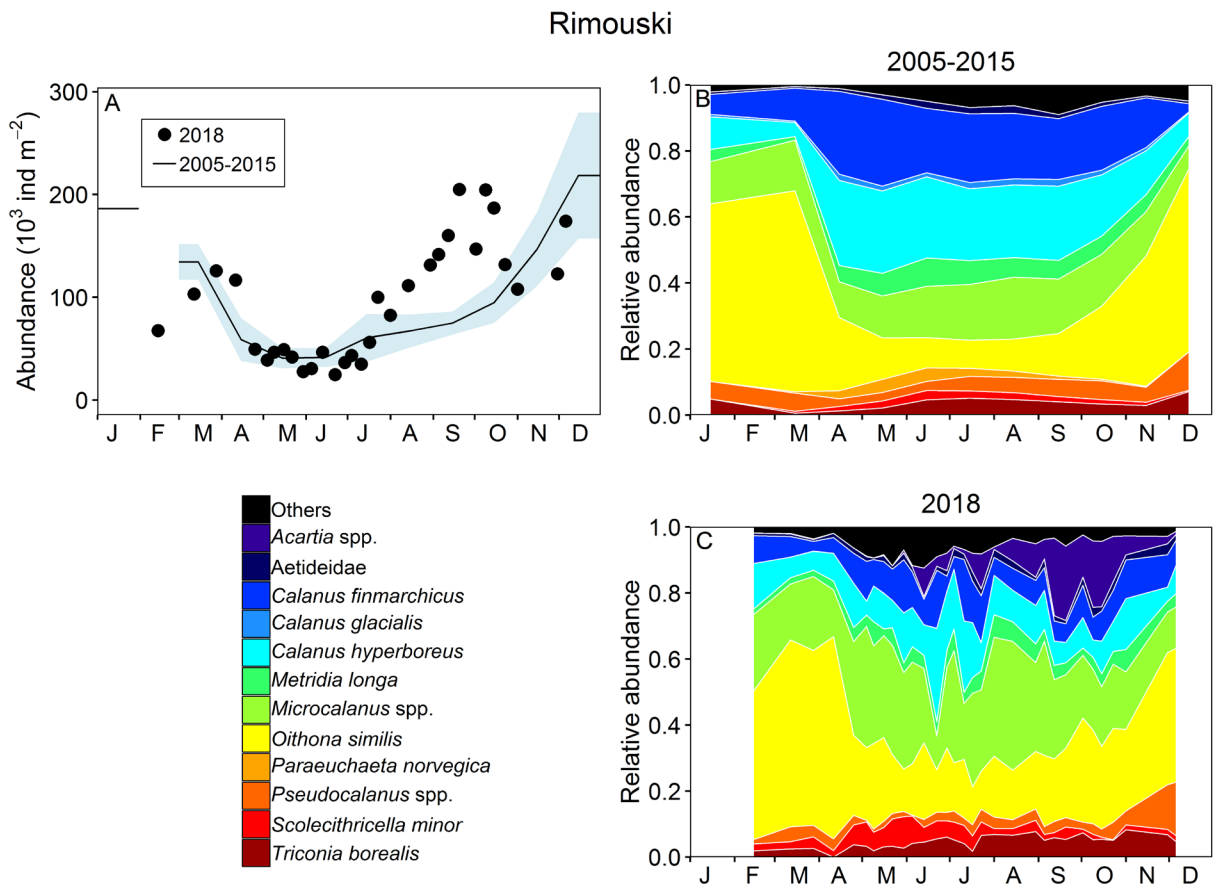

Figure 28. Seasonal variability of dominant copepods at Rimouski station. Copepod abundance (excluding nauplii) during the reference period (black line with blue shading indicating ± 0.5 SD) and in 2018 (circles) (A); climatology of the relative abundance of the top 95% of identified copepod taxa during the 2005–2015 period (B) and in 2018 (C).

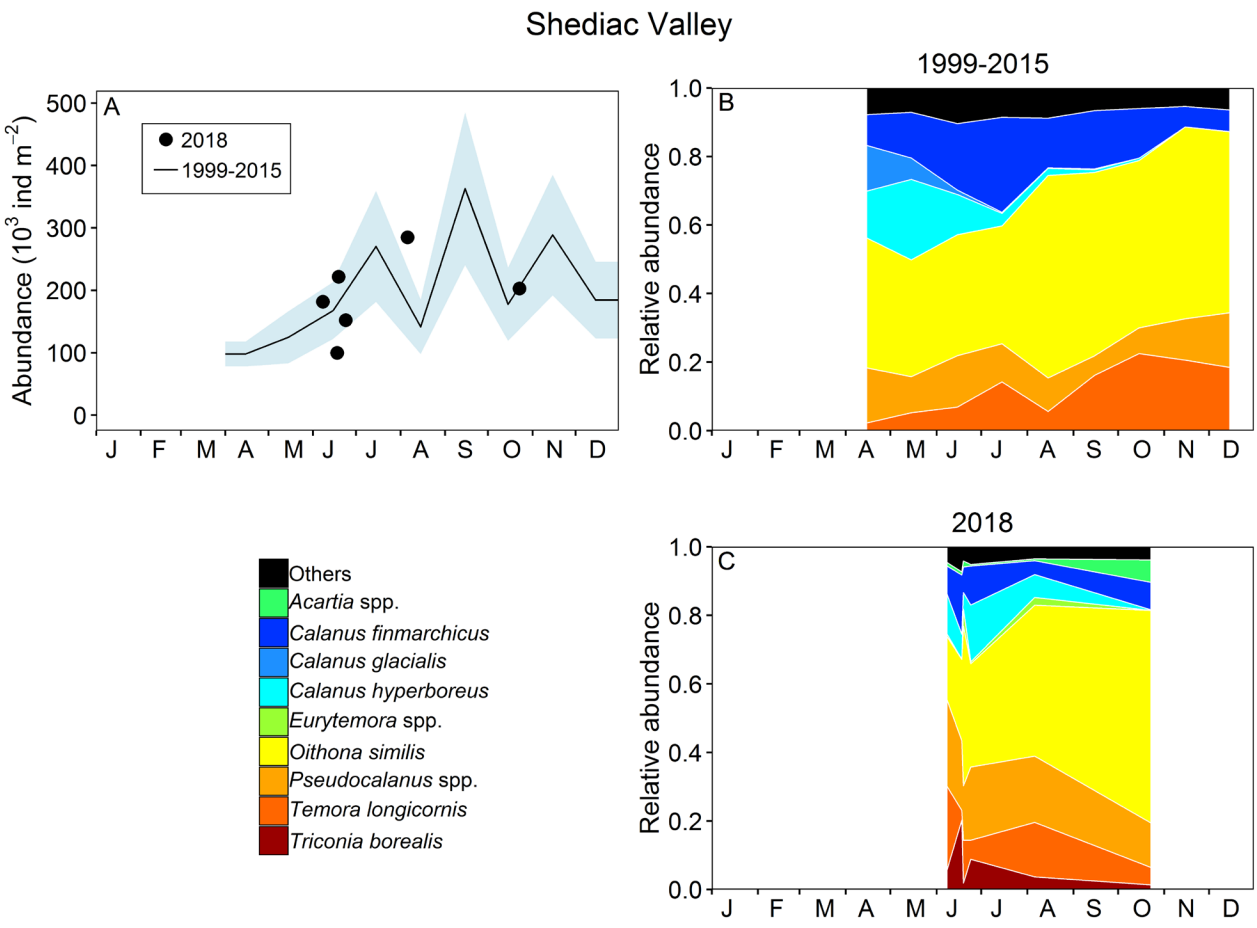

Figure 29. Seasonal variability of dominant copepods at Shediac Valley station. Copepod abundance (excluding nauplii) during the reference period (black line with blue shading indicating ± 0.5 SD) and 2018 (circles) (A); climatology of the relative abundance of the top 95% of identified copepod taxa during the 1999–2015 period (B) and in 2018 (C).

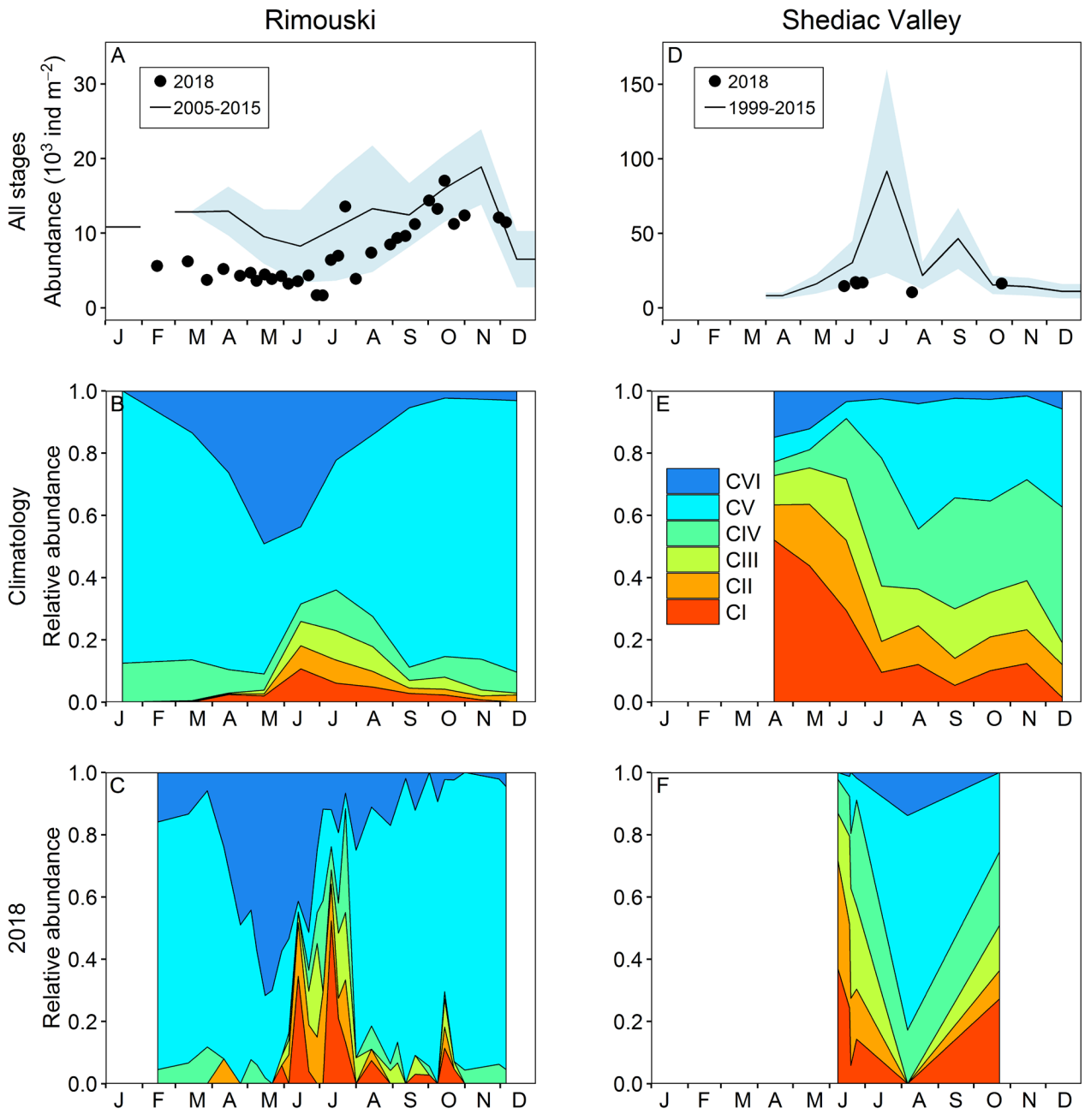

Figure 30. Seasonal variability in Calanus finmarchicus *copepodite abundance at Rimouski (A–C) and Shediac Valley (D–F) stations. The climatologies of the combined counts for the reference periods (black line with blue shading indicating ± 0.5 SD) are plotted with data from 2018 (circles) (A, D). The seasonal variabilities for the individual copepodite stages for the reference periods (B, E) and for 2018 (C, F) are also shown.*

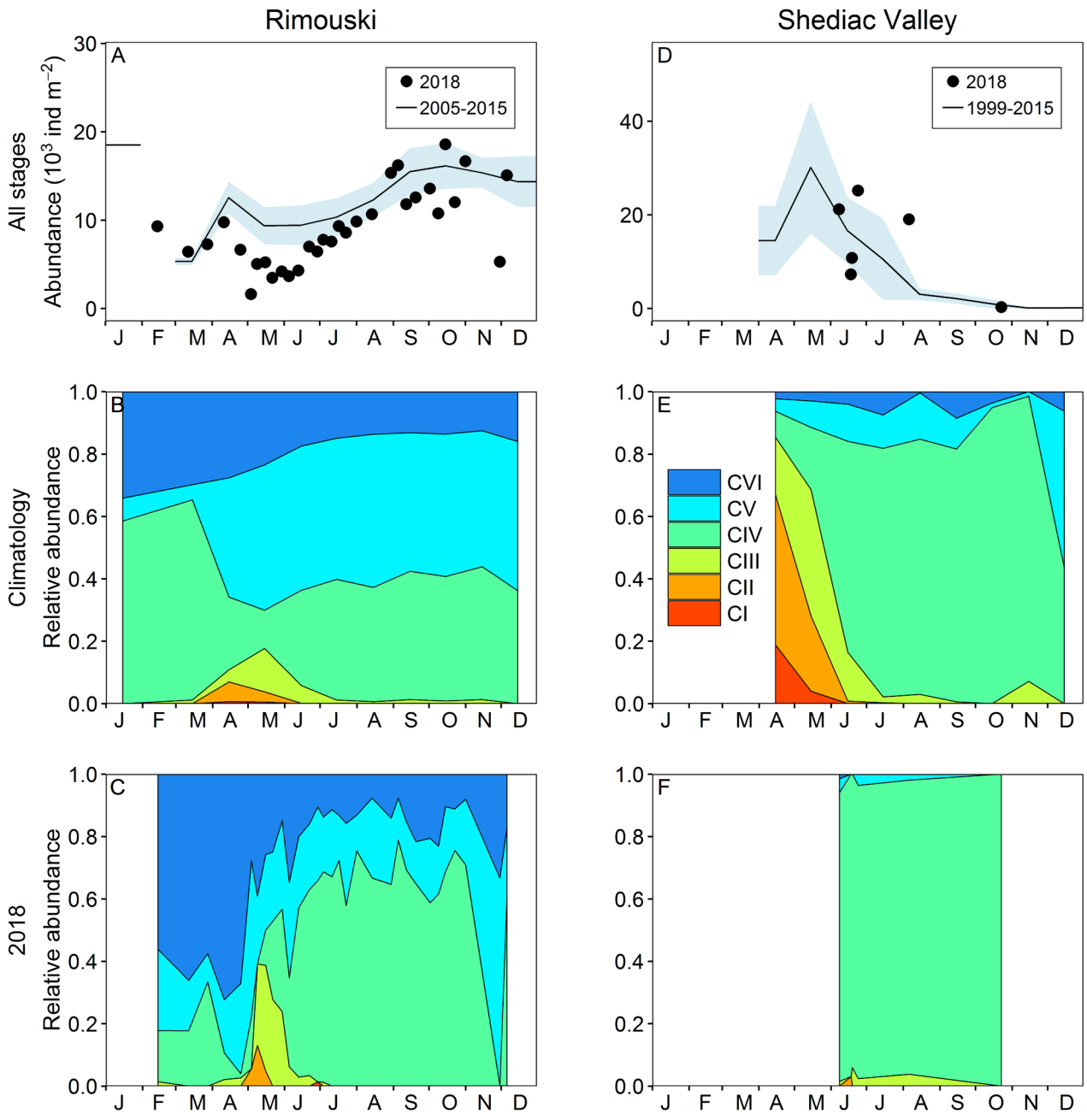

Figure 31. Seasonal variability in Calanus hyperboreus *copepodite abundance at Rimouski (A–C) and Shediac Valley (D–F) stations. The climatologies of the combined counts for the reference periods (black line with blue shading indicating ± 0.5 SD) are plotted with data from 2018 (circles) (A, D). The seasonal variabilities for the individual copepodite stages for the reference periods (B, E) and for 2018 (C, F) are also shown.*

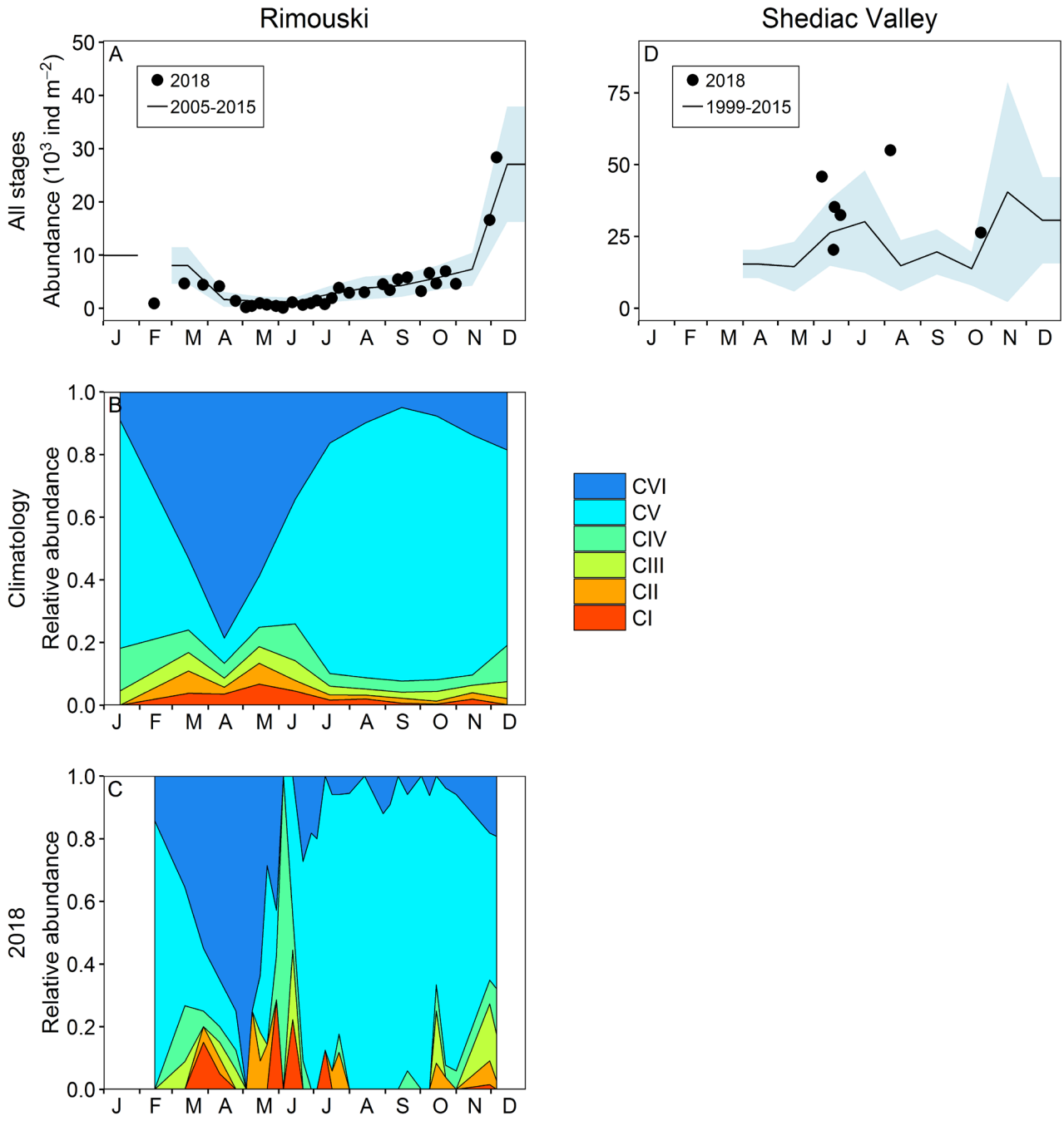

Figure 32. Seasonal variability in Pseudocalanus *spp. copepodite abundance at Rimouski (A–C) and Shediac Valley (D) stations. The climatologies of the combined counts for the reference periods (black line with blue shading indicating ± 0.5 SD) are plotted with data from 2018 (circles) (A, D). Seasonal variability for the individual copepodite stages for the reference period (B) and for 2018 (C) are also shown. No stage information is available for Shediac Valley.*

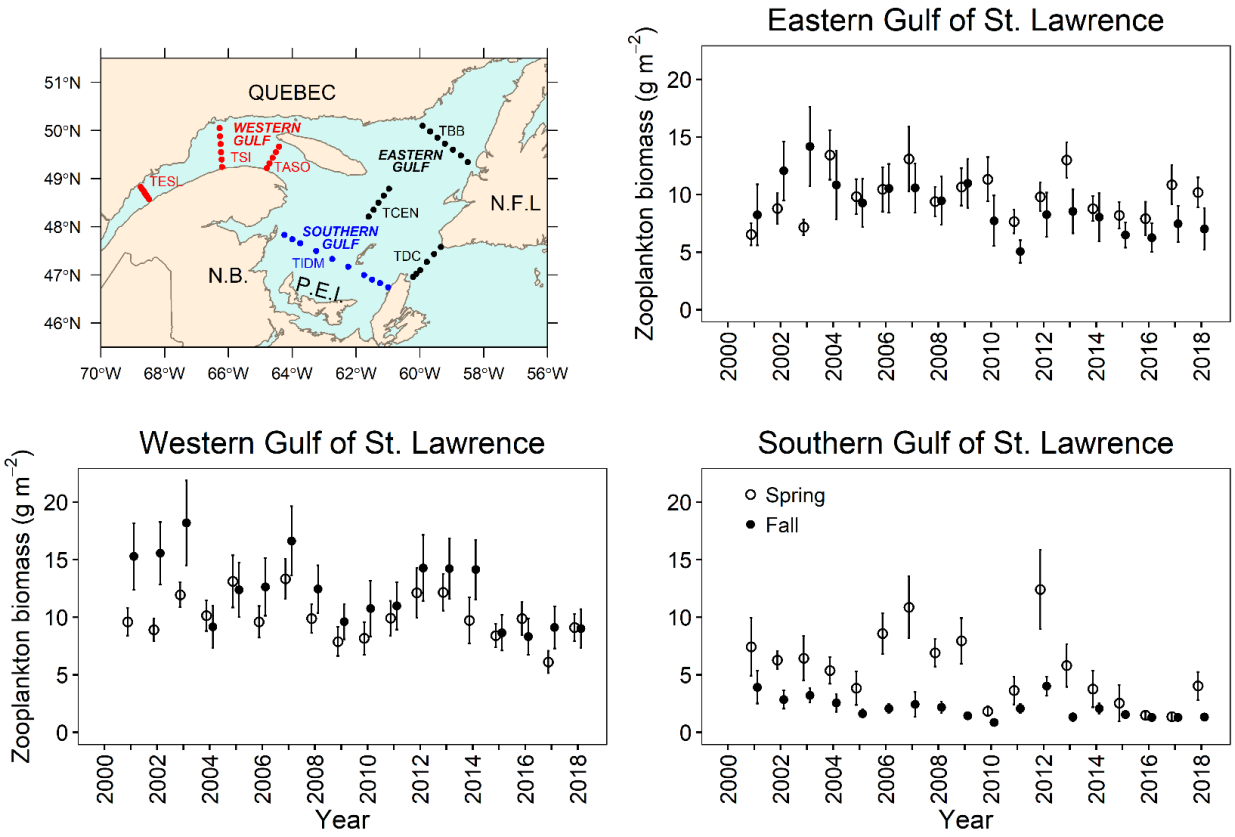

Figure 33. Time series of mean total zooplankton biomass (dry weight) during spring (open circles) and fall (filled circles) for the three subregions of the Gulf of St. Lawrence. Vertical lines represent standard errors.

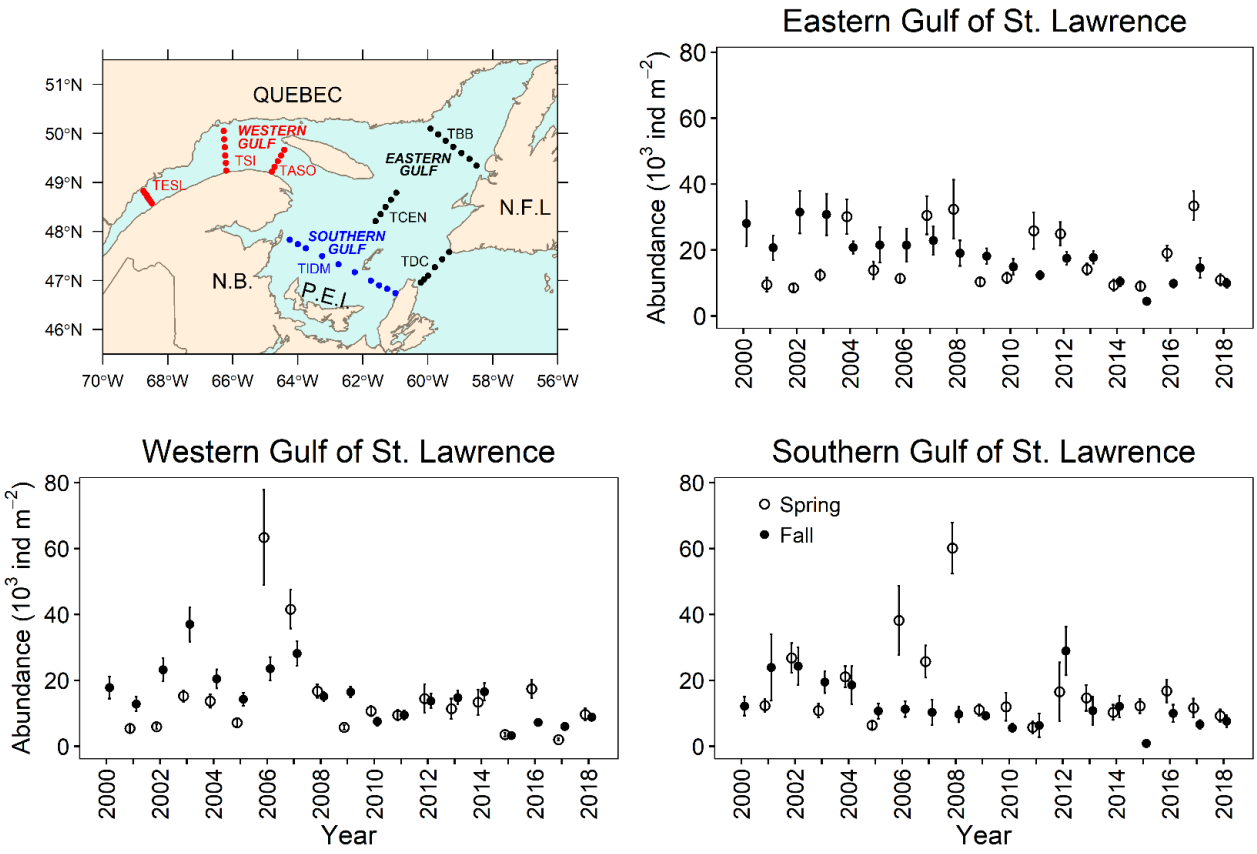

Figure 34. Time series of mean total abundance of Calanus finmarchicus *during spring (open circles) and fall (filled circles) for the three subregions of the Gulf of St. Lawrence. Vertical lines represent standard errors.*

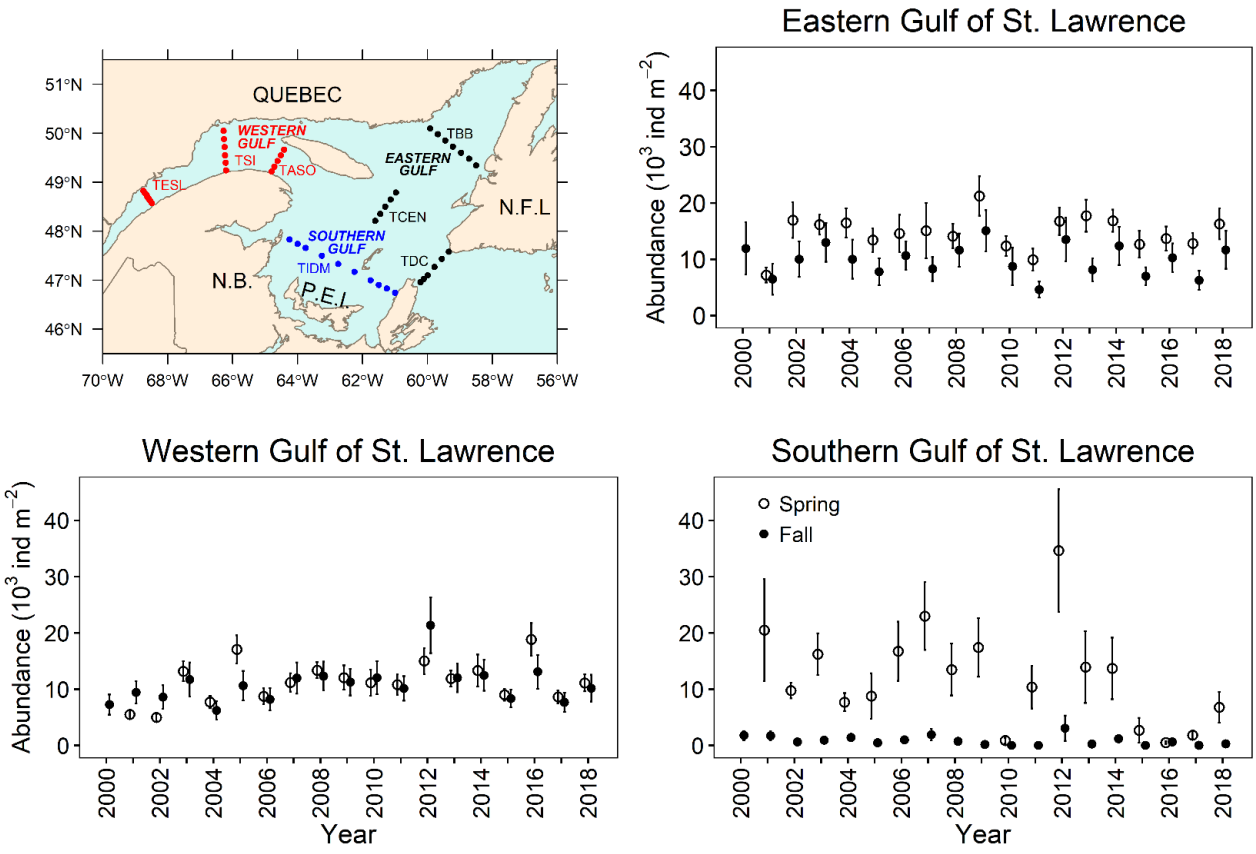

Figure 35. Time series of mean total abundance of Calanus hyperboreus *during spring (open circles) and fall (filled circles) for the three subregions of the Gulf of St. Lawrence. Vertical lines represent standard errors.*

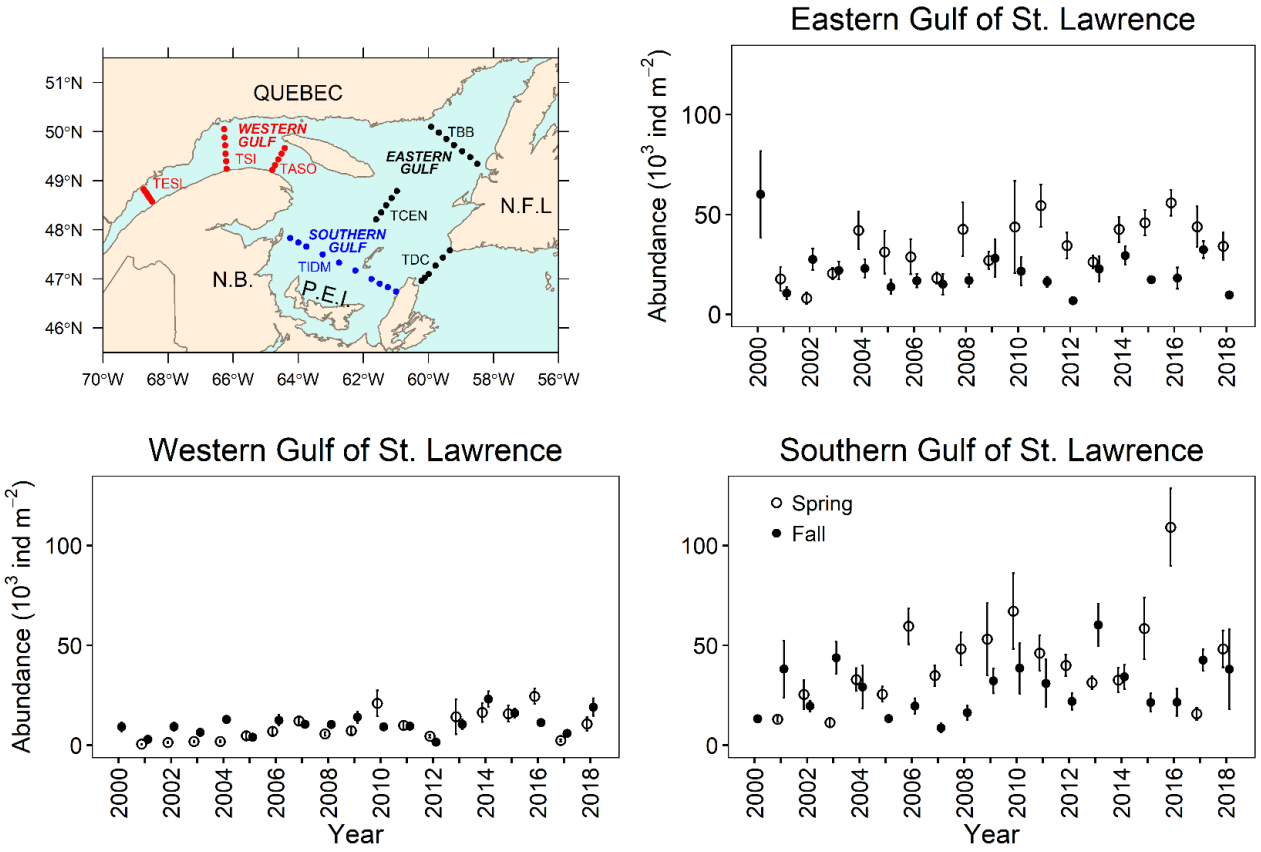

Figure 36. Time series of mean total abundance of Pseudocalanus *spp. during spring (open circles) and fall (filled circles) for the three subregions of the Gulf of St. Lawrence. Vertical lines represent standard errors.*

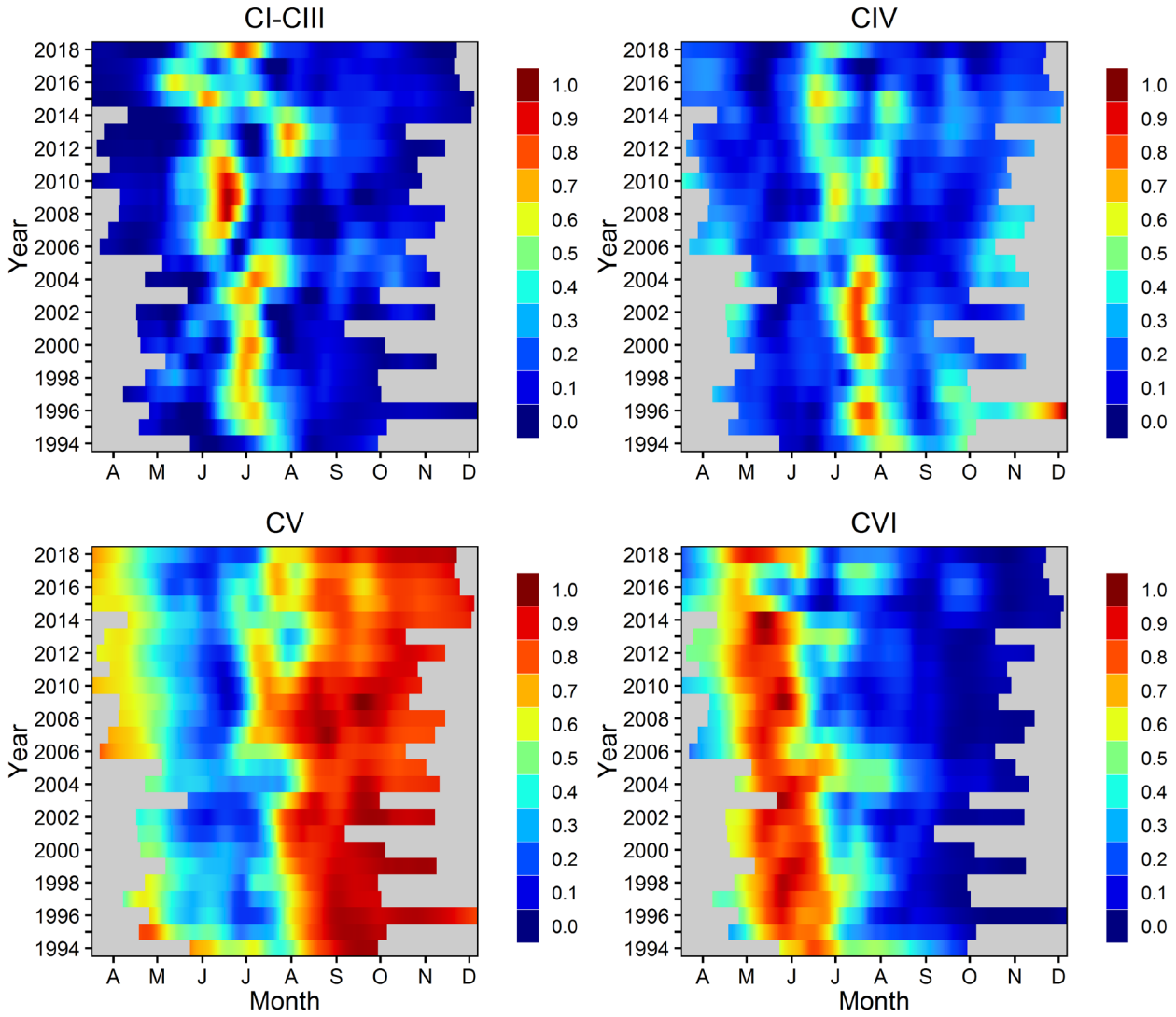

Figure 37. Time series of the seasonal cycle in relative proportion of total abundance for Calanus finmarchicus *copepodite stages (CI–CIII, CIV, CV, and CVI male + female) at Rimouski station. Proportions are normalized by the annual maximum and smoothed using a Loess.*

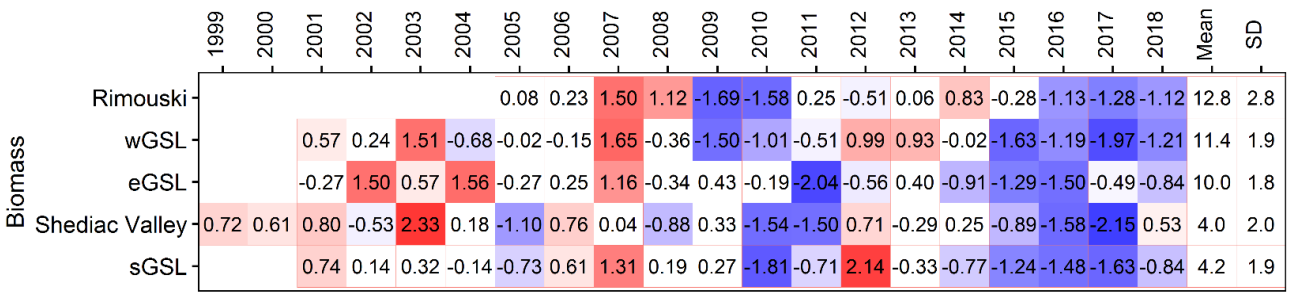

Figure 38. Time series of normalized annual anomalies of zooplankton biomass (dry weight; g m^{-2}) at the high-frequency monitoring sites and the three subregions of the Gulf of St. Lawrence. Variable means and standard deviations for the1999–2015 (2005–2015 for Rimouski) reference period are shown to the right of the scorecard. Blue colours indicate anomalies below the mean and reds are anomalies above the mean, and white representing normal conditions.

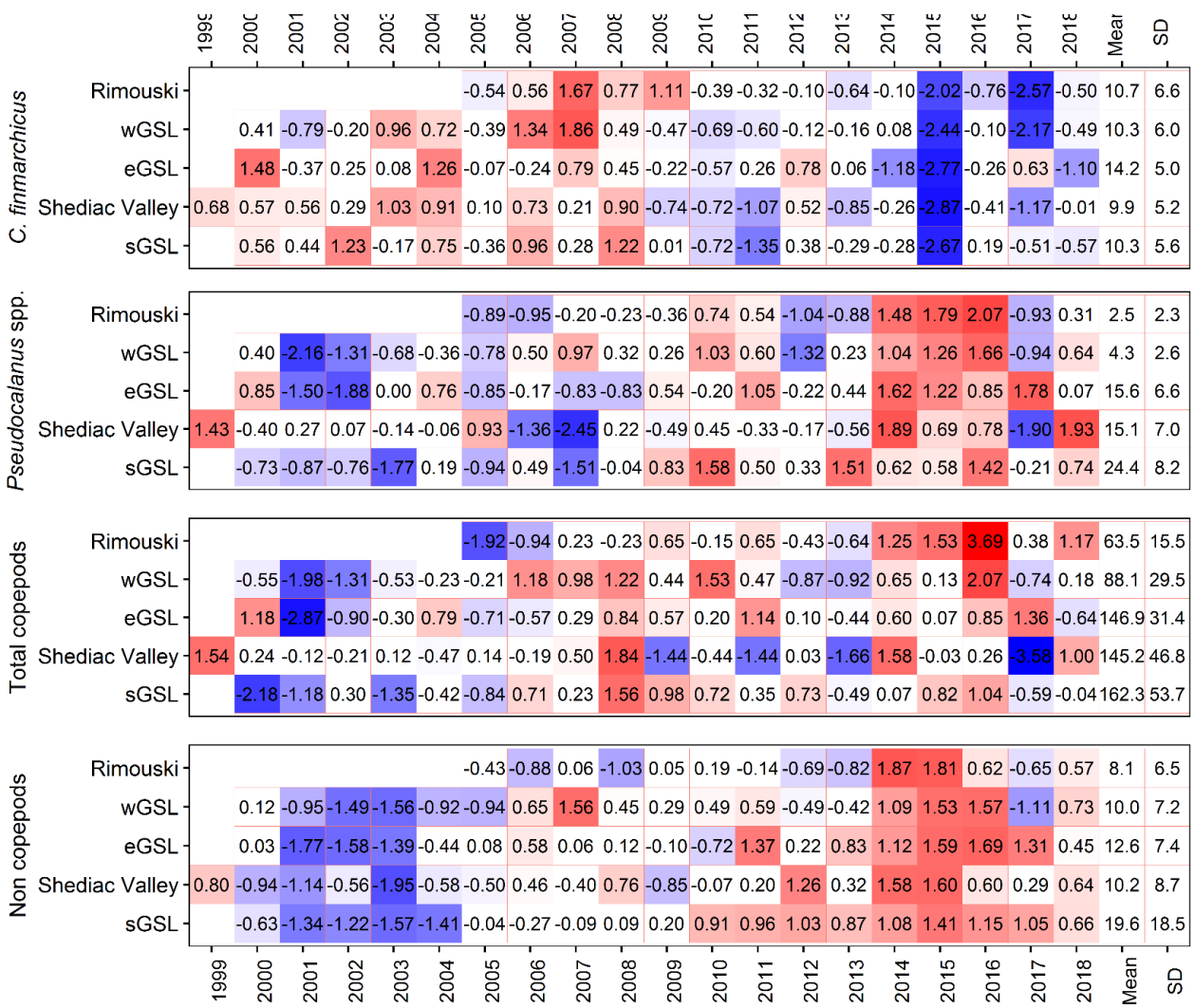

Figure 39. Time series of normalized annual anomalies for the abundance (×10³ ind m⁻²) of four zooplankton categories at the high-frequency monitoring sites and the three subregions of the Gulf of St. Lawrence. Variable means and standard deviations for the1999–2015 (2005–2015 for Rimouski) reference period are shown to the right of the scorecard. Blue colours indicate anomalies below the mean and reds are anomalies above the mean, and white representing normal conditions.

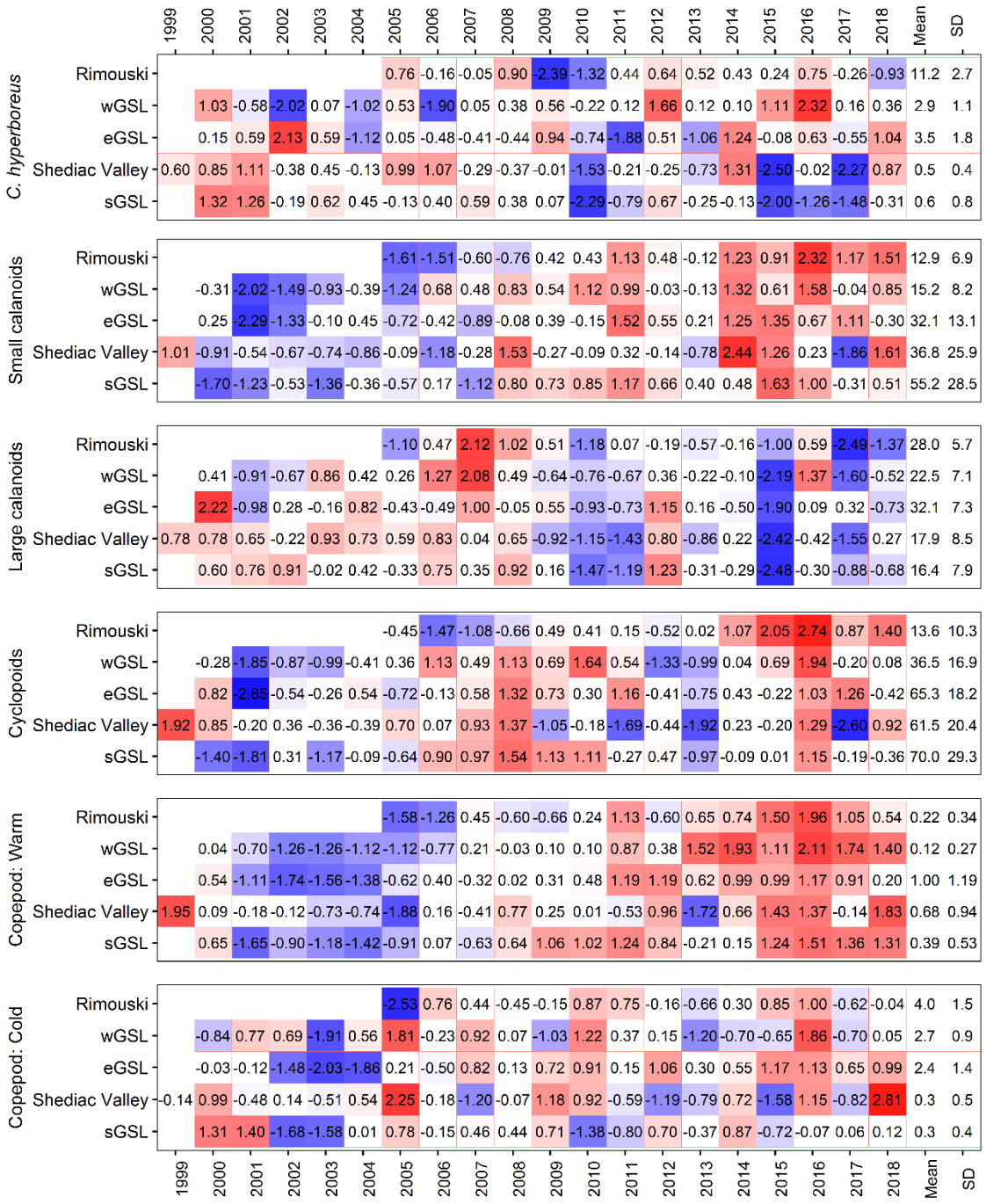

Figure 40. Time series of normalized annual anomalies for the abundance (×10³ ind m⁻²) of six categories of zooplankton assemblages at the high-frequency monitoring sites and the three subregions of the Gulf of St. Lawrence. Variable means and standard deviations for the1999–2015 (2005–2015 for Rimouski) reference period are shown to the right of the scorecard. Blue colours indicate anomalies below the mean and reds are anomalies above the mean, and white representing normal conditions. Small calanoids: mostly neritic species such as Pseudocalanus *spp.,* Acartia *spp.,* Temora longicornis*, and* Centropages *spp.; large calanoids: mostly* Calanus *and* Metridia *species; cyclopoids: mostly* Oithona *spp. and* Triconia *spp.; warm-water species:* Metridia lucens*,* Centropages *spp.,* Paracalanus *spp., and* Clausocalanus *spp.; and cold/arctic species:* Calanus glacialis *and* Metridia longa*. A detailed list of species included in each large copepod index is presented in Appendix 1*

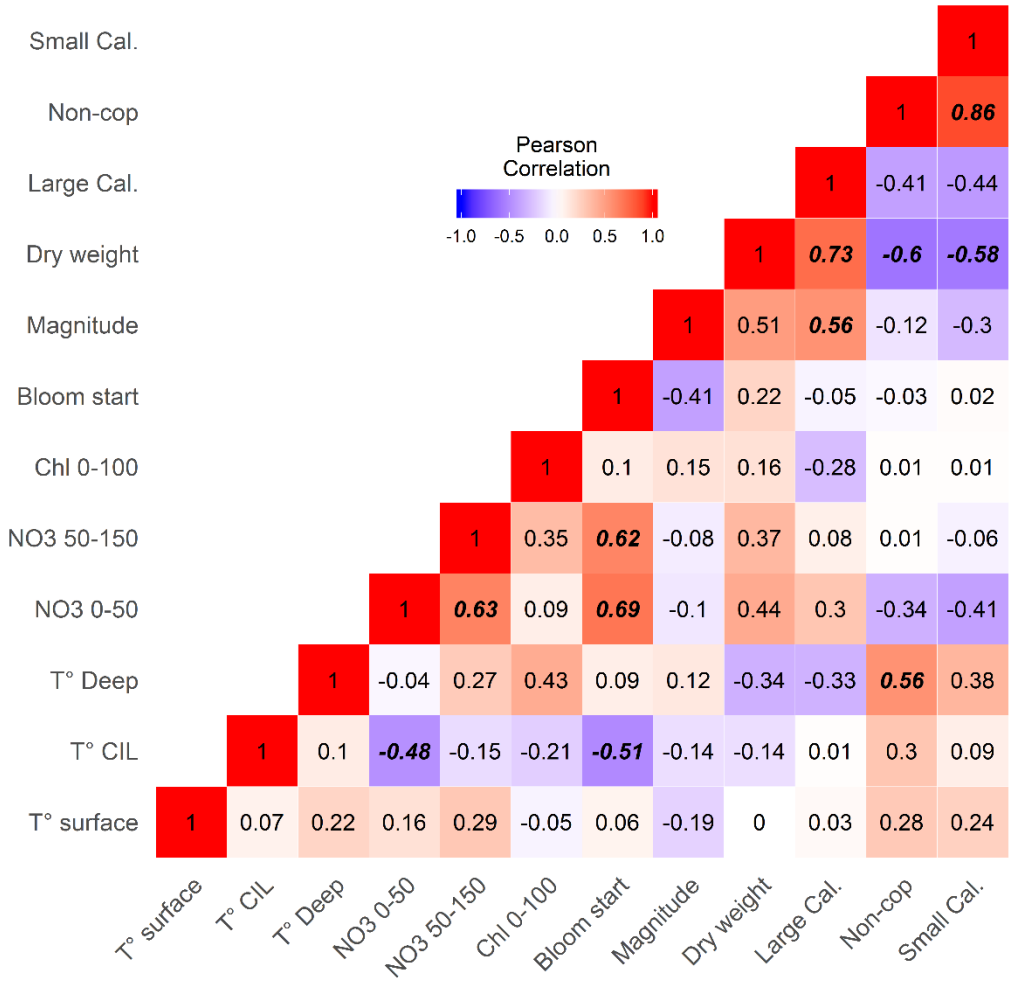

Figure 41. Correlation matrix for summed anomalies of some GSL indices. Red colours indicate positive correlations and blue colours negative correlations. Significant correlations ($p < 0.05$) are indicated in bold-italic.

APPENDICES

Appendix 1. List of species and genus associated with each large copepod index.

Small calanoids	*Acartia* spp.
	Aetideidae
	Centropages spp.
	Clausocalanus spp.
	Eurytemora spp.
	Microcalanus spp.
	Nannocalanus spp.
	Paracalanus parvus
	Pseudocalanus spp.
	Scolecithricella spp.
	Spinocalanus spp.
	Temora spp.
	Tortanus spp.
Large calanoids	*Anamolocera* spp.
	Calanus finmarchicus
	Calanus glacialis
	Calanus hyperboreus
	Euchaeta spp.
	Metridia spp.
	Paraeuchaeta norvegica
	Pleuromamma borealis
	Pleuromamma robusta
Warm copepods	*Centropages* spp.
	Clausocalanus spp.
	Metridia lucens
	Nannocalanus minor
	Paracalanus spp.
	Pleuromamma borealis
	Pleuromamma robusta
Cyclopoids	*Oithona* spp.
	Oncaea spp.
	Triconia borealis
	Triconia conifera
	Triconia similis
Cold copepods	*Metridia longa*
	Calanus glacialis

Appendix 2. GLM results for Rimouski and Shediac Valley stations. Significance of the year and month effects as well as the adjusted R squared of the regression for nutrients or chorophyll a are presented.

Station	Index	year (*p*)	month (*p*)	R^2
Rimouski	Chlorophyll *a* (0–100m)	<0.0001	<0.0001	0.40
	Nitrate (0–50m)	<0.0001	<0.0001	0.31
	Phosphate (0–50m)	<0.0001	<0.0001	0.30
	Silicate (0–50m)	<0.0001	<0.001	0.44
	Nitrate (50–150m)	<0.0001	<0.0001	0.24
	Phosphate (50–150m)	<0.0001	<0.0001	0.30
	Silicate (50–150m)	<0.0001	<0.0001	0.25
	Nitrate (300m)	<0.0001	<0.001	0.46
	Phosphate (300m)	<0.0001	0.01	0.36
	Silicate (300m)	<0.0001	<0.0001	0.63
	Nitrate (150–320m)	<0.0001	<0.0001	0.37
Shediac Valley	Chlorophyll *a* (0–100m)	<0.0001	<0.0001	0.40
	Nitrate (0–50m)	<0.001	<0.0001	0.33
	Phosphate (0–50m)	<0.0001	<0.0001	0.33
	Silicate (0–50m)	<0.01	<0.0001	0.27
	Nitrate (50–150m)	0.3	<0.0001	0.15
	Phosphate (50–150m)	<0.01	<0.0001	0.32
	Silicate (50–150m)	0.4	<0.0001	0.20

Appendix 3. GLM results for Rimouski and Shediac Valley stations. Significance of the year and month effects as well as the adjusted R squared of the regression for phytoplankton groups are presented.

Region	Group	year (*p*)	month (*p*)	R^2
Rimouski	Diatoms	<0.0001	<0.0001	0.35
	Dinoflagellates	<0.0001	<0.0001	0.54
	Flagellates	<0.0001	<0.0001	0.39
	Ciliates	<0.0001	<0.0001	0.35
	Total	<0.0001	<0.0001	0.22
	Diatoms/Dinoflagellates	<0.0001	<0.0001	0.30
	Diatoms/Flagellates	<0.0001	<0.0001	0.23
Shediac Valley	Diatoms	<0.0001	<0.0001	0.36
	Dinoflagellates	<0.001	0.03	0.28
	Flagellates	<0.0001	<0.0001	0.42
	Ciliates	0.2	0.4	0.03
	Total	<0.0001	<0.0001	0.35
	Diatoms/Dinoflagellates	<0.0001	<0.001	0.35
	Diatoms/Flagellates	<0.0001	<0.0001	0.41

Appendix 4. GLM results for GSL subregions. Significance of the year, season, and station effects as well as the adjusted R squared of the regression for nutrients or chorophyll a are presented.

Region	Index	year (*p*)	season (*p*)	station(*p*)	R^2
wGSL	Chlorophyll *a* (0–100m)	<0.0001	<0.0001	<0.0001	0.37
	Nitrate (0–50m)	<0.0001	<0.0001	<0.0001	0.69
	Phosphate (0–50m)	<0.0001	<0.0001	<0.0001	0.65
	Silicate (0–50m)	<0.0001	<0.0001	<0.0001	0.68
	Nitrate (50–150m)	<0.0001	0.08	<0.0001	0.48
	Phosphate (50–150m)	<0.0001	0.6	<0.0001	0.45
	Silicate (50–150m)	<0.0001	0.02	<0.0001	0.50
	Nitrate (300m)	<0.0001	<0.001	0.3	0.12
	Phosphate (300m)	<0.0001	<0.001	<0.0001	0.65
	Silicate (300m)	<0.0001	<0.0001	<0.0001	0.67
sGSL	Chlorophyll *a* (0–100m)	<0.0001	<0.001	<0.01	0.27
	Nitrate (0–50m)	<0.0001	<0.0001	<0.0001	0.69
	Phosphate (0–50m)	<0.0001	<0.0001	<0.0001	0.71
	Silicate (0–50m)	<0.0001	<0.0001	<0.0001	0.61
	Nitrate (50–150m)	<0.0001	0.01	<0.0001	0.61
	Phosphate (50–150m)	<0.0001	0.3	<0.0001	0.63
	Silicate (50–150m)	<0.001	0.1	<0.0001	0.62
eGSL	Chlorophyll *a* (0–100m)	<0.0001	<0.0001	<0.0001	0.19
	Nitrate (0–50m)	<0.0001	<0.0001	<0.0001	0.75
	Phosphate (0–50m)	<0.0001	<0.0001	<0.0001	0.77
	Silicate (0–50m)	<0.0001	<0.0001	<0.0001	0.78
	Nitrate (50–150m)	<0.0001	<0.0001	<0.0001	0.63
	Phosphate (50–150m)	<0.0001	<0.01	<0.0001	0.56
	Silicate (50–150m)	<0.0001	<0.0001	<0.0001	0.51
	Nitrate (300m)	<0.0001	<0.0001	<0.0001	0.39
	Phosphate (300m)	<0.0001	<0.0001	<0.0001	0.65
	Silicate (300m)	<0.0001	<0.0001	<0.0001	0.63

Appendix 5. GLM results for Rimouski and Shediac Valley stations. Significance of the year and month effects as well as the adjusted R squared of the regression for each zooplankton index are presented.

Station	Index	year (*p*)	month (*p*)	R^2
Rimouski	*Calanus finmarchicus*	<0.0001	<0.0001	0.55
	Pseudocalanus spp.	<0.0001	<0.0001	0.56
	Total copepods	<0.0001	<0.0001	0.56
	Non-copepods	<0.0001	<0.0001	0.44
	Calanus hyperboreus	<0.0001	<0.0001	0.38
	Small calanoids	<0.0001	<0.0001	0.65
	Large calanoids	<0.0001	<0.0001	0.3
	Cyclopoids	<0.0001	<0.0001	0.58
	Copepods: Warm	<0.0001	0.9	0.54
	Copepods: Cold	<0.0001	<0.0001	0.44
	Dry weight	<0.0001	<0.0001	0.6
Shediac Valley	*Calanus finmarchicus*	<0.0001	<0.0001	0.34
	Pseudocalanus spp.	0.2	0.2	0.03
	Total copepods	0.1	<0.0001	0.18
	Non-copepods	0.001	0.0003	0.24
	Calanus hyperboreus	<0.0001	<0.0001	0.66
	Small calanoids	0.01	0.0003	0.18
	Large calanoids	<0.0001	<0.0001	0.37
	Cyclopoids	0.2	<0.0001	0.24
	Copepods: Warm	0.1	0.06	0.08
	Copepods: Cold	0.1	<0.0001	0.29
	Dry weight	0.3	<0.0001	0.17

Appendix 6. GLM results for GSL subregions. Significance of the year, season, and station effects as well as the adjusted R squared of the regression for each zooplankton group are presented.

Region	Group	year (*p*)	season (*p*)	station(*p*)	R^2
wGSL	*Calanus finmarchicus*	<0.0001	0.001	<0.0001	0.68
	Pseudocalanus spp.	<0.0001	<0.0001	<0.0001	0.53
	Total copepods	<0.0001	<0.0001	<0.0001	0.76
	Non-copepods	<0.0001	<0.0001	<0.0001	0.60
	Calanus hyperboreus	0.003	<0.0001	<0.0001	0.61
	Small calanoids	<0.0001	<0.0001	<0.0001	0.68
	Large calanoids	<0.0001	0.02	<0.0001	0.78
	Cyclopoids	<0.0001	<0.0001	<0.0001	0.71
	Copepods: Warm	<0.0001	0.05	<0.0001	0.52
	Copepods: Cold	<0.0001	<0.0001	<0.0001	0.66
	Dry weight	<0.0001	<0.0001	<0.0001	0.66
sGSL	*Calanus finmarchicus*	<0.0001	<0.0001	<0.0001	0.31
	Pseudocalanus spp.	<0.0001	<0.0001	0.8	0.13
	Total copepods	<0.0001	<0.0001	0.0005	0.32
	Non copepods	<0.0001	<0.0001	<0.0001	0.53
	Calanus hyperboreus	<0.0001	<0.0001	<0.0001	0.49
	Small calanoids	<0.0001	0.003	0.01	0.28
	Large calanoids	<0.0001	<0.0001	<0.0001	0.48
	Cyclopoids	<0.0001	<0.0001	<0.0001	0.37
	Copepods: Warm	<0.0001	<0.0001	0.3	0.52
	Copepods: Cold	<0.0001	<0.0001	<0.0001	0.40
	Dry weight	<0.0001	<0.0001	<0.0001	0.36
eGSL	*Calanus finmarchicus*	<0.0001	0.3	<0.0001	0.22
	Pseudocalanus spp.	<0.0001	<0.0001	<0.0001	0.27
	Total copepods	<0.0001	<0.0001	<0.0001	0.27
	Non-copepods	<0.0001	<0.0001	<0.0001	0.45
	Calanus hyperboreus	0.1	<0.0001	<0.0001	0.54
	Small calanoids	<0.0001	0.9	<0.0001	0.37
	Large calanoids	<0.0001	<0.0001	<0.0001	0.48
	Cyclopoids	<0.0001	<0.0001	0.002	0.32
	Copepods: Warm	<0.0001	<0.0001	<0.0001	0.50
	Copepods: Cold	<0.0001	<0.0001	<0.0001	0.38
	Dry weight	<0.0001	0.02	<0.0001	0.59